Coding Techniques for Backscatter Communications – A Contemporary Survey

Fatemeh Rezaei*, *Member, IEEE*, Diluka Galappaththige*, *Member, IEEE*, Chintha Tellambura, *Fellow, IEEE,* Sanjeewa Herath, *Member, IEEE*

***Abstract*—Backscatter communication (BackCom) networks enable passive/battery-free Internet-of-Thing devices, providing reliable, massive connectivity while ensuring self-sustainability, low maintenance, and low costs. Effective channel codes and decoding algorithms are necessary to achieve these objectives. However, a comprehensive survey/review paper on such techniques for BackCom networks has not been available. This paper aims to fill this gap. Because tags have limited computational resources, traditional coding techniques may not suit them. We first describe the basics of BackCom, channel codes and their relevant design parameters, and codes for general communication networks. We address the BackCom limitations, requirements, and channel characteristics. As conventional codes may not seamlessly move to the BackCom arena, we identify the potential BackCom coding techniques and multiple access schemes. We further highlight potential approaches for addressing code implementation complexity and reliability. Finally, we discuss open issues, challenges, and potential future research directions.**

***Index Terms*—Backscatter communications, Coding and decoding, Error correcting codes, Space-time codes, Multiple access coding schemes.**

I. Introduction

Backscatter communication (BackCom) was introduced by Stockman in 1948 [1]. It allows a tag to communicate with a reader without generating a radio frequency (RF) signal by the tag. The backscatter tag simply reflects an incident RF signal, and this reflection process is called backscatter modulation [2] (Fig. 1). Backscatter tags are thus inexpensive and have ultra-low energy requirements (a few nW–$\mu\mathrm{W}$) because of the simple RF design [3]. The receiver (reader) has its power supply and RF components. The reader, a dedicated RF carrier emitter, or an ambient legacy transmitter can generate the incident RF signal. Section II will describe these.

Inexpensive, passive tags have significant and multiple applications, including logistics, inventory management, warehousing, manufacturing, energy industry, healthcare, agriculture, aerospace and defense, farming, retail, sports, and many more. The potential market will grow exponentially, e.g., parcel volume will reach 163.4 billion in China by 2025 and 220-262 billion globally by 2026 [4]. Hence, these potential use cases and the market values will establish an excellent platform for BackCom use.

Radio frequency identification (RFID) is the prime example of commercial, short-range use of this technology. RFID systems read data such as the electronic product code (EPC) and other relevant information stored on a tag attached to an object [5]. There has been an enormous upsurge in RFID use due to its diverse sectors such as medicine and health care, agriculture, livestock, logistics, retail chains, and others [6], [7]. According to industry research [8], the RFID market will reach \$35.6 billion by 2030 from \$14.6 billion in 2022; growing at a compound annual growth rate (CAGR) of 11.9%.

BackCom can also work with massive machine-type communications (mMTC), one of the core fifth-generation (5G) service areas. This approach enables the collection of a huge volume of small data packets from large numbers of devices simultaneously. mMTC supports applications using Internet of Things (IoT) sensors, meaning that data can reduce energy consumption, make work more efficient, or improve our lives in other ways [9]–[11]. Over 2021-2026, the mMTC market is expected to reach \$3.1 billion, growing at a CAGR of $9.2\,\%$ [12]. Many mMTC devices will be less mobile, which reduces demand for the handover of ongoing communications with short delay-tolerant transmissions. Since mMTC typically involves the automated transmission of infrequent, low-volume, and non-delay-sensitive data via a massive number of devices, it differs significantly from conventional mobile networks.

For example, an mMTC device must be ultra-low complex and low cost. It also needs a long battery life, a $5\,\mathrm{Wh}$ battery allowing for a more than 10 years [13]. Hence, the devices that require frequent recharging are not suitable. And the number of mMTC devices might be $10\times$ to $100\times$ more than mobile phones [13]. Additionally, at least $20\,\mathrm{dB}$ improvement in coverage over conventional cellular networks is required for machine-type communications (MTC) in 5G [11], [13]. Many technologies such as Bluetooth 5, Wireless Fidelity (Wi-Fi), long term evolution (LTE) MTC, narrow-band IoT (NB-IoT), and wake-up radios have the potential to meet MTC network requirements [14], [15]. BackCom is another emerging solution to facilitate MTC goals.

Billions of IoT devices will seek access to the Internet [16], [17]. However, powering them is a significant challenge. Charging/changing batteries is inefficient and expensive. Hence, passive IoT, also known as battery-free IoT, based on energy harvesting (EH), is emerging [4], [18]–[20], which supports ultra-low power consumption, i.e., $1\,\mu\mathrm{W}\sim100\,\mu\mathrm{W}$ [4]. Passive IoT requires (i) small packet transmissions, (ii) connectivity for numerous low-energy and low-complexity user devices, and (iii) uplink-dominated transmissions [21], [22]. BackCom can thus enable passive IoT towards sixth-generation (6G) network [3], [23]–[25].

However, due to the reliance on EH, backscatter tags are extremely power limited (Section II-C). Moreover, double path-losses and other impairments (Section IV) decrease the

*F. Rezaei and D. Galappaththige contributed equally to this work.

F. Rezaei, D. Galappaththige, and C. Tellambura are with the Department of Electrical and Computer Engineering, University of Alberta, Edmonton, AB, T6G 1H9, Canada (e-mail: rezaeidi, diluka.lg, ct4@ualberta.ca).

S. Herath is with the Huawei Canada, 303 Terry Fox Drive, Suite 400, Ottawa, Ontario K2K 3J1 (e-mail: sanjeewa.herath@huawei.com).

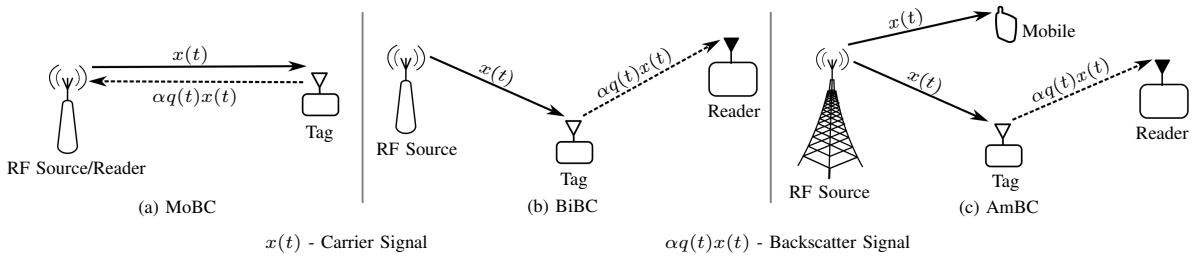

Fig. 1: BackCom configurations.

TABLE I: Channel codes adopted in wireless standards.

Year	Standard	Channel code type	Year	Standard	Channel code type
1992	GSM	Convolutional	2011	3GPP v=V10.1.0	Convolutional, Turbo
1999	IEEE 802.11a/b	Convolutional	2012	IEEE 802.16m	Convolutional, Turbo, Duo-binary
2000	CDMA 2000	Convolutional, Turbo		LTE-Advanced	Convolutional, Turbo
	TD-SCDMA	Convolutional, Turbo		IEEE 802.11ac	Convolutional, LDPC
	WCDMA	Convolutional, Turbo, Reed-Soloman		IEEE 802.11ad	Reed-Soloman, LDPC
2003	IEEE 802.11g	Convolutional	2014	ISA100.11a	No
2006	IEEE 802.16e	Turbo, LDPC	2015	WIA-FA	Convolutional, LDPC
2009	IEEE 802.11n	Convolutional, LDPC	2018	5G (Release 15)	LDPC, Polar
	PNO/WSAN	Repeat, Cyclic redundancy check	2020	5G (Release 16)	LDPC, Polar

achievable data rates and the communication distance [26]. Channel codes offer coding gains, which can help increase the reliability and communication range. However, there are challenges to adopting classical coding solutions to BackCom networks. This survey article aims to explore those issues in depth.

A. Channel Codes in Wireless Standards

Before discussing specific BackCom channel codes, we briefly review channel codes for conventional wireless standards (Table I). Third-generation (3G) and fourth-generation (4G) standards use turbo codes due to their high performance and reliability [27], [28]. However, the 5G standardization process of the 3rd generation partnership project (3GPP) considers low-density parity-check (LDPC) codes and polar codes [29], [30]. This change is due to the delay of iterative decoding of turbo codes, a drawback for 5G, which requires high rates and low delays. Since one code cannot meet all 5G requirements, 3GPP uses both of these. Section III-C and Section V-C describe the pros and cons of them.

We can thus learn from the channel codes used for conventional standards to design/select codes for BackCom systems. Previous research has shown that poor selection of channel codes will degrade the coverage, data rates, capacity, and other quality-of-service (QoS) parameters. As well, channel codes must satisfy 5G requirements (Section I). In particular, 5G mMTC systems require energy-efficient, near-optimal short codes with a strong error detection capability [31], [32], and low-complexity decoding algorithms operating with partial or no channel state information (CSI) [33].

B. Contribution and Organization

BackCom networks can enable massive connectivity, helping to achieve sustainable IoT deployments and meeting the needs of emerging applications. BackCom links are vulnerable to excess path-losses and impairments, causing low rates and limited range. Channel codes provide coding gains, which can alleviate those impairments. However, conventional codes may not work with ultra-low-power tags with low processing capability. Thus, we need to develop codes matching backscatter channel characteristics. However, this research area has yet to be fully explored or developed. This article thus comprehensively surveys existing coding solutions and potential solutions for practitioners and researchers.

Although several surveys and tutorials cover a wide range of BackCom topics, including architectures, physical layer, benefits, limitations, and applications [34]–[39], only a few consider coding aspects [24], [25], [40], [41]. Hence, we limit our attention to those. In particular, [24] describes AmBC fundamentals, general architecture, challenges, design techniques, applications, and research efforts/progress. It briefly describes non-return-to-zero (NRZ), Manchester, Miller, and FM0. It also discusses orthogonal space-time block code (OSTBC), balanced code, short block-length cyclic channel code, and μ-code. Overall, this discussion is extremely brief. Reference [25] addresses the integral aspects of BackCom wireless-powered networks and reviews their performance improvement techniques, emphasizing large-scale networks. It also discusses the pros and cons of some conventional coding schemes. Besides, [40] discusses BackCom-based green IoT through joint communication and sensing, operating principles, architecture, evolution, and applications. It has a brief discussion of coding and modulation solutions. Moreover, reference [41] specifically focuses on antenna design, RF system integration, and advanced packaging technologies for BackCom systems. It has an interesting discussion on rectifying antennas and circuits, and waveforms for EH. The discussion on coding,

however, is limited to future research directions.

To the best of our knowledge, no papers have focused on coding techniques for BackCom. This paper thus fills this gap exclusively (Fig. 2). Table II compares and contrasts our work with related works.

We summarize the contributions of this paper as follows:

1) We start with the basics of BackCom systems. We briefly discuss different BackCom configurations and describe the two critical tasks of passive tags, namely backscatter modulation and EH.
2) We address the general principles of channel codes, their design guidelines, and encoding and decoding techniques. We also highlight conventional codes that have evolved with communication networks and standards over the last few decades.
3) We then discuss the limitations and requirements of BackCom networks by considering their specific channel characteristics. We also provide several simulations to highlight the performance in terms of capacity and bit error rate (BER). These simulations demonstrate the benefits of channel codes in BackCom.
4) We thus identify line codes, error-correcting codes, and space-time codes (STCs) to improve reliability and data rate while overcoming deeper fading in backscatter channels. To this end, we summarize Backcom adopted codes and give their performance simulations.
5) We also review codes to support concurrent transmissions of multiple tags, a critical requirement of BackCom-assisted MTC networks.
6) Finally, we discuss the potential approaches to address the implementation complexity and reliability. We also touch upon open issues, challenges, and future research directions.

We organized the rest of the paper as follows. Section II describes different BackCom configurations and the critical tasks of passive tags, including backscatter modulation and EH. Section III discusses the basic principles of channel coding (including channel capacity, code design criteria, code rate, and coding gain) and describes the basic channel codes. The interplay between coding and modulation and the antenna effects on coding is also explained. Section IV discusses the BackCom channel characteristics and requirements. We address the potential BackCom coding techniques in Section V. In Section VI, we summarize the coding schemes adopted for BackCom. Section VII discusses multiple access coding schemes for BackCom. Section VIII addresses the open issues and future research directions. Finally, we conclude the paper in Section IX. Table III and Table IV respectively summarize the abbreviations and notations used in this article.

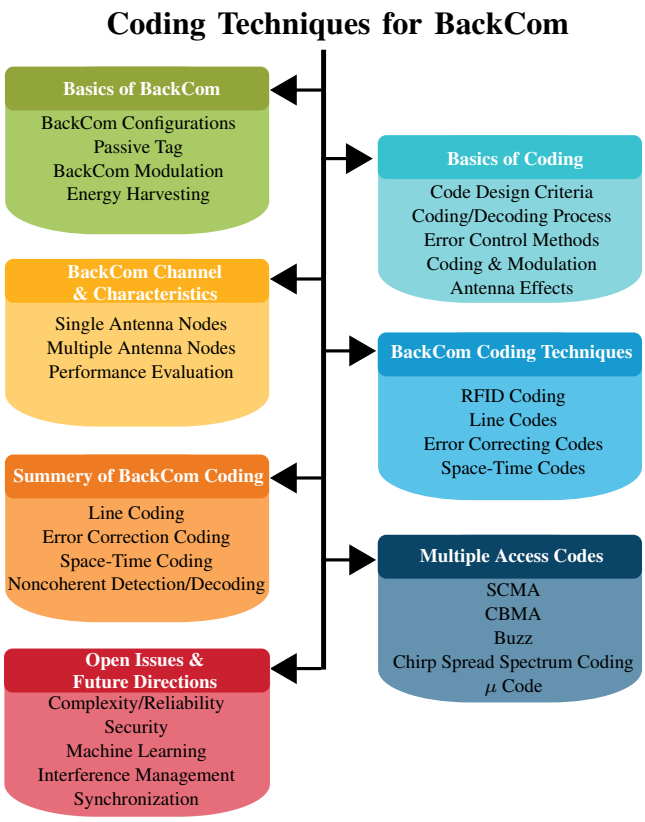

Fig. 2: Outline of the main contributions of this survey.

II. Basics of BackCom

The three types of BackCom are described below.

1) *Monostatic Backscatter Communication (MoBC) Systems*: These comprise a backscatter tag and a reader (Fig. 1 (a)). The reader first emits an RF signal to activate the tag, which reflects it to communicate its data. Thus, the RF emitter and the receiver of the reflected signal are co-located at the reader. However, because the RF signal travels from the reader to the tag and back, the path-loss doubles up [42]. Therefore, MoBC systems suit short-range applications, e.g., RFID [5], [43].
2) *Bistatic Backscatter Communication (BiBC) Systems*: To mitigate the double path-loss, the total distance traveled by the RF signal must be minimized. This can be done by dislocating the two functions of the reader. Thus, a dedicated RF emitter transmits the RF signal reflected by the tag. The reader receives the tag reflections. Thus, this system can include multiple RF carrier emitters to cover an area. These emitters' locations should be optimized to maximize coverage and performance. Each tag can be close to at least one of these emitters. This physical proximity boosts the EH capability of the tag. Therefore, the BiBC configuration (Fig. 1 (b)) [42] offers two advantages: (i) the ability to optimize the locations of the RF emitters, and (ii) the lower fabrication costs of the RF emitter and the reader relative to that in MoBC [42], [44].
3) *Ambient Backscatter Communication (AmBC) Systems*: However, a key problem with BiBC is the high cost/complexity of dedicated carrier emitters. Is there another way to find RF carrier signals? Ambient legacy RF sources, e.g., cellular base stations (BSs), television (TV) towers, and Wi-Fi access points (APs) are ubiquitous and operate on a 24/7 basis. No cost is associated with using such signals to the BackCom system. Tags can thus use them to harvest energy and backscatter data

TABLE II: Summary of related works.

Reference	Objective	Contribution						
		(a)	(b)	(c)	(d)	(e)	(f)	(g)
[24]	Comprehensive survey on AmBC	✓	✗	✗	✗	✗	✗	✓
[25]	Wireless-powered networks integrated with BackCom systems	✓	✗	✗	✗	✗	✓	✓
[41]	Antenna design and RF system integration for BackCom	✓	✗	✗	✗	✓	✓	✓
[40]	Comprehensive survey from signal processing aspects	✓	✗	✗	✗	✗	✓	✓
This paper	Comprehensive survey on potential BackCom coding methods	✓	✓	✓	✓	✗	✗	✓

(a) Fundamentals of BackCom (b) Coding techniques for BackCom (c) Gains of coding schemes in BackCom
(d) Multiple-access coding schemes (e) Practical experiments (f) EH aspects (g) BackCom challenges

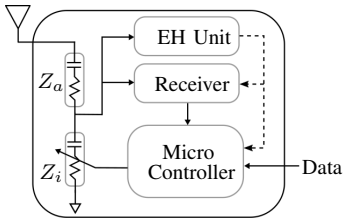

Fig. 3: Passive tag.

(Fig. 1 (c)) [3], [45]–[47]. These ambient transmitters' output power levels affect the tag's harvested energy level, which must exceed the sensitivity threshold of tags. However, regulations from governmental agencies such as the federal communications commission (FCC) limit the RF output power levels. For instance, effective radiated power (ERP) is $60\,\mathrm{dBm}$ in TV towers [48] and $36\,\mathrm{dBm}$ for cellular BSs [49].

This AmBC approach has several pros and cons. Using ambient RF sources rather than dedicated ones saves costs and energy, benefiting IoT networks. New spectrum allocations are unnecessary, avoiding licensing and regulatory hurdles. However, legacy signals can directly interfere with AmBC systems, limiting their performance. The reader's signal detection task is highly challenging because the critical parameters of ambient RF signals (e.g., power levels, phase, timing, and others) are unknown. Furthermore, such ambient signals can be unpredictable and uncontrollable. Finally, tag-reflected signals can interfere with legacy receivers [21], [50].

A. Passive Tags

We can categorize tags into two types: (i) Active or semi-passive tags and (ii) Passive tags. Active tags have both RF circuits and a battery. Semi-passive tags include a battery but no active RF modulation. Because of more power availability, such tags can communicate over longer distances than passive tags [51], [52]. Since we focus on passive tags only, we do not further discuss active and semi-passive tags.

A passive backscatter tag (Fig. 3) comprises a low-cost/power integrated circuit with limited processing capability, a passive backscatter modulator, and an RF energy harvester. It thus harvests RF energy and operates using direct current (DC) power derived from the RF signal from the dedicated/ambient RF sources. Many practical applications of passive tags are listed in [53], [54]. From the perspective of this survey, the tag's critical tasks are passive modulation and energy harvesting. We describe these next.

B. Passive Backscatter Modulation

Passive modulation is a process where the tag does not use an active circuit to map its data to an RF signal. Instead, the tag utilizes a set of load impedances. By switching among these, the tag can vary its signal reflection coefficient, which is given by [3]

$$\Gamma_i = \begin{cases} \sqrt{\alpha_i} q_{b,i} = \frac{Z_i - Z_a^\star}{Z_i + Z_a}, & i = 1, \ldots, \bar{M}, \\ 0, & i = 0, \end{cases} \tag{1}$$

where $0 < \alpha_i \leq 1$ is the fraction of power reflected at the tag and $q_{b,i}$ is the normalized backscatter symbol selected from a multi-level ($\bar{M}$-ary) modulation (i.e., $|q_{b,i}|^2 \leq 1$). Moreover, Z_i is the load impedance of state i, Z_a is the antenna impedance, and $(\cdot)^\star$ is the complex conjugate operator. When the load impedance perfectly matches to the antenna impedance, we have $Z_0 = Z_a^\star$. The reflection coefficient is then zero.

Based on (1), on-off keying (OOK) and binary phase-shift keying (PSK) modulation schemes, i.e., $\bar{M} = 2$, can be readily implemented [5]. Higher-order modulations are also possible, e.g., QPSK and 16-PSK [47], QPSK [55], [56], 16-quadrature amplitude modulation (QAM) [57], [58], 32-QAM [59].

To illustrate this process, we next show the design of a simple, passive modulator. It must generate a constellation of modulated symbols. The load impedance value Z_i must be chosen appropriately to design these constellation points. These values can be calculated from Γ_i or by utilizing the Smith chart [3], [60], [61]. From (1), for real-valued antenna impedance, i.e., $Z_a = R_a$, the load impedance Z_i can be calculated via

$$Z_i = \frac{1 + \Gamma_i}{1 - \Gamma_i} Z_a, \quad i = 1, \ldots, \bar{M}. \tag{2}$$

Normalizing the load impedance Z_i in (2), we have $z_i = Z_i / R_a = r_i + j x_i$, where r_i and x_i are can be readily derived from (2) [3, Section 3.4.1]. Note that normalized load impedance resistance, r_i, and reactance, x_i, can be obtained directly from the Smith chart [3]. Fig. 4 and Table V summarize the QPSK and 8-PSK backscatter modulator designs for $|\Gamma_i|^2 = 0.8, \forall\, i$. Similarly, the tag can implement higher-order modulations such as $\bar{M}$-QAM and $\bar{M}$-PSK [3]. We omit the details for brevity.

Frequency shift keying (FSK) modulation too is sometimes used for data communications. This modulation is widely

TABLE III: List of abbreviations.

Abbreviation	Definition	Abbreviation	Definition
3GPP	3rd Generation Partnership Project	**ML**	Maximum-Likelihood
3G/4G/5G/6G	Third/Forth/Fifth/Sixth-Generation	**mMTC**	Massive Machine-Type Communication
ACK	Acknowledgment	**MoBC**	Monostatic Backscatter Communication
AmBC	Ambient Backscatter Communication	**mOSTBC**	Modified Orthogonal Space-Time Block Code
AP	Access Point	**MPA**	Message Passing Algorithm
ARQ	Automatic Repeat-for-Request	**MTC**	Machine-Type Communication
AWGN	Additive White Gaussian Noise	**NAK**	Negative Acknowledgment
BackCom	Backscatter Communication	**NB-IoT**	Narrow-Band Internet of Thing
BCH	Bose-Chaudhuri-Hocquenghem	**NOMA**	Non-Orthogonal Multiple Access
BER	Bit Error Rate	**NR**	New Radio
BiBC	Bistatic Backscatter Communication	**NRZ**	Non-Return-to-Zero
BPSK	Binary Phase-Shift Keying	**OSD**	Ordered Statistics Decoding
BS	Base Station	**OSTBC**	Orthogonal Space-Time Block Code
BUTQ	Block-Level Unitary Query	**PDF**	Probability Density Function
CAGR	Compound Annual Growth Rate	**PEP**	Pairwise Error Probability
CBMA	Coded-Backscatter Multiple Access	**PLoRa**	Passive Long-Range
CDMA	Code Division Multiple Access	**PN**	Pseudo-Noise
CRC	Cyclic Redundancy Checks	**PSK**	Phase-Shift Keying
CSI	Channel State Information	**QAM**	Quadrature Amplitude Modulation
CSS	Chirp Spread Spectrum	**QoS**	Quality-of-Service
DC	Direct Current	**RF**	Radio Frequency
DPSK	Differential Binary Phase-Shift Keying	**RFID**	Radio Frequency Identification
EH	Energy Harvesting	**RM**	Reed-Muller
EPC	Electronic Product Code	**RS**	Reed-Solomon
ERP	Effective Radiated Power	**RZ**	Return-to-Zero
FDMA	Frequency-Division Multiple Access	**SC**	Successive Cancellation
FEC	Forward Error-Correction	**SCL**	Successive Cancellation List
FER	Frame Error Rate	**SCMA**	Sparse Code Multiple Access
FFT	Fast Fourier Transform	**SER**	Symbol Error Rate
FSA	Framed Slotted ALOHA	**SIC**	Successive Interference Cancellation
FSK	Frequency-Shift Keying	**SISO**	Single Input Single Output
GRAND	Guessing Random Additive Noise Decoding	**SNR**	Signal-to-Noise Ratio
GSM	Generalized Spatial Modulation	**STBC**	Space-Time Block Coding
HARQ	Hybrid Automatic Repeat-for-Request	**STC**	Space-Time Code
I/Q	In/Quadrature-phase	**STTC**	Space-Time Trellis Codes
i.i.d.	Independent Identical Distributed	**TDMA**	Time-Division Multiple-Access
IoT	Internet of Thing	**TV**	Television
LDPC	Low-Density Parity-Check	**UFQ**	Uniform Query
LDS	Low-Density Signature/Spreading	**UHF**	Ultra-High Frequency
LLR	Log-Likelihood Ratio	**UMTS**	Universal Mobile Telecommunications System
LTE	Long Term Evolution	**URLLC**	Ultra-Reliable Low Latency Communication
MAP	Maximum A-Posteriori	**UTQ**	Unitary Query
MIMO	Multiple-Input-Multiple-Output	**Wi-Fi**	Wireless Fidelity

adopted in BiBC which can also facilitate multiple access schemes [62], [63]. It is interesting to see how a passive tag can implement FSK and similar modulations, which is unlike the details mentioned above for constant-envelope modulations such as QPSK. For instance, to implement binary FSK, carrier signal frequency f_c is switched between two frequencies $f_i,\ i \in 1,2$, according to the bit values, $\{0,1\}$ [42], [63]–[66]. Specifically, the tag switches between two distinct reflection coefficient values, $\Gamma_i,\ i \in 1,2$, with different rates f_i for corresponding bits $\{0,1\}$, respectively. The waveforms, $u_i(t),\ i \in 1,2$ shows the fundamental frequency component of a 50% duty cycle square waveform of frequency f_i and random initial phase $\Phi_i \in [0, 2\pi)$, given as [63]

$$u_i(t) = u_0 + \frac{\Gamma_1 - \Gamma_2}{2}\frac{4}{\pi}\cos\left(2\pi f_i t + \Phi_i\right),\ i \in \{1,2\}, \quad (3)$$

where u_0 is a constant depending on the tag antenna structural mode and the tag reflection coefficients Γ_i [61].

A complete summary of BackCom modulation schemes, along with their performance, is provided in [3], [25].

C. Energy Harvesting

The other critical task of the tag is to harvest energy to power itself. The tag employs an EH circuit to convert RF to DC. The key parts of such systems are the antenna and rectifier circuit that allows the incident RF power to be converted into DC energy. For further details on EH circuits, we refer the reader to [41].

The EH unit is characterized by two key parameters: sensitivity and energy transfer efficiency, which significantly influence the tag's performance, range, and reliability. The sensitivity is the minimum power required to wake up the EH circuit. This activation threshold for commercial passive RFID tags is about $-20\,\mathrm{dBm}$ [53], [54]. On the other hand, the RF-to-DC conversion efficiency - the ratio of input power to output power - is determined by the performance of the receiving antenna, the impedance matching network between the antenna and the rectifying circuit, and the overall power conversion efficiency of the rectifier [67]–[70]. Practical EH units can output from $\sim 1\,\mu\mathrm{W}$ to $\sim 100\,\mu\mathrm{W}$ [41].

The EH unit operates one of the two modes [71]: (i) time-

TABLE IV: Notations

Notation	Definition	Notation	Definition
$\bar{M}$	Modulation order	$\mathbf{C}$	STC matrix
Z_a	Antenna impedance	c^a	space-time codeword
Z_i	Tag's load impedance	D_{in}	Interleaver depth
Γ_i	Tag's reflection coefficient	M, N	Transmit and receive antennas
$\alpha = \lvert\Gamma_i\rvert^2$	Fraction of power reflected at the tag	L	Tag's antennas
R	Coding gain	δ	Diversity gain
k, n	Information bit sequence and codeword length	μ	Rate gain
d_{min}	Hamming distance	q_b	Tag's signal
$\mathbf{d}, \mathbf{c}$	Information bits and codeword	p_h	Tag's harvested power
T	STC block length	η	EH circuit conversion efficiency

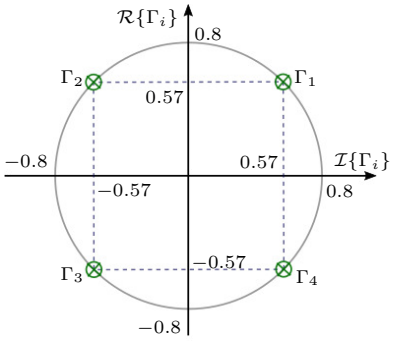

(a) QPSK

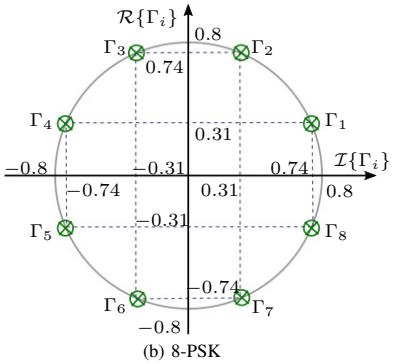

(b) 8-PSK

Fig. 4: Examples of QPSK and 8-PSK backscatter modulator designs.

TABLE V: Examples of QPSK and 8-PSK backscatter modulator designs.

Modulation scheme	Index	Γ_i	z_i (Ω)
QPSK	1	$0.57 + j0.57$	$0.69 + j2.24$
	2	$-0.57 + j0.57$	$0.13 + j0.41$
	3	$-0.57 - j0.57$	$0.13 - j0.41$
	4	$0.57 - j0.57$	$0.69 - j2.24$
8-PSK	1	$0.74 + j0.31$	$2.18 + j3.79$
	2	$0.31 + j0.74$	$0.35 + j1.45$
	3	$-0.31 + j0.74$	$0.16 + j0.65$
	4	$-0.74 + j0.31$	$0.11 + j0.20$
	5	$-0.74 - j0.31$	$0.11 - j0.20$
	6	$-0.31 - j0.74$	$0.16 - j0.65$
	7	$0.31 - j0.74$	$0.35 - j1.45$
	8	$0.74 - j0.31$	$2.18 - j3.79$

switching mode, where EH and data processing (e.g., information sending/decoding) operations occur in two distinct time slots, and (ii) power-splitting mode, where both operations occur simultaneously but each is allocated a fraction of the RF power captured by the antenna. However, for passive tags, the power-splitting mode is widely implemented [72]. To understand how it operates in this case, we consider the tag to use $\bar{M}$-ary modulation, (1). The power-splitting (PS) ratio can be variable or fixed. As mentioned earlier, the tag uses a set of impedance values to generate the signal constellation. When the tag load impedance matches the antenna impedance, i.e., $Z_i = Z_a$ for $i = 0$, resulting in $\Gamma_0 = 0$ and the absorption state. In this state, the tag completely harvests energy without reflecting the RF signal.

With a fixed PS ratio or $\bar{M}$-ary PSK, the reflection coefficients of all other impedance values have a constant magnitude, i.e., $|\Gamma_i|^2 = \alpha_i = \alpha$. Hence, the received power at the tag antenna, P_a, is split, and αP_a is used for data communication and the remaining $P_b = (1 - \alpha)P_a$ for EH. On the other hand, when the tag employs $\bar{M}$-ary ASK, the reflection coefficient depends on the data value, i.e., $|\Gamma_i|^2 = \alpha_i$, and hence the PS ratio varies. Therefore, the reflected power at the tag, i.e., $\alpha_i P_a$, changes accordingly. Then, the rest, i.e., $P_b = (1-\alpha_i)P_a$, is used for EH. Regardless of the modulation scheme, the EH rectifier converts the incident RF power to a DC voltage to power the tag.

To model an EH circuit and quantify the amount of harvested power, the linear EH model is convenient and analytically tractable. As the name implies, it suggests that the harvested power is given by $P_h = \eta P_b$, where $0 < \eta \leq 1$ is the power conversion efficiency (PCE). However, energy harvesters comprise nonlinear components (e.g., diodes, resistors, capacitors) and the output power is a nonlinear function of the input power; that is (i) high input powers cause a saturation plateau, (ii) the output of the EH circuit drops to zero if the input RF is below the sensitivity level. Thus, the linear model does not represent these key nonlinear properties. Thus, several nonlinear EH models may more accurately model practical EH circuits, including a piece-wise linear function [73], a rational function [74], a polynomial function [75], a sigmoid function [76], or an improved sigmoid function [77], and a nonlinear model based on error function [78].

Another EH parameter is the activation threshold. The system needs RF signals that "wake up" tags – the activation process. Thus, the activation threshold is the minimum of incident RF power to wake up a tag. It is around -20 dBm for some tags, but values even below -20 dBm are highly desirable. Thus, decreasing the activation threshold and also improving the PCE are desirable [79], i.e., low activation thresholds enable the tag to harvest power at low input powers, and high PCE ensures that more DC power is available to the tag for coding, modulation, and other operations.

Overall, the EH process yields only a limited amount of

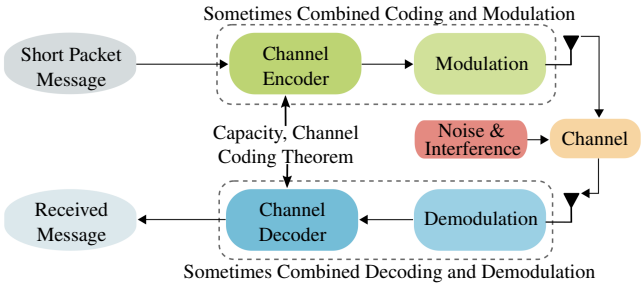

Fig. 5: A general framework for digital communication.

power to the tag, e.g., $5\,\mu$W harvested power in $1.8\,$GHz to $2.5\,$GHz using crossed dipole antenna and full-wave rectifier [80]. Thus, passive tags are power limited, a fact that has great ramifications for the choice of codes.

III. Basics of Coding

This section provides a brief background on channel coding, decoding, and code design guidelines.

Fig. 5 represents a general digital communication link to transport data packets. The channel encoder and modulator are the key components of the transmitter side. The channel encoder maps data bits to coded bits based on the channel code. We will discuss popular channel codes in Section V. The modulator maps the code bits to complex or real symbols to create the transmitted signal. For brevity, we do not discuss this process here. As the transmitted signal travels through the channel, noise, interference, and other impairments can occur. Thus, the receiver gets a distorted version of it. The receiver then maps it back to data bits. To do that, the receiver eliminates the effects of noise, interference, channel fading, and others. As this process is not perfect, the decoded bits may contain some errors. Channel codes will help detect and correct those bit errors and thus will significantly improve system performance.

The encoder adds extra bits (parity bits) to the original data bits (Fig. 5). These parity bits are computed according to the channel code. The original data bits and parity bits together form codewords. Each codeword is then mapped to a sequence of symbols that are sent through the channel. The decoder performs the reverse operation of the encoder, and it detects and/or corrects errors during transmission. As per Fig. 5, demodulation and decoding may be combined to extract data from the received signal.

Channel capacity is a tight upper bound on the reliable information transfer rate over the channel. This concept has been central to the development of modern wired and wireless communication systems, and the advent of novel error correction codes achieves performance close to the channel capacity [81]. A rigorous statement of this notion is expressed by the following theorem.

Theorem 1. ***Shannon's Noisy Channel Coding Theorem****: If the rate of transmission R is less than the channel capacity, for any given probability of error P_e, there exists length n_0 such that codes of length n exceeding n_0 can decode with a probability of error less than P_e.*

Theorem 1 suggests that an arbitrarily low error probability is achievable if a sufficiently long code is employed for information rates less than capacity [81, Section 1.12.7]. This theorem guarantees that such codes exist but does not tell how to find them. Nevertheless, practical codes have been discovered with low-complexity decoding and high error-correcting capabilities. Before discussing them, we define some basic terms.

A. Channel Coding Design Criteria

These depend on the characteristics of the channel and the QoS parameters. Before describing those, we first introduce some relevant coding parameters.

- *Hamming Distance*: It is the number of bit differences between two codewords $\mathbf{v} = (v_1, v_2, \ldots, v_n)$ and $\mathbf{w} = (w_1, w_2, \ldots, w_n)$, both of length n, i.e.,
$$d_H(\mathbf{v}, \mathbf{w}) = |\{i | v_i \neq w_i, i = 1, \cdots, n\}|, \tag{4}$$
where $|A|$ is the number of elements in set A. Hamming distance is useful for the characterization of the error detection and error correction capabilities of a code. The minimum Hamming distance between any two distinct codewords of a code is denoted by d_{min}. A code with minimum Hamming distance d_{min} can detect up to $(d_{min} - 1)$ errors and can correct up to $(d_{min} - 1)/2$ errors [82].
- *Coding Gain*: This is the signal-to-noise ratio (SNR) difference required between uncoded and coded systems to achieve the same probability of error [81]. Coding gain is expressed in dB units. A tradeoff exists between coding gain and complexity; long codes can provide larger coding gains at the cost of increased decoding complexity.
- *Code Rate*: It is the ratio of the number of data bits (k) to the total number of bits (n) in each codeword. Thus, the code rate $R = k/n$. As $R \to 0$, the ability to correct and/or detect errors increases. However, since the added $(n - k)$ bits do not carry information, physical resources such as bandwidth and power expended to transmit them constitute an inefficiency.

The minimum Hamming distance, d_{min}, determines the error correction/detection capability of a coding scheme. Consequently, maximizing d_{min} helps to minimize the probability of errors. This is done by generating sets of symbol sequences having larger distances than with uncoded sequences, while not sacrificing data rate or increasing system bandwidth. To that end, the standard channel code design criterion is to maximize d_{min} among the set of all possible codewords. However, for the non-fading, additive white Gaussian noise (AWGN) channel, the minimum Euclidean distance among all possible codeword pairs is the design criterion.

Other factors also affect the design of channel coding schemes (Fig. 6). Hence, designing a coding scheme for a particular channel involves many design trade-offs. For example, an optimized code may achieve a lower BER or better coding gain, but it may increase decoding complexity and transmission delay or reduce the throughput [83]–[85]. Therefore, design trade-offs must be carefully considered.

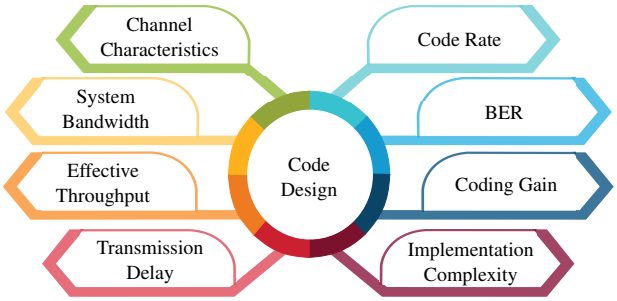

Fig. 6: Design parameters for channel codes.

B. Encoding and Decoding Processes

As per Fig. 5, channel encoder adds redundant bits to its input bits $\mathbf{d} = (d_1, \cdots, d_k)$ and generates a codeword $\mathbf{c} = (c_1, \cdots, c_n), n \geq k$. The transmitter maps the codeword to a signal sent through the channel. The demodulator converts the channel output into a sequence of symbols to be fed to the decoder. These decisions may be "hard" (e.g., a particular bit is 0 or 1), or "soft" (e.g., the likelihood of a particular bit being 0 or 1). The decoder exploits the code's redundancy to correct/detect the bit errors.

To decode the data and estimate the transmitted bits $\mathbf{d}$ (embedded in codeword $\mathbf{c}$), the decoder processes the output of the channel, $\mathbf{y}$. The channel is specified by the conditional probability distribution $P(\mathbf{y}|\mathbf{c})$ given that $\mathbf{c}$ was transmitted. This distribution $P(\mathbf{y}|\mathbf{c})$ is called the likelihood function.

An optimal detector minimizes the probability of error P_e for $\mathbf{c}$, i.e., [81], [86]

$$P_{e,min} = \min P(\mathbf{c} \neq \hat{\mathbf{c}}), \tag{5}$$

where $\hat{\mathbf{c}}$ is the codeword output by the decoder. A popular choice is the maximum likelihood (ML) rule.

Theorem 2. *Let $\mathcal{C}$ be the collection of all codewords, i.e., $\mathcal{C} = \{\mathbf{c}_1, \cdots, \mathbf{c}_m\}$. The ML decoder outputs the most probable codeword by maximizing $P(\mathbf{y}|\mathbf{c}_j)$[1], i.e.,*

$$\hat{\mathbf{c}} = \max_{\mathbf{c}_j \in \mathcal{C}} P(\mathbf{y}|\mathbf{c}_j). \tag{6}$$

The ML rule minimizes the error probability when all codewords are equally likely. Otherwise, the maximum a posteriori (MAP) rule may be used, which maximizes $P(\mathbf{c}|\mathbf{y}) \propto P(\mathbf{y}|\mathbf{c})P(\mathbf{c})$, with prior probabilities $P(\mathbf{c})$.

Decoders can be iterative or non-iterative types. The latter includes syndrome decoding, nearest-distance decoding, algebraic decoding for Reed-Solomon (RS) and Bose-Chaudhuri-Hocquenghem (BCH) codes, and viterbi decoding for convolutional codes [87]. Turbo decoding with component MAP decoders for each component [88], [89], the sum-product algorithm and min-sum decoding for LDPC codes [90], [91], are among the iterative decoding algorithms (see Section V-C).

These algorithms can be hard-decision and soft-decision decoders [81]. The former makes a final decision on the most likely codeword, while the latter gives soft information in the form of probabilities or log-likelihood ratios (LLRs)[2], on each bit of the codeword. On the other hand, all iterative decoding algorithms use soft-decision algorithms.

C. Error Control Methods

Channel impairments such as noise and interference cause bit errors in transmit data packets and thus significantly impact system performance. Thus, many error control techniques have been developed, which can be classified into [92]: (i) automatic repeat-for-request (ARQ) and (ii) forward error-correction (FEC).

1) ARQ Schemes: ARQ is an error control strategy based on the idea that if a received codeword contains bit errors, the receiver can request that the sender retransmit the codeword several times until it is received without errors. Thus, the receiver must be able to detect the presence of errors in the received codeword. A channel code can enable this task. Commonly, a cyclic redundancy check (CRC) code[3] is used to encode the message bits prior to transmission. The receiver uses the code to detect the presence of bit errors. If bit errors are detected, the receiver asks for retransmissions. We can generally classify these schemes into (i) stop-and-wait ARQ, (ii) go-back-N ARQ, (iii) selective-repeat ARQ, and (iv) incremental-redundancy ARQ.

In stop-and-wait ARQ, the sender transmits a codeword and waits for the receiver to respond with an ACK or negative acknowledgment (NAK) signal. If an ACK is received, the sender transmits a new codeword; otherwise, it retransmits the same one. This strategy is inefficient because the sender must idle for an ACK or NAK signal. The go-back-N strategy eliminates this idle waiting time by letting the sender transmit codewords continuously while waiting for ACK or NAK signals. If a NAK is received for a particular codeword, the sender retransmits that codeword and the $(N-1)$ subsequent codewords during the round-trip delay. This helps in the preservation of codeword ordering at the receiver.

Like go-back-N ARQ, in selective-repeat ARQ, the sender continuously transmits codewords. However, the sender retransmits the codeword corresponding to the NAK. The codewords contain headers used for identification and re-ordering at the receiver. This method has a greater throughput than the go-back-N ARQ because only one codeword is retransmitted, instead of N. However, additional buffer space is needed at the receiver to allow for block re-ordering.

In incremental-redundancy ARQ, when the transmitter receives a NAK message, it sends additional bits to the receiver. The decoder employs those extra bits and the received codeword to recover the original data. The process is repeated until

[1] In (6), $\mathcal{C}$ can be considered as the set of transmitted signal vectors induced by the chosen channel code and modulation.

[2] The LLR for a bit $b \in \{0, 1\}$ is defined as $\text{LLR}(b) = \log(p(b=0)/p(b=1))$ [81].

[3] It is a type of linear block code (cyclic codes - Section V-C), which is mainly used for error detection purposes. It is defined by a unique monic generator polynomial $g(x)$ of degree $n-k$; an (n, k) CRC code appends $n-k$ checksum bits to k message bits. It can detect (i) error bursts with length up to $n-k$, (ii) any combination of $d_{min}-1$ errors, and (iii) any error pattern with an odd weight if $g(x)$ has an even number of nonzero coefficients [93]. For a wide set of configurations, [94], [95] list optimal CRC generator polynomials. In 5G NR systems, 16-bit CRC (CRC-16) and 24-bit CRC (CRC-24) are specified for downlink transmission [29].

the data is retrieved or declared lost. More details of ARQ schemes can be found [92].

2) FEC Codes: FEC algorithms add an extra number of coded bits (e.g., parity bits) to data bits, allowing the receiver to detect and correct errors without ARQ [96]. Various FEC codes have been developed throughout the evolution of modern communication networks and standards. However, linear codes are widely used due to simpler encoding and decoding processes (Table I). They can be *block codes* or *convolutional codes* which are briefly described below.

- *Linear block codes*: A (n, k, d_{min}) linear block code $\mathcal{C}$, with the code rate $R = k/n$, transforms a message of k bits into a codeword of $n > k$ bits by adding $n - k$ redundant parity bits, and d_{min} is the minimum Hamming distance of the code, which determines the error detecting and correcting capability [81]. Linearity implies that the sum of two codewords is another codeword, and the all-zeros word is a valid codeword. Thus, the minimum Hamming distance d_{min} is the smallest weight of the nonzero codewords in the code. The codewords are generated according to

$$\mathbf{c} = \mathbf{dG}, \tag{7}$$

  where $\mathbf{c} \in \mathcal{C}$ is the codeword for message $\mathbf{d}$, and $\mathbf{G}$ is the $k \times n$ generator matrix, all with entries from $\{0, 1\}$. To perform error detection, one uses $(n-k)\times n$ binary parity check matrix $\mathbf{H}$ such that, $\mathbf{HG}^{\mathrm{T}} = \mathbf{0}$, or equivalently $\mathbf{cH}^{\mathrm{T}} = \mathbf{0}$, where $(\cdot)^{\mathrm{T}}$ is the transpose operator. The $\mathbf{H}$ matrix lists the parity-check equations that each codeword must satisfy. Therefore, a linear block code is uniquely specified by $\mathbf{G}$ or $\mathbf{H}$.
  Perhaps the most well-known linear block codes are *Hamming codes*, characterized by $m = n - k$ and $n = 2^m - 1$, for any positive integers $m \geq 3$. They have $d_{min} = 3$ and can correct single-bit errors only or detect up to two-bit errors. BCH, RS, Polar, and LDPC codes are other ones for conventional communication systems and BackCom (Section V-C).
  Encoding any linear block code requires the multiplication of $\mathbf{G}$ by $\mathbf{d}$, (7). This entails k multiplications and $k - 1$ additions for each coded bit. Nevertheless, for a systematic code, the first k bits are simply the message bits. However, each of the remaining $n-k$ parity bits requires $\mathcal{O}(k)$ operations. Thus, the overall encoding complexity is $\mathcal{O}(nk)$ [81].
- *Convolutional Codes*: These operate on a continuous stream of bits. The structure of the generator matrix of such codes makes the encoding operation a form of filtering - or convolution. For an (n, k, K) convolutional code, at each time step, k bits are shifted through a set of K registers and n new bits are produced by performing a convolution, in modulo-2 arithmetic, of the data stored in the registers, leading to the code rate $R = k/n$ [81], [92]. The integer K is called constraint length, i.e., encoder memory; the output is a function of the current input and the previous $K - 1$ inputs. The memory must be large enough to increase the minimum distances and reduce error probabilities, but complexity increases exponentially with K [92].
  There are several decoders for convolutional codes. The Viterbi algorithm is the most commonly used one based on the trellis diagram of the code [87]. It can be either hard-decision or soft-decision, with a $2\,\mathrm{dB}$ gain for the latter [97].
  Turbo codes are a class of convolutional codes adopted by the 3G universal mobile telecommunications system (UMTS) [27] and 4G LTE mobile standards, and 4G NB-IoT standard [28], [98]. A turbo encoder concatenates two parallel convolutional encoders, which are separated by an interleaver [89]. It accepts a data block of k bits and rearranges the order of the bits based on a predetermined interleaving pattern. Thus, each convolutional encoder produces a k-bit parity block which is then concatenated together with a third replica of the data block, to generate a n-bit encoded block.

On the other hand, a hybrid ARQ scheme (HARQ) leverages a combination of FEC and ARQ to ensure the reliable and robust delivery of data packets. HARQ offers significant advantages over ARQ schemes for relatively large packet lengths and for high noise and/or interference levels [99]. To this end, CRC is used with the adopted channel codes in different wireless standards, e.g., 3G UMTS [27], 4G LTE mobile standards, 4G NB-IoT standard [28], [98] and 5G and 5G NR [29], [30] (see Table I).

D. Interplay Between Coding & Modulation

The channel's expected noise primarily determines the selection of channel code and the modulator design, interference, and distortion characteristics [100]. Cooperation between channel coding/decoding and modulation/demodulation can greatly improve efficiency. For example, when a channel imposes severe bandwidth limitation, modulation methods that use spectral spectrum shaping techniques to minimize distortion and simplify decoding are preferred [101, Chapter 6]. Otherwise, design options may be used that lowered the required SNR ratio for greater bandwidth occupancy.

Channel coding always forces the system to use a larger constellation to keep the same data rate as an uncoded system [102]. Going to a larger constellation reduces the distance between the symbols, which implies a higher BER at the output of the demodulator. However, the BER is significantly reduced at the channel decoder output. For instance, compared to uncoded QPSK, coded 8-PSK with a trellis code of rate two lowers the SNR to achieve a given BER. Specifically, this reduction amounts to a $3.3\,\mathrm{dB}$ coding gain at a BER of 10^{-5} [103].

To reduce the BER, the code rate can be lowered, which increases the code's redundancy at the cost of bandwidth expansion. Trellis Coded Modulation (TCM), however, can improve the reliability of a digital link without bandwidth expansion or reduction of data rate. It treats the coding and the modulation as one operation [104]. TCM includes a $k/(k+1)$-rate convolutional coder and $\bar{M}$-QAM/$\bar{M}$-PSK modulator. The decoding process then uses a Viterbi decoder with a soft metric

- the Euclidian distance from the constellation point. One of the first commercial applications of TCM was high-speed telephone modems that use substantial constellation sizes to reach data rates up 33 kbits/s over the telephone line [102].

Adapting the modulation and coding rate to the channel fading can also increase average throughput, reduce the required transmit power, or reduce the average probability of bit error by taking advantage of favorable channel conditions to send at higher data rates or lower power – and by reducing the data rate or increasing power as the channel degrades [105]. Adaptive modulation and coding use the CSI to determine the order of the modulation and the coding scheme. In LTE and 5G-NR [106], radio link quality is estimated based on channel quality indicator (CQI), which is reported by the user equipment and measured based on the cell-specific reference signal and channel state information reference signal in LTE and 5G-NR, respectively [107], [108]. The better the radio conditions, the higher CQI and the higher the coding rate. Modulation and coding rate is thus determined to maintain the error probability, not more than 10%.

E. Antenna Effects on Coding

Besides coding, multiple transmit/receive antennas can provide diversity (δ) and multiplexing (rate) gains (μ) [109]. These are functions of the number of transmit and receive antennas M and N, respectively. MIMO creates multiple spatial channels by exploiting rich-scattering channels. For instance, when compared to single input single output (SISO), (M, N) MIMO can increase the data rate by a factor of $\min(M, N)$ [109]. The latter is obtained by exploiting the independent fading gains affecting the same signal, i.e., the number of independent paths traversed by each signal, which has a maximum value of MN [109]. Between these two gains, there is a fundamental trade-off: for example, maximum rate gain, attained by simultaneously sending independent signals, has no diversity gain, whereas maximum diversity gain, attained by simultaneously sending the same signal from all antennas, has no rate gain [109]. This curve depicts the maximum achievable diversity gain, $\delta^*(\mu)$, as a function of μ. For example, the piecewise-linear function connecting the points $(i, \delta^*(i))$ denotes the trade-off curve for a code with block length $T \geq M + N - 1$, where $i \in \{0, 1, \ldots, \min(M, N)\}$ and $\delta^*(i) \triangleq (M - i)(N - i)$ (Section V-D) [109].

Fig. 7 depicts the diversity-rate trade-off for $M = 8$ and $N = 4$. We observe that the maximum values for μ and δ are $\min(M, N)$ and MN, respectively. It also demonstrates that the maximum diversity gain is only possible with zero-rate gain, and the maximum rate gain is only possible with zero-diversity gain.

Given a specific antenna configuration and those gain trade-offs of MIMO, the challenge is to design codes that achieve high rates, high diversity orders, and low decoding complexity. To do this, space-time block codes (STBCs), space-time trellis codes (STTCs), and layered STCs, which use the degrees of freedom in both space and time, have been developed [109]. We discuss these in more detail in Section V-D.

The number, M, of transmit antennas significantly impacts space-time code designs. For $M = 2$, the Alamouti code

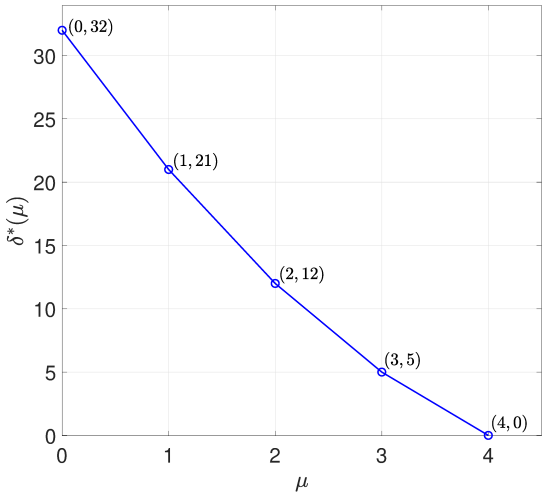

Fig. 7: Diversity-rate trade-off for (8,4) MIMO channel.

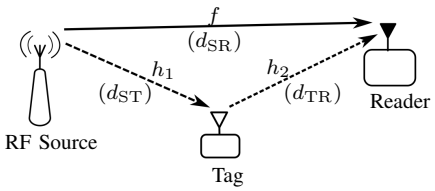

Fig. 8: A single-antenna BackCom setup. We will refer to the source-to-tag, tag-to-reader, and source-to-reader channels as forward, backscatter, and direct channels, respectively.

provides full diversity at the full data rate (one data symbol per channel use). However, for $M > 2$, no complex valued STBCs with full diversity and full data rate exist [109].

A subset of transmit antennas can be selected on demand to form spatial modulation (SM) [110] to increase the coding gain for low decoding complexity [111]. In SM, the transmit antenna on/off status provides an additional dimension to send bits, and therefore both STBC symbols and antenna indices convey information, increasing the rate. We discuss the resulting BER and spectral efficiency in BackCom systems (Section VI-C). Additionally, Multiple receive antennas (N) also leverage power gain, and receive diversity gain to increase the received power and enhance signal detection, thereby improving the BER and communication range (Section VI-C) [112]–[114].

IV. BackCom Channels and Characteristics

This section discusses these and provides the simulations of the capacity and BER. We also quantify the performance gains due to using channel codes in BackCom. These are transmit power reductions, rate gains, and communication distance improvements.

A. Single-Antenna Nodes

For simplicity, we start with single-antenna nodes (Fig. 8). The reader receives the data signal via the tag-to-reader, h_2, (backscatter) and the RF source-to-tag, h_1, (forward) channels. This gives rise to three different cases of the effective channel coefficient seen by the reader:

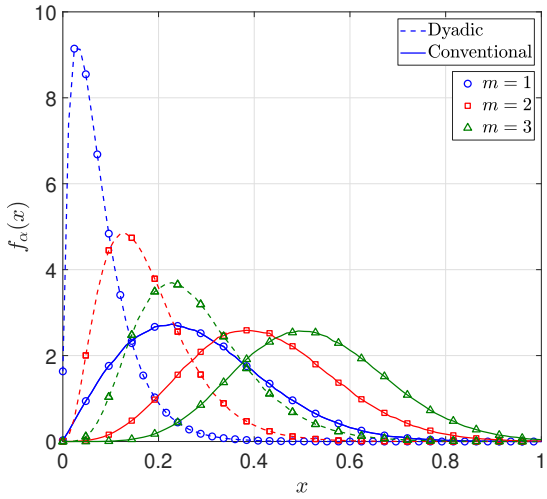

Fig. 9: A comparison of $(1,1,1)$ dyadic PDF and conventional $(1,1)$ channel PDF. For the dyadic channel, both $|h_1|$ and $|h_2|$ have the same m, which is their Nakagami-m parameter.

1) It is $h_1 h_2$ for AmBC,
2) It is h_1^2 for MoBC because of the co-located RF source and the receiver,
3) It is $h_1 h_2$ for AmBC because of the dislocated RF source and the receiver.

Such channels form a product or dyadic channel, i.e., the product of the forward link and backscatter link. It has the following properties: (i) if the forward and backscatter channels are frequency selective, the product channel will be the convolution of the two channel responses. Convolution results in a longer channel impulse response and dispersed peaks [26], (ii) correlation between h_1 and h_2 for closely spaced or co-located transmitter and reader antennas degrades the overall channel [34], [115], [116], and (iii) the statistics of the worst of h_1 and h_2 dominates the statistics of the BackCom channel [117]. These unusual characteristics will play a key role in the performance of BackCom systems and thus be considered in code designs.

Generally, the overall statistics of a dyadic channel are drastically different from a one-way channel, resulting in deeper and more frequent small-scale fading [26]. To see this, in Fig. 9, we plot the envelope probability density function (PDF) of the single-antenna dyadic channel for different Nakagami-m factors[4]. The conventional Nakagami-m channel PDFs are also plotted for comparison. Independent forward and backscatter links are assumed while each PDF has been normalized to unit power, i.e., $\mathbb{E}\{\alpha^2\} = 1$, where α is $|h_1|$ or $|h_2|$.

To quantify the deeper fading of the dyadic channel, we use the coefficient of variation (c_v), which measures the dispersion of a random variable. The c_v of X is defined as the ratio between the mean and the standard deviation of X. For wireless channels, high c_v values of α show deeper fading and vice versa. Hence, a low c_v tends to avoid deeper fading.

[4]The parameter m can model a myriad of channel fading conditions. For instance, $m = 1$ models Rayleigh fading, $m > 1$ models less severe fading, including Rician channels ($m \approx (K_r+1)^2/(2K_r+1)$, where K_r is the Ricean factor), and $m \to \infty$ gives an AWGN channel [118].

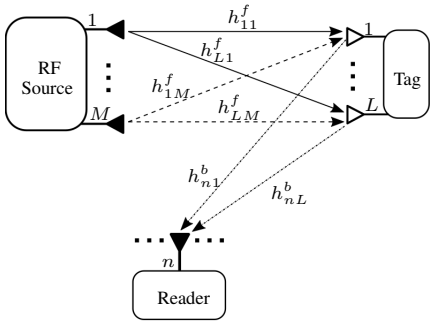

Fig. 10: A general multi-antenna BackCom setup. The forward and backscatter channels are $\mathbf{H}^f = [h^f_{11},\ldots,h^f_{L1};\ldots;h^f_{1M},\ldots,h^f_{LM}] \in \mathbb{C}^{M\times L}$ and $\mathbf{H}_b = [h^b_{11},\ldots,h^b_{N1};\ldots;h^b_{1L},\ldots,h^b_{NL}] \in \mathbb{C}^{L\times N}$, respectively.

Table VI lists it for the dyadic backscatter and conventional channels (Fig. 9). It clearly reveals the deeper fading effects of the dyadic channel, leading to outages and higher error rates.

The diversity order measures how many independent copies of the transmitted signal are available at the receiver. These copies are created by means of multiple time and/or space channels by using multiple antennas at the transmitter and/or receiver sides. Diversity gains help to overcome the effects of fading [105]. Performance analysis techniques can also be developed based on conventional analysis methods [119], [120]. The diversity order of a conventional $(1,1)$ Nakagami-m channel is m, whereas a $(1,1,1)$ dyadic channel has the diversity order of $\min(m_1, m_2)$. Thus, the statistics of the worst of forward and backscatter channels dominate the BackCom link performance [117].

B. Multiple-Antenna Nodes

With M-RF source, L-tag, and N-receiver antennas, the dyadic channel is described by the tuple (M, L, N) (Fig. 10). The so-called pinhole effect can be observed in this dyadic channel. The pinhole concept arises in conventional MIMO channels. The ratio between the MIMO channel capacity and that of the SISO channel is equal to r, which is the rank of the MIMO channel matrix. Under rich-scattering channels, r is the smaller number of M and N. Essentially, r is the multiplexing or rate gain described earlier (Section III-E). However, due to spatial correlation, the rank can collapse to one, which is the pinhole or keyhole effect. This effect can also be observed in BackCom networks.

Each tag antenna behaves as a pinhole, i.e., it collects all incoming multipath components and reflects them to the reader (Fig. 10). Thus, the propagation paths converge at the tag. Such channels are also known as keyhole, dyadic, or double-fading channels [115], [116], [121]. The pinhole channel shows severe small-scale fading even under the line-of-sight conditions [65]. The link envelope (received signal envelope) correlation can occur between propagation paths that terminate or originate on the tag antenna [34], [115].

However, multiple tag antennas provide additional statistically independent pinhole diversity. Therefore, multiple-antenna tags will create pinhole diversity gain, which in turn enhances the BER performance [116].

TABLE VI: The coefficient of variation of α.

c_v	$m=1$	$m=2$	$m=3$
Dyadic	78.7 %	53.0 %	42.5 %
Conventional	52.3 %	36.3 %	29.4 %

We next study different practical BackCom setups in terms of capacity and BER.

C. Performance Evaluation of BackCom

As before, we consider an RF source (carrier emitter), a backscatter tag, and a receiver (reader) (Fig. 8). For the AmBC setup, the carrier signal is an ambient modulated RF signal for a typical legacy transmission (primary user), while for BiBC and MoBC systems, the carrier signal is a dedicated ummodulated RF signal. In fact, MoBC systems utilize a co-located RF source and receiver.

For the system (Fig. 8), the RF source transmits the RF signal s, where $\mathbb{E}[|s|^2]=1$, and both reader and tag receive it. The tag harvests energy from the RF signal and reflects it with its signal q_b to the reader. We assume that, the direct channel f and the forward and backscatter channels are modeled as $v=\zeta_v^{1/2}\tilde{v}$, where $v=\{f,h_1,h_2\}$, $\tilde{v}\sim\mathcal{CN}(0,1)$ captures the quasi-static Rayleigh fading, and ζ_v accounts for path-loss, which is modeled via free-space path-loss model [122]. Moreover, we assume a constant tag reflection coefficient, i.e., $|\Gamma_i|^2=\alpha$ in (1). The received signal at the reader is then

$$y_R=\sqrt{P_t}fs+\sqrt{P_t}\sqrt{\alpha}h_2h_1sq_b+w_R, \tag{8}$$

where the first term, $\sqrt{P_t}fs$, is the direct link signal, the second term, $\sqrt{P_t}\sqrt{\alpha}h_2h_1sq_b$, is the backscattered signal, and w_R is the AWGN noise at the reader having zero mean and variance σ_w^2, i.e., $w_R\sim\mathcal{CN}(0,\sigma_w^2)$. Besides, P_t is the transmit power at the RF source. Note that, for the MoBC setup, both the tag-terminated channel (h_1) and tag-originated channel (h_2) are equal, $h_1=h_2$.

For a typical AmBC setup, as in the other two setups, the reader decodes with successive interference cancellation (SIC)[5], i.e., $T_b=N_sT_s$ where T_b is the tag's symbol duration, T_s is the primary symbol duration, and $N_s\geq 1$ is an integer. The received signal after SIC is thus given as

$$\hat{\mathbf{y}}_R=\sqrt{P_t}f(\mathbf{s}-\hat{\mathbf{s}})+\sqrt{P_t}\sqrt{\alpha}h_2h_1\mathbf{s}q_b+\mathbf{w}_R, \tag{9}$$

where $\hat{\mathbf{y}}_R\in\mathbb{C}^{N_s\times 1}$ is the received signal vector after SIC, in the tag's symbol duration. In (9), the first term is the residual interference due to the imperfect SIC, where $\mathbf{s}\in\mathbb{C}^{N_s\times 1}$ is the modulated RF signal vector and $\hat{\mathbf{s}}\in\mathbb{C}^{N_s\times 1}$ is the estimates of $\mathbf{s}$, i.e., $\mathbf{s}=\rho\hat{\mathbf{s}}+\mathbf{e}$, where $\mathbf{e}\in\mathbb{C}^{N_s\times 1}$ is the estimation error, i.e., $\mathbf{e}\sim\mathcal{CN}(\mathbf{0},\sigma_e^2/[1+\sigma_e^2]\mathbf{I})$, statically independent of the $\hat{\mathbf{s}}$, and $\rho=1/\sqrt{1+\sigma_e^2}$ $(0\leq\rho\leq 1)$, determines the quality of the estimation [123]. Besides, $\mathbf{w}_R\in\mathbb{C}^{N_s\times 1}$ is the noise vector.

[5]For a passive IoT network of tags coexisting with a primary network, the reader can be considered as a common receiver that decodes the signals of both the ambient RF source (primary) and the backscatter tag [46]., i.e., assuming perfect CSI, it first decodes the direct link legacy signal (primary), subtracts it from the received signal y_R to decode the backscatter data. The direct link signal is typically much stronger than the backscatter link signal. It is therefore reasonable to assume that the rate of the backscatter tag is equal or lower than the rate of the primary transmission.

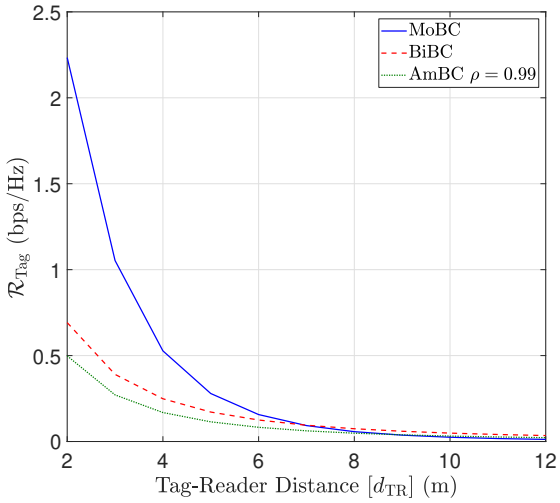

Fig. 11: The achievable rate as a function of tag-reader distance for $d_{\text{ST}}=5\,\text{m}$, $d_{\text{SR}}=7\,\text{m}$, $\alpha=0.9$ and $P_t=10\,\text{dBm}$. For MoBC setup, $d_{\text{ST}}=d_{\text{SR}}$ and $d_{\text{SR}}=0\,\text{m}$.

The channel capacity of the AmBC system is the maximum of the mutual information between input and output:

$$C_{\text{Tag}}=\max_{P(q_b)} I(q_b;\hat{\mathbf{y}}_R) \tag{10}$$

Thereby, the average achievable backscatter rate can be given as[6]

$$\mathcal{R}_{\text{Tag}}=\frac{1}{N_s}\mathbb{E}\left[\log_2\left(1+\frac{\alpha P_t\|\mathbf{s}\|^2|h_2h_1|^2}{P_t\|\mathbf{s}-\hat{\mathbf{s}}\|^2|f|^2+\sigma_w^2}\right)\right]. \tag{11}$$

Next, we consider both the tag and the primary transmissions have the same symbol rate, i.e., $N_s=1$, and provide simulations to evaluate the achievable rate[7] and BER. Moreover, AWGN variance is $\sigma_w^2=10\log_{10}(N_0BN_f)$ dBm, where $N_0=-174\,\text{dBm/Hz}$, $B=10\,\text{MHz}$ is the bandwidth, and $N_f=10\,\text{dB}$ is the noise figure.

Fig. 11 depicts the average achievable bacscatter rate as a function of the tag-reader distance (d_{SR}) for different BackCom setups. As observed, due to backscattering and the dyadic path-losses, the achieved rate is low. As the tag-reader distance increases, the achieved rate decreases. For the AmBC setup, the tag achieves the rates of $0.5\,\text{bps/Hz}$ and $0.2\,\text{bps/Hz}$ for $d_{\text{SR}}=2\,\text{m}$ and $d_{\text{SR}}=4\,\text{m}$, respectively.

Fig. 12 plots the average achievable rate trade-off between the primary and the backscatter transmissions as a function of the tag reflection coefficient (α). As α approaches zero, the primary achievable rate reaches a maximum, whereas the backscatter achievable rate becomes infinitesimal since the tag

[6]When the tag's rate is lower than the primary rate, the primary signal can be viewed as a spread-spectrum code. Thus, with perfect SIC, the SNR for decoding tag's symbol increased by N_s times at the cost of symbol rate decreased by $1/N_s$ [46].

[7]For $N_s=1$, the tag's signal interferes with the primary signal and the average achievable primary rate can be computed as $\mathcal{R}_{\text{Primary}}=\mathbb{E}\left[\log_2\left(1+\frac{P_t|f|^2}{\alpha P_t|h_2h_1|^2+\sigma_w^2}\right)\right]$. This is only applicable to AmBC systems, as dedicated RF signals used in MoBC and BiBC are unmodulated.

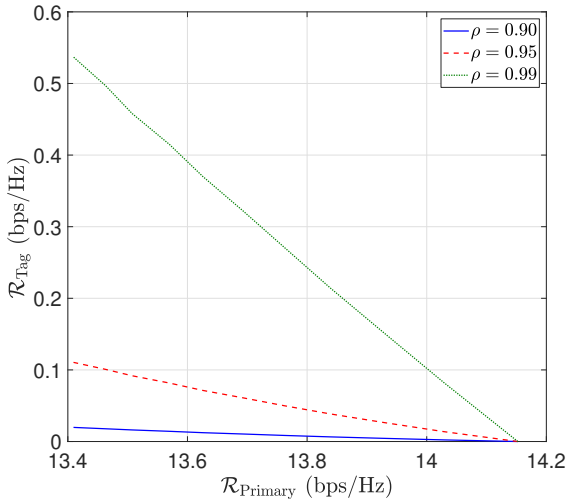

Fig. 12: The primary rate versus the tag rate as a function of the reflection coefficient (α) for $d_{\text{ST}} = 5\,\text{m}$, $d_{\text{TR}} = 2\,\text{m}$, $d_{\text{SR}} = 7\,\text{m}$, and $P_t = 10\,\text{dBm}$.

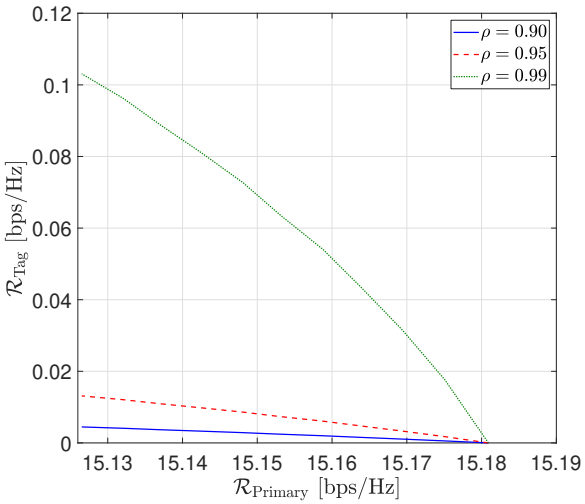

Fig. 13: The achievable primary rate versus the achievable rate of the tag as a function of the AmBC tag reflection coefficient (α) for $N_s = 5$, $d_{\text{ST}} = 5\,\text{m}$, $d_{\text{TR}} = 2\,\text{m}$, $d_{\text{SR}} = 7\,\text{m}$, and $P_t = 10\,\text{dBm}$.

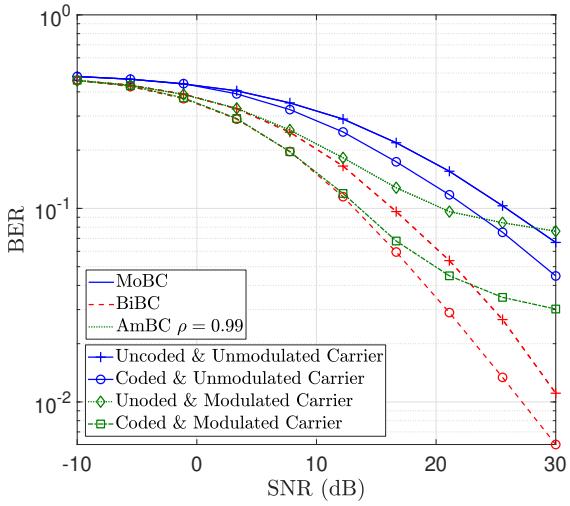

Fig. 14: The BER versus the transmit power at the RF source for $d_{\text{ST}} = 5\,\text{m}$, $d_{\text{TR}} = 2\,\text{m}$, $d_{\text{SR}} = 7\,\text{m}$, and $\alpha = 0.8$. The tag uses BCH(31,6) code and BPSK. MoBC and BiBC tags reflect an unmodulated carrier signal. AmBC tags reflect a BPSK-modulated carrier. For MoBC setup, $d_{\text{ST}} = d_{\text{SR}} = 5\,\text{m}$ and $d_{\text{SR}} = 0\,\text{m}$.

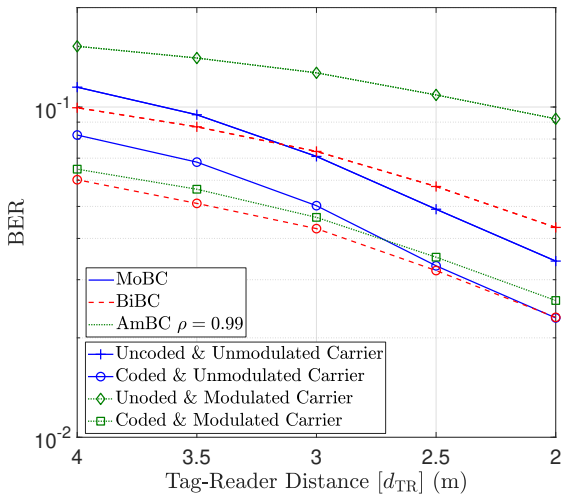

Fig. 15: The BER versus the tag-reader distance for $d_{\text{ST}} = 4\,\text{m}$, $d_{\text{SR}} = d_{\text{ST}} + d_{\text{TR}}$, $P_t = 20\,\text{dBm}$ and $\alpha = 0.8$. The tag uses BCH(31,6) code and BPSK. MoBC and BiBC employ an unmodulated carrier signal. AmBC employs a BPSK modulated carrier.

does not reflect any signal. On the other hand, when the α approaches unity, the backscatter achievable rate reaches its maximum, and the primary achievable rate slightly degrades due to interference from the backscatter transmission. Therefore, for a given α, the achievable rates of the primary and BackCom can be obtained by traversing the trade-off curves. We also consider $N_s = 5$, i.e., $T_b = 5T_s$ in Fig. 13, where the tag's signal is treated as a multi-path component, not interference, for the primary transmission (see [46, Sec II-B]).

The BER of the three BackCom setups is investigated in Fig. 14 and Fig. 15. To study the effects of FEC codes, we use cyclic BCH code (Section V-C) to encode tag data. Fig. 14 shows that FEC codes can reduce the BER for the same transmit power compared to the uncoded system (e.g., coding gain). In particular, for the AmBC setup, a BER of 10^{-1} is achieved at $14\,\text{dBm}$ and $21\,\text{dBm}$ of transmit powers for the coded system and uncoded one, respectively. Therefore, FEC codes lower the required transmit power for a certain BER and eventually increase the range (Fig. 15).

V. Coding Techniques in BackCom Systems

This section discusses coding requirements for BackCom, RFID coding techniques, line codes, FEC codes, and space-time codes.

The signal attenuation in the tag-to-reader and the emitter-to-reader channels depends on distances between nodes, location, propagation environment, and others. It can seriously limit capacity and reliability. Channel codes can help to alleviate this problem [124]–[126]. But code design for BackCom networks is different from that for conventional networks and is challenging due to several reasons: (i) tags can only do simple processing because of significant energy constraints (Section II-A), (ii) the capacity-approaching codes, such as

turbo and LDPC codes (Section III-C and Section V-C, respectively), require long codes, which is problematic for tags, and (iii) there are currently no coding standards for non-coherent and BackCom systems [125], [127], [128]. Thus, we need novel or existing coding schemes to extend the communication range, enhancing the application potential of BackCom.

Coherent decoding requires the availability of CSI, which is typically estimated with pilot signals [129]–[131]. The quality of estimated CSI depends on several factors and determines the BER performance [132]. However, the passive tag itself may not be able to transmit long pilot sequences for accurate CSI estimation. Moreover, CSI estimation is also affected by channel impairments such as multi-path fading, shadowing, noise, Doppler shifts, and interference. Consequently, the poor quality of CSI may degrade performance, resulting in high error floors. Rather than CSI estimation, we may use non-coherent encoding/decoding techniques, which are robust against fading [133]. They avoid CSI and achieve low complexity and cost. Thus, they may be exploited to enhance BackCom systems.

A. RFID Coding Techniques

RFID, commercial implementation of BackCom, adopts line codes [5], [64], [65], e.g., FM0 and Miller codes, due to their simplicity, along with CRC-16 to ensure the integrity of data transmission. In passive ultra-high frequency (UHF) Gen2 RFID, the tag communicates with the reader in a slot through framed slotted ALOHA (FSA)-based scheme [5]. The interrogator (reader) recovers tag data using two types of command sets $\{\mathrm{ACK}, \mathrm{EPC}\}$ and $\{\mathrm{Read}, \mathrm{Data}\}$ in the identification and read procedures, respectively. Initially, the reader transmits a query command that sets up communication parameters, such as tag rate, number of slots and the tag line code (i.e., FM0 vs Miller). Upon receiving the query from the reader, the tag picks a random value in the range $(0, 2^q - 1)$, where q is an integer between 0 and 15, and loads this value into its slot counter. For 0 value, the tag backscatters a 16-bit random or pseudo-random number (RN16). The interrogator then acknowledges the tag by sending an ACK with the same RN16. When the tag receives it correctly, it replies and backscatters the reply including the protocol control (PC) bits (16 bits), the EPC bits (minimum of 96 bits) and the 16-bit CRC (CRC-16). This procedure is the identification process. On the other hand, in the read procedure, the tag replies to the read command and backscatters its reply comprising a header (a 0-bit), memory word (data with variable length), 16-bit tag identifier (handle) and CRC-16 which is calculated over the 0-bit header, memory words, and handle. We note that there is option of activating an extra pilot sequence, that could be further exploited for channel estimation and respective coherent detection. The tag-to-reader link is thus protected with a CRC-16 along with with FM0/Miller codes.

Nonetheless, designing feasible BackCom channel codes remains a challenge since (i) lack of coding standards because BackCom systems are still in infancy, and (ii) passive tags have limited resources. By considering these factors, we next present several current and potential BackCom channel codes.

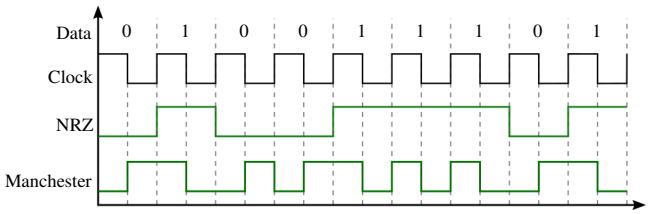

Fig. 16: NRZ and Manchester. **NRZ**: "1" represented by a high voltage value and "0" represented by a low voltage value. **Manchester**: "1" and "0" represented by a high-to-low and a low-to-high transition at the middle of the clock period, respectively [64].

B. Line Codes

Line coding, also known as digital baseband modulation (transmission), maps binary data into a baseband digital signal [65], [82]. Line codes have varying degrees of complexity. For instance, simple unipolar schemes employ the presence or absence of a voltage to represent a binary one or a binary zero, whereas more complicated multilevel schemes use different signal amplitudes to represent a distinct group of binary digits [82]. The simplest line codes are preferable for low-speed asynchronous transmission ($< 32\,\mathrm{kbps}$), where data is transmitted in short blocks. Thus, the receiver can synchronize itself with the transmitter at the beginning of each incoming block. For high-speed synchronous applications ($56\,\mathrm{kbps}$ to $100\,\mathrm{Mbps}$), where larger blocks of data are sent, timing and other factors such as noise and the DC component become significant factors. Thus, those applications must use more complex line codes.

There are five main categories of line coding schemes: (i) unipolar, (ii) polar, (iii) bipolar, (iv) differential (multi-transition), and (v) multi-level [82]. The unipolar, polar, and bipolar line codes are further categorized as either NRZ or return-to-zero (RZ) schemes.

We next briefly discuss some line codes.

- ***NRZ***: For NRZ, the 1's and 0's are clocked from the data to output voltages (Fig. 16). Despite its simplicity, it presents problems if the data have long runs of 1's or 0's because these may be misunderstood as the presence of a DC voltage, leading to synchronization failures [64].
- ***Manchester Codes***: This is a variation of NRZ encoding that ensures a transition in the middle of the clock cycle, thus allowing the receiver to extract the clock signal from the data signal (Fig. 16) [64]. Because of the frequent transitions, this code consumes up to approximately twice the bandwidth of the original signal. The physical layer of Ethernet local area networks (LANs) uses Manchester encoding.
- ***FM0 Codes***: The FM0 coding (Fig. 17) uses several basis functions for generating FM0 (bi-phase space) encoding. It offers four possible waveforms, two for each bit. It inverts the baseband phase at every symbol boundary (a phase inversion between bits "1" and "0" or "0" and "1"); a data-0 has an additional mid-symbol phase inversion. Therefore, the decoder only needs to determine if any phase inversion at the center of the symbol [5]. FM0 signaling shall always end with a "dummy" data-1 bit at the end of a transmission (Fig. 17 (c)). FM0 has the same spectrum as a Manchester-encoded signal. With a shift in

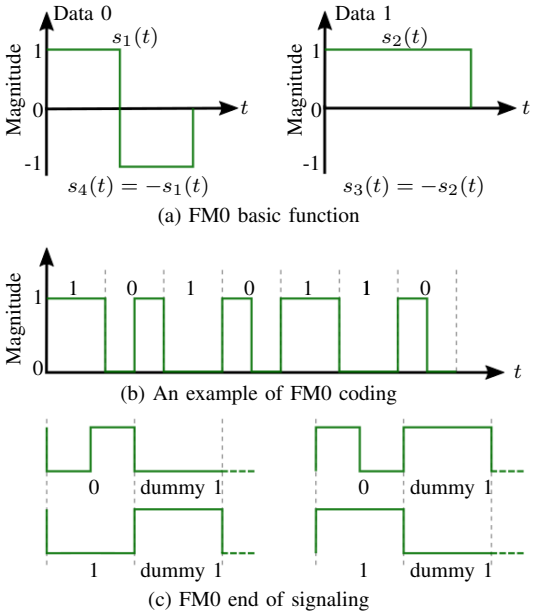

Fig. 17: FM0 basic function, encoding, and end of signaling. There is a phase inversion between symbols "1" and "0", and a phase inversion at the center of symbol "0" (no phase inversion at the center of symbol "1") [5].

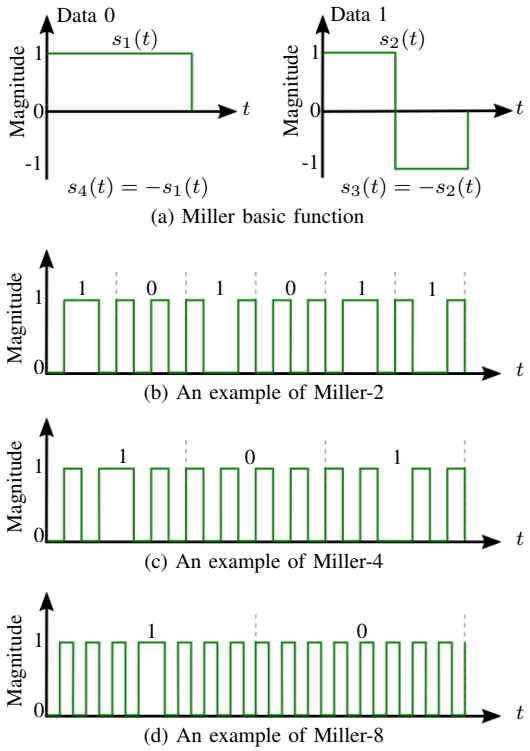

Fig. 18: Miller basic function and encoding. A phase inversion occurs between two consecutive symbols "0" and another in the middle of a symbol "1" [5], [135]. Miller-modulated subcarrier, i.e., Miller-$\hat{M}$, is obtained by multiplying the baseband Miller encoded data with a square wave whose frequency is $\hat{M}$ times that of the baseband data [134].

time of one-half of a data bit period, an FM0 signal can be represented as a Manchester encoded waveform, albeit with a different set of informative 1s and 0s constituting the data.

- ***Miller Codes***: These offer four possible waveforms, two for each bit [5], [66]. Fig. 18 shows the basic functions and an example of Miller code. The Miller sequence shall contain exactly two, four, or eight subcarrier cycles per bit [134, Section 3.4]. The waveforms of the tag for information bit "1" do not change the line level at the middle of the bit, whereas the waveforms for bit "0" do. Additionally, the starting line level of each waveform must be opposite than that of the preceding waveform. The exception to that rule is when there is transmission of bit "1" after bit "0"; in that case, the line level at the start of both waveforms must be the same. Miller codes always end with a "dummy" data-1 bit at the end of a transmission (Fig. 19).
  The baseband Miller code's subcarriers can be eliminated at the receiver via XOR operation with the system's synchronous clock. The signal waveform obtained at this stage is similar to the signal of the FM0 code (Fig. 20) and can be easily decoded [135].
  Several subcarriers (transitions per bit) are added to each bit of Miller code, which results in higher bit duration, while FM0 code has only one subcarrier. FM0 provides faster communication rates but is less robustness to noise. On the other hand, Miller encodings allow for increasing levels of noise resistance at the expense of slower tag data rate. Moreover, higher Miller indices provide better interference rejection (collision tag separation) at the cost of lower tag data rates [136].

Table VII describes the pros/cons of these line codes.

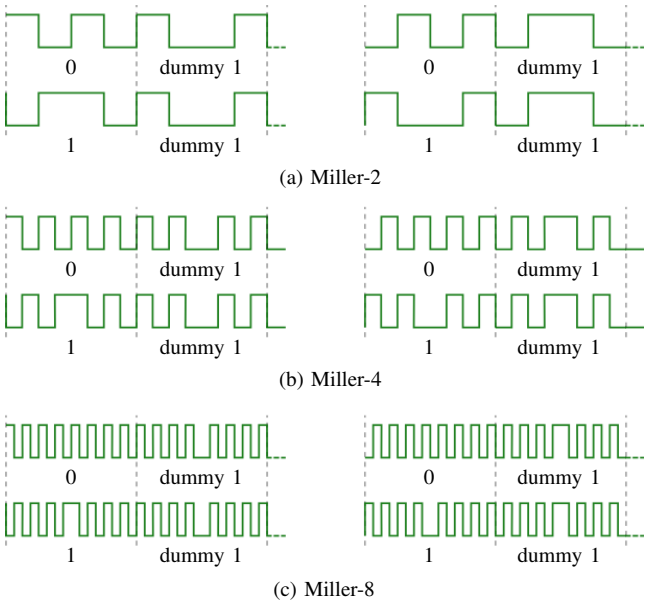

Fig. 19: Miller end of signaling [5]. The transmission ends with a "dummy" data-1 bit.

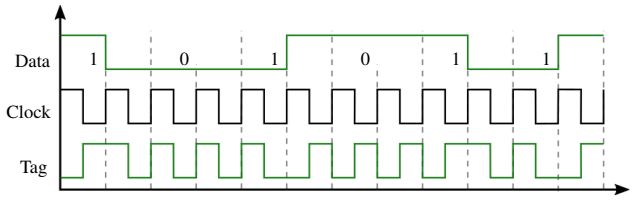

Fig. 20: Subcarrier elimination in Miller-2 [135]. Data is the baseband signal after subcarrier removal which is similar to the signal of FM0 code.

TABLE VII: Popular line codes.

Line codes	Advantages	Disadvantages
NRZ codes	• Ease of generation • Relatively low bandwidth requirement [137, Section 28.2]	• Signal distortion due to DC component • Synchronization failures due to the absence of voltage transitions • No error detection capability • Weak error rate performance
Manchester codes	• DC balanced • Easy clock recovery and synchronization • Better than NRZ error rate [137, Section 28.2]	• The minimum bandwidth is twice that of NRZ • No error detection capability [137, Section 28.2]
FM0 codes	• DC balanced • Data-embedded timing • High data rate	• Less robustness to noise/interference compared to Miller codes [135] • High bandwidth requirement [134, Section 3.6] • No error detection capability
Miller codes	• DC balanced • Timing information is embedded in data • Good interference and noise rejection • High separation efficiency for collision tags [135] • Low bandwidth requirement compared to Manchester codes [134, Section 3.4] • Good error rate performance	• Lower data rate compared to FM0 [136, Section 8.5.2] • Lower data rate by increasing the number of sub-carriers [136, Section 8.5.2] • No error detection capability [137, Section 28.2]

Remark 1. *Tags can use differential encoding, albeit with a slight degradation in error performance. That will reduce the complexity of the receiver and avoid power-consuming training sequences needed for channel estimation [50], [138]–[140]. Specifically, differential encoding works when the channel is unknown but is unchanged over a coherence interval that spans several (two) symbol durations. The data is encoded as a change rather than absolute values of the signals. Differential coding is popularly applied to PSK-signalling, where the information bits are encoded as the phase difference between current and previous symbols. For differential BPSK (DPSK), the encoding operation can be expressed at the bit level. Thus, the output of the differential encoder is given as*

$$b_n = b_{n-1} \oplus d_n, \tag{12}$$

where $\oplus$ is the XOR operation, b_n and b_{n-1} are is the transmitted bit at the current time instant, is the transmitted bit at the previous time instant, and d_n is the binary message bit of the tag ($d_n \in \{0, 1\}$) to be transmitted at the current time instant. At the receiver, d_n is decoded with a similar XOR operation [138].

Using (12)*, 180^o phase ambiguity can be resolved, which is enough for the binary case. However, for a general $\bar{M}$-array case, an $\bar{M}$-fold phase ambiguity occurs. The differential encoder can thus be formulated as [141, Section 3.5.2]*

$$b_n = b_{n-1} \exp(j\frac{2\pi}{\bar{M}} d_n), \tag{13}$$

which is equivalent to

$$\varphi_n - \varphi_{n-1} = \frac{2\pi}{\bar{M}} d_n, \tag{14}$$

where $b_n = e^{j\varphi_n}$, and $\varphi_n = 2\pi(n-1)/\bar{M}, n = 1, \ldots, \bar{M}$. Therefore, differential encoding maps the nth information symbol d_n into the phase change from the last transmitted symbol b_{n-1} to the following one b_n. At the receiver, the phase difference between the signals received at two subsequent symbol samples is used for detection. In general, the energy efficiency of $\bar{M}$-DPSK is quit poor for $\bar{M} \geq 8$ [100]. These designs are thus rarely found in practice when energy efficiency is the primary concern.

C. Error Correcting Codes

These can increase the reliability of the backscatter link and the communication range [62], [63], [125], [142]–[144]. Although long FEC codes approach the channel capacity, they consume significant computations and power and need accurate CSI. Passive tags, as mentioned before, have limited memory, energy, and computational power. Thus, CSI acquisition is challenging. Hence, existing long FEC codes may need substantial changes to be adopted for BackCom [63].

Adopting FEC codes to power-constrained and low-complexity backscatter tags needs several properties: (i) near-optimal short FEC codes and low-complexity encoders [31], [145], (ii) significant error detection capability at low overheads, (iii) low-complexity decoding algorithms operating with limited or no CSI [33], [62], [146]. Decoding delays could limit the potential number of tags served by a single receiver.

These concerns show that channel coding design for BackCom systems with the aim to achieve a favorable trade-off between complexity and reliability remains an open research problem. To this end, a modified version of short block length FEC codes, e.g., polar codes [142] and cyclic codes [143], [144], have been developed for BackCom systems.

One problem with short channel codes is that the coding gain will drop off and the gap to the Shannon capacity will increase [145], thereby channel capacity losses are experienced[8]. Moreover, short channel codes have small minimum Hamming distance, small bit-error correction capability and cannot overcome the deep fading effects which are even more frequent in BackCom systems, due to the product of two fading channels [125]. To overcome this difficulty, interleaving techniques, which provide time diversity efficiently [147], can be employed with the FEC codes with relatively small codeword length [63], [148]. With the help of interleaving, signal diversity can be achieved such that burst errors affects bits of different codewords rather than consecutive bits of the same codewords. The main drawback of this technique is the

[8]The utilization of relatively smaller (than larger) packets in low rate applications, such as environmental monitoring, in conjunction with the need for multi-user detection, is preferred to reduce the processing delay.

added delay at both the transmitter and receiver. In particular, for an interleaving depth D_{in}[9], both the tag and the receiver (reader) need to process a block of D_{in} codewords upon transmission and reception, respectively. Due to the limited tag's memory, relatively small values of D_{in} should be considered. One insightful approach to overcome this limitation is to take advantage of mathematical structure of the adopted FEC codes to reduce the memory requirement [63]. For instance, for a cyclic code $\mathcal{C}(k, n, d_{min})$, interleaving $\mathcal{C}$ with the interleaving depth D_{in} results in another cyclic code with the same minimum distance of d_{min}, i.e., $\mathcal{C}^{D_{in}}(D_{in}k, D_{in}n, d_{min})$ [149]. Thus, instead of processing D_{in} blocks of n bits each, the tag can easily produce the interleaved code with a shift register encoder of $(n-k)D_{in}$ memory elements.

Coherent detection/decoding, which relies on accurate CSI estimation, seems formidable in BackCom. Accurate channel estimation may require long enough training signals, which is time-consuming and energy-intensive [150]. Passive tags however possess inherently limited resources and have strict energy constraints and are unable to support such training or pilot signals [139]. Moreover, compared to conventional systems, backscatter link introduces multiple challenges, (i) the passive tags may reflect ambient sources, which are unknown to the reader. If the reader performs coherent detection, it requires a pilot-assisted channel estimation phase and strong coordination between the legacy and the BackCom system [50], [139], [140], [151], and (ii) a tag further introduces additional parameters, e.g., tag reflection coefficients and scattering efficiency, and the reader may not know them [63]. A solution to overcome these challenges of coherent detection is the non-coherent detection/decoding approach (Section VI-D) [62], [125], [140], [152] .

Next, we briefly review the principles of popular FEC codes (linear block codes) adopted in BackCom systems.

1) ***Cyclic Codes****:* A cyclic code has the property that a cyclic shift of a codeword is another codeword [81]. A (n, k) cyclic code has a unique monic generator polynomial $g(x)$ of degree $n-k$, i.e., $g(x) = g_0 + g_1x + g_2x^2 + \cdots + x^{n-k}$, which is a factor of $(1+x^n)$. For example, $g(x)$ of degree 5 can be $g(x) = (1+x)(1+x+x^4)$ or $g(x) = (1+x)(1+x+x^2+x^3+x^4)$ [81]. Each codeword can be generated as $c(x) = m(x)g(x)$, where $m(x)$ is a message polynomial of degree $k-1$.

Cyclic codes have efficient encoding and decoding algorithms and thus find applications in various systems. Examples of cyclic codes include:

- *CRC Codes*: These are mainly used for error detection purposes. An (n, k) CRC code can detect (i) error bursts with length up to $n-k$, (ii) any combination of $d_{min}-1$ errors, and (iii) any error pattern with an odd weight if $g(x)$ has an even number of nonzero coefficients, e.g., $g(x) = x^{12} + x^{11} + x^3 + x^2 + x + 1$ for 12-bit CRC (CRC-12) and $g(x) = x^{16} + x^{15} + x^2 + 1$ for 16-bit CRC (CRC-16) [93]. For a wide set of configurations, optimal generator polynomials can be found in [94], [95]. In 5G NR systems, CRC-16 and 24-bit CRC (CRC-24) are specified for downlink transmission [29].
- *BCH Codes*: BCH codes, a generalization of Hamming codes, are among the best cyclic codes in terms of their error-correcting capability. They can be designed to correct almost any required number of errors. In general, for any positive integers $m \geq 3$ and $t_e < 2^{m-1}$ (error-correcting capability), there exists a binary t_e-error-correcting BCH code, denoted $\mathrm{BCH}(n, k, d_{min})$, with codeword length of $n = 2^m - 1$, parity bit number of $n - k \leq mt_e$ and minimum distance of $d_{min} \geq 2t_e + 1$. For example, BCH(15,11) has $g(x) = x^4 + x + 1$ [93]. BCH codes can be decoded via syndrome decoding [153], which allows for simple decoding hardware. The Berlekamp-Massey (BM) decoder (a bounded distance decoder) is the standard decoder for BCH codes [92].
- *RS Codes* are a subset of non-binary BCH codes. Each RS symbol represents two or more bits. For a given (n, k, d_{min}) RS code, n and k are the numbers of the message and codeword symbols. Thus, there are $n-k$ parity symbols. RS codes are efficient because they achieve the Singleton bound as $d_{min} = n - k + 1$. They can correct up to $t_e = (n-k)/2$ errors. They are especially effective against burst errors because RS codes operate on the symbol level. A burst of bit errors can be mapped to a few symbols, which can be corrected efficiently [93]. A general form of the generator polynomial is $g(x) = (x-\alpha^i)(x-\alpha^{i+1})\ldots(x-\alpha^{i+2t_e})$, where α is a primitive element of the Galois field [93]. For example, the $g(x)$ of RS(15,11) is $g(x) = x^4 + \alpha^{13}x^3 + \alpha^6x^2 + \alpha^3x + \alpha^{10}$ and has the minimum distance 5 [93].
- *Reed-Muller (RM) codes*: For any integer $m \geq 0$ and $0 \leq r \leq m$, there exists an RM code, denoted by RM(r,m), which has the length $n = 2^m$ and minimum Hamming distance $d_{\min} = 2^{m-r}$. The message length is $k = \sum_{i=0}^{r} \binom{m}{i}$ [154]. The algebraic RM channel codes have an effectual error-rate performance under ML decoding, even for short lengths [155]. RM(2,5) has the best coding gain over all RM codes up to length $n = 32$ [154].

2) ***Polar Codes****:* These recently-developed linear block codes can achieve channel capacity and have simpler encoding and decoding algorithms [156]. Consequently, 5G wireless standards already incorporate them [157], [158]. They are based on the concept of channel polarization, where a channel is either noiseless (ideal) or useless [156]. Thus, a channel is split into n sub-channels, each with a capacity zero or one. Thus, $I(W)$ number of channels will become perfect channels with no noise, while the remaining channels, $n - I(W)$, will become completely noisy. The former ones, also known as reliable or noiseless channels, are used to transmit information, whereas the latter ones communicate zero information or frozen bits.

Consider length-n polar codes of rate R with $k = n \times R$ information bits. The encoder encodes the data for an input binary sequence, $\mathbf{d}$, so that there are $n-k$ frozen bits or fixed bit positions. As a consequence, for the given input sequence,

[9]The choice of D_{in} usually depends on how delay tolerant is the system and the channel coherence time [147].

the encoder generates the output sequence, $\mathbf{c}$, as follows:

$$\mathbf{c} = \mathbf{d}\mathbf{F}_n = \mathbf{d}(\mathbf{F}_2)^{\otimes m}, \tag{15}$$

where $m = \log_2(n)$, $\mathbf{A}^{\otimes m}$ denotes the m-th Kronecker power of matrix $\mathbf{A}$, and $\mathbf{F}_2 = \begin{bmatrix} 1 & 0 \\ 1 & 1 \end{bmatrix}$.

Polar codes can be decoded in several ways. First, successive cancellation (SC) decoding has been proposed. As well, successive cancellation list (SCL) decoding, CRC-aided SCL (CRC-SCL) decoding, and adaptive successive cancellation list (adaptive-SCL) decoding have been proposed [159]–[162]. Nonetheless, 5G NR adopts the SC-based decoder due to higher error correction performance.

*3) **LDPC Codes**:* These use sparse parity-check matrices and bipartite graphs. They received massive interest due to the development of belief propagation algorithms. LDPC codes, when combined with such algorithms, can achieve near-Shannon capacity [163]. When the block length is large, LDPC codes provide better performances, greater flexibility, and reduced decoding complexity than turbo codes. They also allow for parallel processing and simple hardware implementation, while high throughput ensures efficient decoding. The applications include optical, and 4G mobile communications, digital subscriber loop (DSL), and others. Others are second-generation digital video broadcasting (DVB-S2) and worldwide interoperability for microwave access (WiMAX) and 5G wireless standards [9].

The LDPC encoding is a two-stage process. First, a sparse parity-check matrix is selected via randomization. Second, the codewords are generated with it. LDPC codes can be decoded with the bit-flipping algorithm, sum-product algorithm, logarithmic sum-product algorithm, and min-sum algorithm [90], [91]. Among these, bit-flipping algorithms are the fastest and simplest [164], [165], making them suitable for high-speed and error-tolerance applications. However, because they can correct only a small fraction of correctable errors, they do not perform well on finite-length codes but need longer codes [164]. To improve performance, many versions have been developed, including weighted bit-flipping, gradient descent bit-flipping, parallel bit-flipping, and serial bit-flipping [164].

The sum-product algorithm operating on the factor graph can effectively decode long-length LDPC codewords [166], [167]. The factor graph (also known as the Tanner graph) is a representation of the parity check matrix of the code. The algorithm relies on the difference between two probability values and is sensitive to the quantization effects [167], [168]. The enhanced version of the sum-product algorithm, i.e., the logarithmic sum-product algorithm, can substantially reduce the required quantization levels by adopting the logarithmic likelihood ratio [167]. The min-sum algorithm is essentially a simplified version of the logarithmic sum-product algorithm. It trades precision for speed by eliminating the need for addition in the message update process, which may increase the number of iterations [90], [169].

D. Space-Time Codes

Recently, researchers have adopted MIMO backscatter to improve the reliability and data rates while overcoming fading [116], [170]–[172]. MIMO channel codes are known as STCs. These spread symbols across space (i.e., antennas) and time. Highly optimized STCs can reap both multiplexing and diversity gains. Another advantage is that STCs do not require the availability of CSI at the transmitter. There are two types of STCs [173]: (i) STBC and (ii) STTC. An STBC maps a block of input symbols to a matrix output with columns representing antennas and rows representing time slots. STBCs may not provide coding gain unless concatenated with an outer code. Their main advantages are diversity gains and simple decoding. A popular class of STBCs is the OSTBC [112]. Any two columns of an OSTBC code matrix are mutually orthogonal. This property has two fundamental consequences. First, it enables a simple ML decoding (Theorem 2) with linear processing. Second, it helps achieve full transmit diversity given uncorrelated fading channels.

STTC, however, operates on one input symbol at a time, resulting in a sequence of vector symbols whose length represents the number of antennas. Similar to SISO trellis-coded modulation, STTC provides a coding gain. The key advantage of STTC over STBC is that it provides both coding and diversity gains. However, the main downsides are the design challenges and the need for high-complexity encoders and decoders [174].

STCs for conventional MIMO channels with L-transmit antennas and N-receiver antennas are designed with two important criteria: (i) rank criterion and (ii) determinant criterion. First, let $\mathbf{D} \in \mathbb{C}^{T \times L}$ be the code difference matrix as

$$\mathbf{D} = \mathbf{C} - \mathbf{C}', \tag{16}$$

where $\mathbf{C} \in \mathbb{C}^{T \times L}$ is the transmitted code matrix (an STC codeword) of duration (block length) T and $\mathbf{C}'$ is the decoded code matrix at the receiver. Then, the pairwise error probability (PEP) of the general STC is given as [175]

$$P(\mathbf{C} \to \mathbf{C}') = P(\mathbf{D}) \leq \left(\prod_{i=1}^{r} \lambda_i \right)^{-N} \left(\frac{\bar{\epsilon}_x}{4N_0} \right)^{-rN}, \tag{17}$$

where r is the rank of $\mathbf{D}$, $\bar{\epsilon}_x$ is the average symbol energy, and $N_0/2$ is the power spectral density of AWGN per dimension at the receiver. Moreover, λ_i's are the non-zero eigen values of $\mathbf{A}^{\mathrm{T}} \triangleq \mathbf{D}^{+}\mathbf{D}$, where $(\cdot)^{+}$ is the Hermitian transpose operator.

1) *Rank Criterion*: The matrix $\mathbf{D}$ must have full rank for any codewords $\mathbf{C}$ and $\mathbf{C}'$ to achieve maximal LN diversity. Diversity order of rN is achieved if matrix $\mathbf{D}$ has a minimum rank of r over the set of two tuples of different codewords. Thus, the STC rank design criterion is to maximize $\mathcal{M}_{\text{conventional}}(\mathbf{C}) = \mathrm{rank}(\mathbf{D})$, for all codewords difference matrix $\mathbf{D}$ [175].
2) *Determinant Criterion*: The minimum determinant of $\mathbf{A}$ over all possible combinations of different codewords corresponds to the STC diversity gain. Thus, the design target is to make this determinant as large as possible to maximize the diversity gain [175].

However, analytical closed-form solutions for PEP in BackCom are challenging [114], [176]. Nonetheless, it has been

proved that for a (M, L, N) dyadic backscatter channel[10] with constant continuous wave transmit signal across all M antennas and T time slots, uniform query (UFQ)[11], and full CSI at the receiver, for an OSTBC, the PEP can be bounded above by [51], [112],

$$P\left(\mathbf{C} \to \mathbf{C}^{'}\right) = P(\mathbf{D}) \leq \frac{1}{2}\left(\frac{4}{\text{SNR}}\right)^{LN} \times \exp\left(\frac{4L}{\text{SNR}}\right)\Gamma\left(1-N, \frac{4}{\text{SNR}}\right)^{L}, \quad (18)$$

where $\Gamma(\cdot,\cdot)$ is the upper incomplete gamma function [177, Eq. (8.350.2)].

The best known OSTBC is the Alamouti code [178], whose code matrix (rows denote time and columns denote antennas) is given by[12]

$$\mathbf{C}_{\text{Alamouti}} = \begin{pmatrix} c_1^a & c_2^a \\ -c_2^{a*} & c_1^{a*} \end{pmatrix}, \quad (19)$$

where c_1^a and c_2^a are two symbols from a standard signal constellation. For the diversity order defined as

$$\delta \triangleq \lim_{\text{SNR}\to\infty} -\frac{\log P\left(\mathbf{C} \to \mathbf{C}^{'}\right)}{\log \text{SNR}}, \quad (20)$$

OSTBCs can achieve $\delta = L$ ($\delta = 2$ for Alamouti code) in dyadic backscatter channel under UFQ [112].

Unlike [112], which considers UFQ at the reader transmitter, i.e., all the M query antennas send out the same signals over T time slots, reference [176] investigates unitary query (UTQ)[13] which can create time diversity within channel coherent time for the (M, L, N) backscatter channel. Fig. 21 shows that with a uniform query, the channel behaviour is quasi-static, i.e., it changes every T time slots (symbol times). In contrast, with a unitary query, the channel changes every 1 symbol time. Therefore, by employing the UTQ, the channel is independent for each symbol time in ideal situations, and thus the risk of all codewords in the coherent time being wiped out decreases. This type of time diversity within the coherent time does not exist in the conventional one-way channel. In asymptotic high SNR regimes, the PEP performances of STCs with the UTQ and the UFQ in the (M, L, N) dyadic backscatter channel can be measured by [176]

[10]A general (M, L, N) dyadic backscatter channel (BiBC setup which employs spatially separated transmit (query) and receive antennas) has M query antennas, L tag antennas and N receiving antennas [51], [112]. The received signal at the receiver, over T time slots is represented by matrix $\mathbf{R} \in \mathbb{C}^{T\times N}$, as $\mathbf{R} = ((\mathbf{QH}) \circ \mathbf{C})\,\mathbf{G} + \mathbf{W}$, where $\mathbf{Q} \in \mathbb{C}^{T\times M}$ is the query matrix, the query signals sent from the M transmitting antennas to the tag over T time slots (i.e., T symbol times), $\mathbf{H} \in \mathbb{C}^{M\times L}$ is the the forward sub-channels, $\mathbf{C} \in \mathbb{C}^{T\times L}$ is the coding matrix, where the tag transmits coded or uncoded symbols from its L antennas over T time slots; and $\mathbf{G} \in \mathbb{C}^{L\times N}$ is the backscattering sub-channels. Besides, $\circ$ is the Hadamard product, and the matrix $\mathbf{W}$ is the same size as that of $\mathbf{R}$, representing the noise at the N receiving antennas over T time slots. Typically, both $\mathbf{H}$ and $\mathbf{G}$ are modeled as full rank matrices with independent identical distributed (i.i.d.) complex Gaussian entries, and $\mathbf{W}$ is the AWGN matrix.

[11]The uniform rank-1 query matrix is given as $\mathbf{Q}_{\text{UFQ}} = [1/\sqrt{M}]\mathbf{E}$, where $\mathbf{E}$ is a matrix with dimension $T \times M$ and all its elements are 1 [176].

[12]Each OSTBC code matrix is created from a set of vector information symbols $\mathbf{c}^a \in \mathbb{C}^{RT}$ that belong to some symbol alphabet [112].

[13]The full-rank unitary query matrix $\mathbf{Q}_{\text{UTQ}}$ satisfies $\mathbf{Q}_{\text{UTQ}}\mathbf{Q}_{\text{UTQ}}^{\text{H}} = \mathbf{I}$ [176].

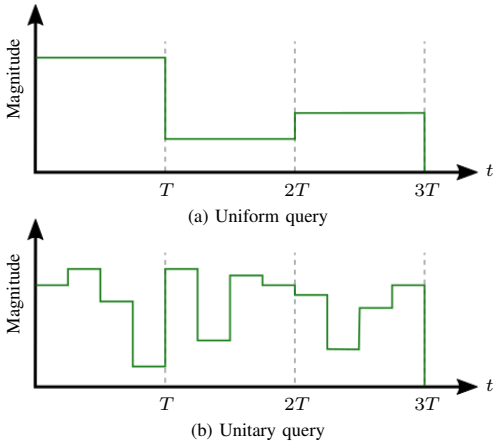

Fig. 21: Time diversity comparison between uniform query and the unitary query. The unitary query creates time diversity within channel coherent time for the (M, L, N) backscatter channel [176].

$$\mathcal{M}_{\text{Unitary}}(\mathbf{C}) = \sum_{t=1}^{T} \min(N, |\mathbf{D}_t|_0), \quad (21)$$

$$\mathcal{M}_{\text{Uniform}}(\mathbf{C}) = \min\left(N \times \text{rank}(\mathbf{D}), L\right), \quad (22)$$

where $|\mathbf{X}|_0$ is the L_0 norm of $\mathbf{X}$, and $\mathbf{D}_t$ is the tth row of the code difference matrix $\mathbf{D}$. Thus, the design criterion is to maximize the above quantity for all $\mathbf{D}$. Therefore, when UFQ is employed, no matter how many antennas are there and whatever the STC is, the performance bottleneck is determined by L, i.e., $\mathcal{M}_{\text{Uniform}}(\mathbf{C}) \leq L$. In contrast, the UTQ can break through this bottleneck and bring a significant improvement, $\mathcal{M}_{\text{Unitary}}(\mathbf{C}) \leq TL$ [176].

Therefore, the conventional and backscatter channels have different STC design criteria. In the former, full rank is essential for all codewords difference matrices to maximize the diversity order; however, in the backscatter channel full rank is not needed, and other metrics must be satisfied.

Some MIMO BackCom space-time coding and beamforming approaches can achieve a large performance gain [114], [176], [179], [180]. Specifically, a 2×2 STC which performs substantially worse than the Alamouti code in the conventional channel, performs much better in the backscatter channel and achieves almost the same performance as the Alamouti code [179]. Furthermore, a tag can implement this code with significantly lower circuit complexity than that of the Alamouti code, making it more desirable for low-cost and hardware-limited tags. Therefore, many overlooked STCs with lower circuit complexity may perform well in BackCom. This provides potential research opportunities.

VI. Summary of BackCom Coding Schemes

Due to recent research, BackCom technology, applications, and scalability are improving. However, there are different and more challenging communication requirements and limitations than conventional networks. Nevertheless, conventional techniques, such as higher-order modulations, MIMO, channel codes, and others have been adopted to improve communication range, reliability, energy efficiency, and data

rates of BackCom. Specifically, channel coding, mitigating interference and noise, can significantly improve BackCom performance. Hence, we next review adopted coding schemes.

A. Line Coding

NRZ and Manchester have been widely adopted in RFID [65], [181]. Differential Manchester encoding[14], a modified version of Manchester coding, has been also implemented for AmBC [140]. However, the NRZ code loses synchronization with long runs of "0" or "1", and the Manchester code effectively doubles the bandwidth usage. Thus, Miller and FM0 techniques (with the maximum rate of one-half) are usually adopted in existing BackCom systems (i.e., UHF Class-1 Gen 2 RFID [5], BiBC, and AmBC systems) because of their advantages, such as enhanced signal reliability, reduced noise, and simplicity [2], [5], [66]. However, energy consumption differs widely between transmitting/receiving bit "0" and a bit "1" under FM0 and Miller codes, i.e., the transmitting bit "0" consumes much greater energy than that for a bit "1" [182]. A wireless identification sensing platform in [182] has in fact measured the energy consumption of transmitting/receiving bits "0" and "1" under FM0 baseband encoding.

To exploit this energy consumption disparity, [182] investigates an energy-efficient data delivery scheme that generates a codebook with more bit "1"s than bit "0"s. The codebook of size 2^k is shared between the sender and the receiver. Each codeword has n bits for a k-bit data block. The receiver recovers the original data by using the shared codebook. There are several challenges with this code: (i) the codewords are of equal length n, which imposes a decoding delay of at least n bit duration and (ii) to save more energy, large k is needed, increasing the memory to hold the codebook. Hence, this code fails with limited-memory tags. To overcome this limitation, it is modified to only encode the blocks with the number of energy-consuming bits being equal to or greater than an encoding threshold, which is determined through an optimization problem [183]. Hence, this update has a smaller codebook size. The sender also uses two different data rates R_1 and R_2 to transmit codewords and uncoded k-bit blocks, respectively.

Discussion: With the line codes, the only available variable to adjust the link's reliability and rate is the symbol period, and the physical layer aspects of backscatter are overlooked [184]. Accordingly, despite their simplicity, the line codes do not provide robust performance under poor link conditions. They cannot achieve the targeted quality to satisfy the emerging requirements, such as high data rates, long communication range, and robustness [51]. More sophisticated coding schemes are thus required. Adapting FEC codes, primarily designed for active radios, is one practical solution [142]–[144]. For instance, STCs can further increase the reliability of multi-antenna tags [51], [112].

[14]Each bit is represented by the presence or absence of a change compared with the previous bit, i.e., no change denotes "0" while change denotes "1" [140].

B. Error Correction Coding

To enhance the reliability, lower the transmit power, and increase the communication range, FEC/CRC codes (Section III-C) have been developed for MoBC, BiBC, and AmBC channels. We next summarize these developments.

*1) **Codes for MoBC networks**:* These networks include RFID networks. Reference [185] investigates Hamming and RS codes and achieves coding gains of $1\,\mathrm{dB}$ and $4\,\mathrm{dB}$ in low-power, small message wireless networks [186], for passive UHF Gen2 RFID communications over two noise models AWGN and burst noise to capture the effect of channel imperfections. Tags use these codes to reply to an ACK command (EPC bits). Hamming code $(7, 4)$ is used, which can correct single bit error only or detect up to two bit errors. The Hamming code suffers from bad reads; which are the corrected received messages that still contain errors. To resolve that, the Hammming code is applied over the entire EPC memory content including CRC-16 to identify the bad reads. This approach could eliminate up to 50% of retransmissions required in the CRC only approach in AWGN channels. However, in the burst noise model, it performs similar to CRC only, both having a retransmission rate above 30% with a burst noise probability of 0.025.

To correct burst errors, an RS code with 8-bit and 16-bit symbols capable of correcting one symbol is further investigated. With the burst noise model, the retransmission rates of the RS code are less than 18% and 4%, respectively, for burst noise probabilities up to 0.025.

RFID tags can also adopt cyclic BCH codes [187], yielding a coding gain up to $8\,\mathrm{dB}$ compared to the uncoded case. However, they also suffer from bad reads. Thus, data spreading technique, e.g., FM0 or Miller-2/4/8, is further utilized to identify the bad reads. The proposed approach with BCH(255,239) code, which can correct two errors and may additionally detect decoding failures, improves the transmission time in certain SNR range compared to CRC based communication.

Moreover, [188] investigates improved-rate $4/6$ and $6/8$ -channel block codes, balanced block code, for RFID tags to address the need for high data rates in limited bandwidth scenarios. A balanced codeword has the same number of 1s and 0s. Reference [189] shows that there are $\bar{n}$ balance codewords for n output bits, where $\bar{n} = n!/[(n/2)!]^2$.

To design a codebook of a k/n-balanced block code, for a given k input bits ($k = \lfloor \log_2 \bar{n} \rfloor$, where $\lfloor a \rfloor$ is the largest integer less than or equal to a), the frequency spectrum of each of the resulting balanced $\bar{n}$ codewords is calculated and 2^k codewords with the deepest spectral nulls at DC are kept; the remaining codewords are discarded. Output codewords are then assigned to a Grey-coded ordered set of input bits.

Their experimental results show that the balanced block code increases the throughput by 50% compared to FM0 without penalties in cost, complexity, and power consumption. The throughput of the $6/8$ and $4/6$ -balanced codes are respectively 1.5 and 1.33 times higher than FM0. Moreover, the balanced code can detect a single-bit error readily, as the decoder can readily check if 1s and 0s are the same or not.

*2) **Codes for BiBC networks**:* Interleaved RM channel code and cyclic BCH codes have been adopted for BER

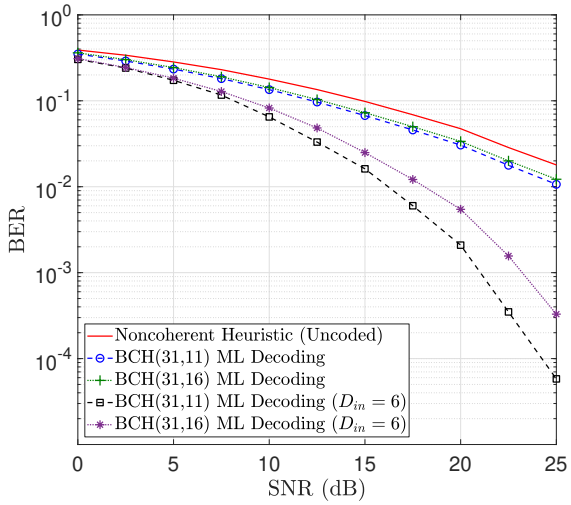

Fig. 22: The impact of interleaving on the BER performance of the coded bistatic setup over Rayleigh fading, i.e., $\{f, h_1, h_2\} \sim \mathcal{CN}(0, 1)$, employing binary FSK and the cyclic BCH code.

reduction or equivalently range increase [63], [125]. Compared to the uncoded case, RM(32,16,8) with FSK modulation[15](Section II-B) at $1\,\text{kbps}$ bit-rate and non-coherent detector can increase the tag-reader range by roughly 10 additional meters for $13\,\text{dBm}$ RF-source power at $867\,\text{MHz}$ [125]. Moreover, the interleaved BCH code considerably improves the BER performance, increasing the reliability and communication range [63]. Specifically, with coherent ML detection (Theorem 2) and FSK, the required SNR to achieve the BER 10^{-2} is $16.25\,\text{dB}$ for depth-6 interleaved BCH(31,11,11) code, while it is $20\,\text{dB}$ without interleaving (Fig. 22). Thus, interleaving yields about a 4 dB gain. Moreover, a coherent coded system with perfect CSI provides significant gains compared to the state-of-the-art non-coherent uncoded receiver.

A larger distance between the reader and the tag is critical because that allows more tags to be deployed economically. Coding can thus be utilized to increase this distance. For a short BCH code, If a tag is $10\,\text{m}$ from the RF exciter and uses a short BCH code, the reader can receive the tag's signal with coherent ML decoding. The tag-reader distance can be up to $150\,\text{m}$ for $1\,\%$ to $5\,\%$ BER [63].

With non-coherent decoding, the choice of BCH or RM codes depends on fading parameters and the design choice for extra diversity (that depends on $d_{\min}$) vs extra power gain (that depends on code rate) [62]. In particular, with non-coherent decoding and full interleaving[16] [147], BCH(31,11,11) outperforms RM(32,16,8) under Rayleigh fading, while they perform similarly under Rician fading. For no fading, the latter slightly outperforms the former.

[15]Multiple access can be naturally facilitated by FSK; each tag within an area can be associated with a unique frequency, thus enabling frequency-division multiple access (FDMA) [63], [190].

[16]For a fully interleaved system, $D_{in}T_b \leq T_{\text{coh}}$, where D_{in} is the depth of the interleaver, T_b is the bit period and T_{coh} is the channel coherence time [147]. A fully interleaved coded system achieves the diversity order d_{min} under ML non-coherent decoding, with classical FSK and Rayleigh fading [62], [147].

*3) **Codes for AmBC networks**:* Adaptive coding schemes, e.g., polar codes, are effective when the tag's data bits are mapped into reliable virtual channels and the code rate is automatically adapted based on channel quality [142]. The identification of channel quality can help to improve performance and throughput. Specifically, in ambient long-range backscatter, e.g., passive long-range (PLoRa) [191], which can support communications over several kms, the packet reception rate considerably decreases with range, an under-utilization of the backscatter link capacity. In contrast, many bytes are received correctly over long communication distances. Channel polarization thus helps the effective utilization of correct bytes, thereby providing reliable and relatively high-rate transmissions across large areas. An encoder is proposed, which comprises two modules: a virtual channel selector and a redundant bit generator; the tags initially encode information bits with a high code rate and then add redundant bits according to the decoding requirement of the receiver, which is estimated based on the frozen bit error ratio (FBER). The tag can adjust automatically to a suitable effective code rate for different channel qualities. Moreover, a small coding matrix is saved to overcome the memory overhead, and large coding matrices are computed iteratively.

At the receiver, the decoding block includes three modules (Fig. 23 (a)): (i) LLR calculator of data bits for each packet using a metric independent of the signal power, (ii) an LLR combiner that merges the LLR provided by different frames to enhance the decoding performance, and (iii) bit decision module. This coding scheme reduces the storage overhead of the coding matrix and energy consumption by several orders of magnitudes, desirable for resource-constrained backscatter tags. This experiment considers an outdoor scenario, where the tags, the RF source (active LoRa node), and the reader are deployed without being blocked by any object, and the RF source-to-tag distance is $1\,\text{m}$. To demodulate the tag's data, the reader first performs a fast Fourier transform (FFT) on the multiplication of the incoming chirp and a down chirp (negative frequency slope with time), and an FFT on the multiplication of the tag's chirp and a down chirp. This scheme can achieve up to $11.5\times$ throughput gain or extends the range limit by $1.9\times$ compared to PLoRa with a Hamming code, with $20\,\text{dBm}$ transmit power at the active LoRa node. Specifically, for a spreading factor of 12, the maximum transmission distances of PLoRa and the proposed scheme are about $1.1\,\text{km}$ and $2.1\,\text{km}$, respectively.

Reference [143] investigates RS codes to improve the reliability of tags reflecting Wi-Fi signals to communicate (Fig. 23 (b)). Wi-Fi signals inherently have silent periods with varying lengths [193], making tag reflections unreliable. Within the silent periods, the reflected bits of a tag are thus consecutively lost, resulting in a burst error channel. To address this, the authors develop an optimized RS code with adaptive rates compatible with Wi-Fi characteristics to maximize efficiency while satisfying reliability. The reader performs the optimization process due to the tag's limited power, and an index indicating the optimal RS code parameters is feedback to the tag. The optimization algorithm includes three steps: (i) estimating the probability distribution of the

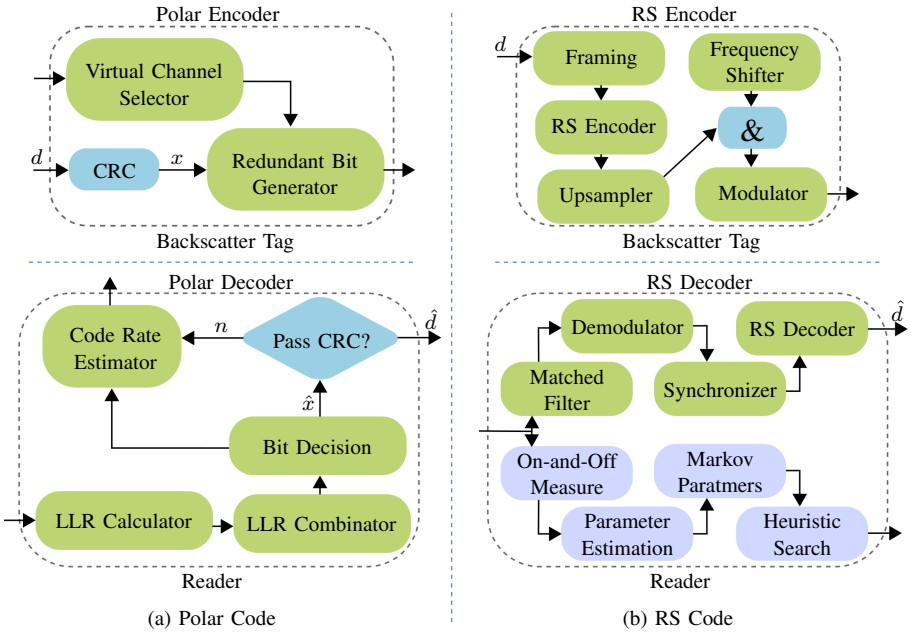

(a) Polar Code (b) RS Code

Fig. 23: Hardware designs for Polar code [142] and RS code [143].

on/off periods of Wi-Fi traffic, (ii) the Markov model for the state transitions, and (iii) RS code optimization to ensure reliability. The experiment is conducted in a $4 \times 6\text{m}^2$ office. A commercial WiFi router transmits regular WiFi signals packet-by-packet as the excitation, the tag which is located $0.3\,\text{m}$ and $0.6\,\text{m}$ away from the WiFi AP and the reader antenna, respectively, reflects the excitation signals to a receiver while conveying its information. The tag shifts the frequency of the reflected signal to another channel to avoid interference. This scheme can achieve significant frame error rate (FER), and BER gains, i.e., $\%99$ error correction in some scenarios.

To enhance AmBC detection without requiring the parameters of the RF source, cyclic BCH code is adopted in [190], with the tag using a hybrid form of FSK-BPSK modulation, a frequency-shifted form of binary phase shift keying (S-BPSK). Semi-coherent detection is then derived, assuming no information about the AmBC carrier, while the tag and channel introduced random phase is estimated. Considerable performance improvement can be achieved, and ambient carrier modulation can constructively enhance the performance under certain conditions. In particular, when the channel and the ambient signal parameter vary between successive bits, the best BER performance is achieved; the required SNR to achieve the BER 0.06 is $6\,\text{dB}$, while it is $10\,\text{dB}$ and $14\,\text{dB}$ when the ambient signal parameter remains constant for the duration of the tag packet (with varying channels between successive bits) and the uncoded case (ML detection with perfect CSI), respectively. This performance improvement is the result of the channel code being fully utilized.

The authors in [192] propose a three-state coding technique, i.e., the tag can be non-reflecting, reflecting, and negative-reflecting, to increase the throughput. The first two states are the same as conventional states. However, the tag switches its antenna impedance to reflect RF signals with an inverse phase in the third state. Thus, the tag requires three different reflection coefficients from three impedance loads. For the RF ambient transmit signal $s(n)$, an OOK modulated signal, the tag transmits its binary signal $b(n)$ to the reader through positive and negative backscattering of $s(n)$ and non-backscattering. Specifically, the tag signal is described as: (i) backscattered signals with the same phase ($b(n) = 1$), (ii) backscattered signals with an inverted phase ($b(n) = -1$), and (iii) no backscattered signals ($b(n) = 0$). The reader then uses a MAP detector. This three-state scheme reduces the BER to 10^{-3} with $15\,\text{dB}$ of the transmitted SNR and increases the throughput to 10^{-1} bps/Hz with $20\,\text{dB}$ of the transmitted SNR.

Table VIII shows the FEC coding schemes for BackCom. It briefly summarises the experimental setups, the desired goals and outcomes, and the tag complexity for different schemes.

Discussion: FEC codes and ARQ schemes offer more flexibility and benefits than line codes. Due to the tag's limited memory and processing capabilities, short linear block codes are more suitable. Therefore, cyclic FEC codes and modified versions of polar suggest themselves. Besides, bit interleaving can provide time diversity. Moreover, the challenge of CSI estimation suggests non-coherent detection/decoding methods. These could achieve acceptable performance compared to coherent ones.

Short channel codes may help ultra-reliable low latency communication (URLLC), mMTC, and control applications [89]. Thus, research has improved the flexibility (i.e., a wide range of use cases), complexity, and error correction capabilities [31], [89], [145]. We highlight several potential approaches to address the complexity and reliability of BackCom next.

For short codes, ordered statistics decoding (OSD), a near ML soft-decision algorithm, works well [31], [145]. It achieves a manageable complexity in conventional channels [146] and can be evaluated for BackCom with BCH and other codes.

In conventional channels, polar codes outperform LDPC codes in short block lengths and low code rates without

TABLE VIII: Summary of BackCom codes.

Setup†	Ref.	RF source	Tag type	Coding scheme	Tag modulation	Detection method	Design goal	Performance gain	Tag complexity
MoBC	[185]	Reader	Passive	Hamming(7,4) +CRC-16	OOK/BPSK	⊖	Error detection and correction	Eliminates up to 50% retransmissions under AWGN, 0.74 % error correction.	$\mathcal{O}(n)$ encoding complexity.
				RS-16/RS-32 +CRC-16	OOK/BPSK	⊖	Burst error detection and correction	Decreases the retransmission rate under burst noise (less than 18% for 16-bit symbols for burst noise probabilities up to 0.025).	$\mathcal{O}(n \log n)$ encoding complexity.
	[187]	Reader	Passive	BCH(255,239) +Miller-4	OOK	⊖	Erroneous packets detection/ BER reduction	8 dB coding gains compared to Miller-4, only.	–
	[188]	Reader	Passive	Balanced block(6/8 - 4/6)	BPSK	⊖	Throughput increase	50 % throughput improvement. The throughput of the $6/8$ and $4/6$ -balanced codes are respectively 1.5 and 1.33 times higher than FM0. It can detect a single bit error.	706/166 transistors are required to implement the logical operations of hard wired 6/8 - 4/6 encoder.
BiBC	[125]	Carrier emitter	Semi-passive	RM(32,16,8)	FSK	Non-coherent	BER reduction/ Range increase	10 m range improvement for tag-reader distance, with 13 dBm transmit power at the RF source and $D_{in} = 2$.	$\mathcal{O}(kn)$ storage/memory to save the generator matrix. Storage overhead and added delays proportional to D_{in}.
	[63]	Carrier emitter	Semi-passive	BCH(31,11)	FSK	Coherent ML	BER reduction/ Range increase	Tag-reader ranges by 150m for BER on the order of $1\% - 5\%$, with 13 dBm transmit power at the RF source.	$(n-k)$ memory elements in shift register encoder.
AmBC	[142]	Ambient LoRa signal	Passive/ PLoRa tag	Polar	CSS*	FFT calculations	Throuput increase	11.5× throughput improvement / extending the range limit by 1.9× compared to PLoRa with Hamming code, with 20 dBm transmit power at the RF source.	Two antennas at the tag to synthesize a LoRa signal. Perform binary operations to obtain coding matrix, reducing storage overhead.
	[143]	WiFi signal	Passive	RS(63,13)	OOK	Matched filter	BER reduction/ Reliability improvement	99 % BER reduction. The BER and FER could be reduced to 10^{-6} when the silent period is short enough. High reliability against the random alternation of on and off states of WiFi signal.	Hankel matrix encoder. Computational complexity and memory proportional to $k(n-k)$.
	[190]	Complex normal signal**	Passive/ Semi-passive	BCH(31,11)	S-BPSK◇	Semi-coherent	Detection improvement without knowledge of the carrier signal	The BER reduces to 10^{-3} with 11 dB SNR under varying channels and varying ambient signal parameter between successive bits.	Frequency switching at the tag.
	[192]	OOK-modulated signal	Passive	Three-state‡	Three-state signal	Coherent MAP	Throughput increase	$>$ 50 % throughput improvement. The BER reduces to 10^{-3} with 15 dB SNR.	Three impedances at the tag.

† These works consider single-antenna nodes, except [142], where the ambient RF source and the tag are with two antennas.
‡ Note that this coding scheme is different from FEC codes. * Chirp spread spectrum ** The ambient signals can attain various modulation schemes, e.g., BPSK, QPSK, and FM modulations. ◇ Frequency-shifted form of BPSK ⊖ Detection methods are not discussed in the respective works.

an error floor [145]. Short polar codes demonstrate their effectiveness using the CRC-aided SCL decoder [159], where a set of parallel SC decoders generates a list of candidates for the given channel output. The adaptation of short polar codes with CRC-aided SCL decoders in different BackCom configurations is thus worth investigating.

Using guessing random additive noise decoding (GRAND) offers significant complexity advantages for the short and high-rate codes in conventional channels [194]. GRAND, an ML decoding algorithm, attempts to identify the noise that corrupts the codeword, rather than directly finding the codeword itself. This algorithm is thus a universal decoder, applicable to any block code. For example, CRC codes can correct errors with GRAND decoder [195]. Specifically, the GRAND CRC decoder provides at least equivalent decoding performance compared BCH codes and CRC-aided polar codes, with ultra-low encoding complexity. GRAND decoders are also effective against burst errors, providing effective error correction without using interleaving, which causes delays [196]. Thus, the GRAND decoder, both hard and soft decision versions, can be evaluated for BackCom to reduce complexity and delays while mitigating fading effects and improving reliability.

C. Space-Time Coding

Due to its low complexity (encoding and decoding) and high performance, classical OSTBC is widely adopted in industrial standards and attractive for power-limited and hardware-limited BackCom [51], [112]. Reference [112] thus investigates STCs to improve the data rate and reliability of BiBC systems (i.e., RFID with separate transmit and receive

antennas at the reader) with multi-antenna passive tags and uniform query at the reader transmitter. The upper bound on the PEP, leading to estimates of the (asymptotic) diversity order, is derived for known orthogonal STCs with UFQ at the transmitter, as given in (18). While adding multiple antennas to the receiver (reader) is a natural solution, the number of antennas per tag is limited by the tag's form factor. Hence the performance gain is investigated with a limited number of tag antennas. The diversity order depends only on the number of tag antennas but not the number of receive antennas, i.e., adding additional transmit/receive antennas has no impact on the asymptotic PEP. However, the number of receive antennas affects the coding gain and the SNR threshold at which the maximum diversity order is achieved. The authors investigate the error performance of OSTBCs and STTCs. OSTBC achieves the maximum diversity order equal to the number of tag antennas, with linear decoding complexity. While, STTCs achieve the same diversity order but with higher decoding complexity since they require viterbi decoding.

Despite [112], which consider UFQ at the reader transmitter, reference [176], investigates UTQ (Fig. 21) and derives the design criteria of STCs with UTQ and UFQ by calculating the PEP in a BiBC setup. When the reader uses UFQ, regardless of the number of antennas and the type of STC, the performance bottleneck is determined by the number of tag antennas, L. In contrast, the use of UTQ can overcome this bottleneck and bring a significant improvement [176]. An improvement as large as $5\,\mathrm{dB}$ to $10\,\mathrm{dB}$ could be achieved comparing with the UFQ in a BiBC setup [176].

Reference [114] further investigates the joint design of reader and tag signals and modified OSTBC (mOSTBC) for MIMO BiBC systems and showed that the diversity order achieved rises from the number of tag antennas L to $\min(M,N)\times L$. OSTBC with UTQ [176] may not properly incorporate the query diversity and OSTBC. Motivated by this, the authors propose the block-level unitary query (BUTQ) at the query end and present the corresponding mOSTBC at the tag end. In particular, the BUTQ is defined by the query matrix $\mathbf{Q}=\mathbf{Q}_0\otimes\mathbf{1}_M$, where $\mathbf{Q}_0$ is a unitary matrix, $\otimes$ is the Kronecker product and $\mathbf{1}_M=(1,1,\cdots,1)^{\mathrm{T}}$. The modified coding matrix, $\mathbf{C}=\mathbf{1}_M\otimes\mathbf{C}_0$, i.e., $\mathbf{C}=(\mathbf{C}_1,\cdots,\mathbf{C}_M)^{\mathrm{T}}$, where $\mathbf{C}_1=\mathbf{C}_2=\cdots=\mathbf{C}_M=\mathbf{C}_0$, with $\mathbf{C}_0$ being an original OSTBC.

Example 1. *For a $2\times2\times2$ dyadic backscatter channel, let $\mathbf{C}_0=\mathbf{C}_{Alamouti}$ and $\mathbf{Q}_0=\mathbf{I}_2$. The design pair for mOSTBC with BUTQ, the BUTQ matrix and the corresponding modified Alamouti code, is respectively given as*

$$\mathbf{Q}=\begin{pmatrix}1&0\\1&0\\0&1\\0&1\end{pmatrix}, \tag{23}$$

$$\mathbf{C}=\begin{pmatrix}c_1^a&c_2^a\\-c_2^{a*}&c_1^{a*}\\c_1^a&c_2^a\\-c_2^{a*}&c_1^{a*}\end{pmatrix}. \tag{24}$$

The asymptotic symbol error rate (SER) is derived for the mOSTBCs with BUTQ. The diversity order that can be achieved is $\min(M,N)\times L$ [114]. Moreover, unlike OSTBC with UTQ at the query end, this scheme enjoys linear decoding complexity, same as OSTBC with UFQ at the query end.

STCs have been also investigated when the reader uses the same set of antennas for transmission and reception, i.e., MoBC setup [113]. For an $N\times L$ MoBC channel[17], the maximum diversity order is $NL/2$, the half of that of the conventional MIMO channel, that can be achieved by mOSTBC and BUTQ design pair. Moreover, this scheme significantly outperforms the OSTBC with UTQ in asymptotically high SNR regimes, indicating that the latter cannot achieve the maximum diversity order. Table IX, summarises the achievable diversity orders for different design pairs for monostatic and bistatic channels.

A 2×2 OSTBC, a rotation of the Alamouti code, is proposed for MIMO BackCom, given as [198]

$$\mathbf{C}_{\text{proposed}}=\frac{\sqrt{2}}{2}\begin{pmatrix}c_1^a+c_2^a&c_2^a-c_1^a\\c_1^{a*}-c_2^{a*}&c_1^{a*}+c_2^{a*}\end{pmatrix}. \tag{25}$$

In BiBC and MoBC channels with UFQ and BUTQ at the query end, the PEP performances of both (25) and Alamouti code are the same with BPSK. And, under UTQ, (25) has lower PEP than the Alamouti code. It always has a better duty cycle, which increases the availability of backscattering signals, reducing outages.

Reference [179] also proposes a simple 2×2 STC for BackCom by removing the minus and conjugate signs from the Alamouti code, i.e.,

$$\mathbf{C}_{\text{simple}}=\begin{pmatrix}c_1^a&c_2^a\\c_2^a&c_1^a\end{pmatrix}. \tag{26}$$

This STC achieves almost the same performance as the Alamouti code in backscatter channels with considerably lower complexity (Fig. 24). It achieves the same performance as the Alamouti code under UTQ. Under the BUTQ scheme, however, its performance is slightly worse. With BPSK, when employing the Alamouti code, each tag requires four different reflection coefficients with four different load impedances. On the other hand, for the simple STC, each tag antenna requires only two different reflection coefficients, i.e., four for both tag antennas. Hence, the number of load impedances is reduced from four to two.

Note that (26) performs worse than the Alamouti code in conventional MIMO wireless channels (Fig. 25). Thus, existing simple codes, which do not perform well in the MIMO channels, may work well in the backscatter channel.

The work [199] further investigates the joint design of the generalized spatial modulation (GSM). GSM exploits the antenna index as an extra dimension to be exploited [200], and STC for BiBC setup. With GSM and the Alamouti scheme in two transmitting antennas, the SER performance improves significantly, and transmit diversity is realized.

[17]For a general $N\times L$ MoBC channel, the reader employs the same set of antennas for transmission and reception (as a full-duplex setup [197]) and the forward and backscatter channel have the same channel gains, i.e., $\mathbf{H}=\mathbf{G}^{\mathrm{T}}$. Consequently, the monostatic backscatter channel is given as $\mathbf{R}=\left((\mathbf{Q}\mathbf{G}^{\mathrm{T}})\circ\mathbf{C}\right)\mathbf{G}+\mathbf{W}$.

TABLE IX: Diversity order comparisons for BackCom systems.

Channel model	MoBC	BiBC	Conventional
Achievable diversity order	$NL/2$ [113]	Not Known	NL
STC with UFQ	$< NL/2$	$\leq L$ [112]	–
OSTBC with UFQ	$< NL/2$	L [112]	–
STC with UTQ	$\leq NL/2$	Can be larger than L with proper design [176]	–
OSTBC with UTQ	$< NL/2$	L [114]	–
mOSTBC with BUTQ	$NL/2$	$L \times \min(M, N)$ [114]	–

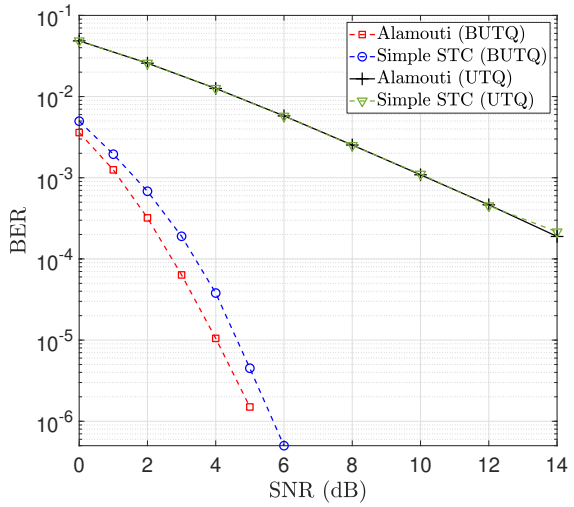

Fig. 24: The BER performances of C_{simple} and Alamouti code in $2 \times 2 \times 2$ backscatter channels with BPSK. The STCs are ML decoded. All channels are Rayleigh fading.

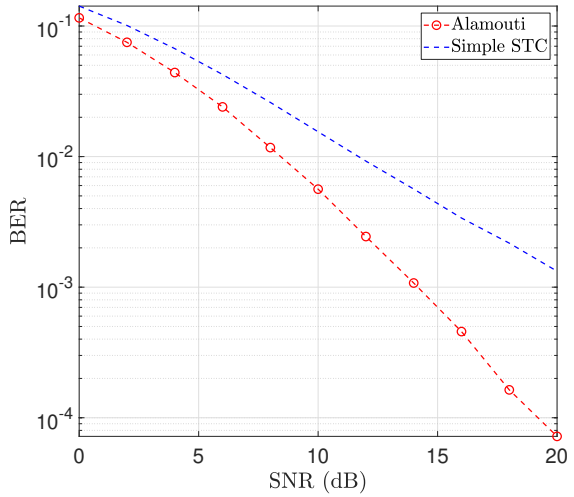

Fig. 25: The BER of C_{simple} and the Alamouti code for the 2×1 conventional channel with ML coherent detection for BPSK and Rayleigh fading.

OSTBCs have also been investigated for AmBC when the tag and the reader are equipped with multiple antennas [180]. First, an approximate linear MIMO ambient backscatter channel model is derived to simplify the detection process by using conventional MIMO techniques. Then, two coherent detectors and a non-coherent detector are provided based on the proposed channel model. The non-coherent detector is based on differential OSTBC where neither the transmitter nor the receiver requires CSI. The proposed linearized and normalized MIMO channel model is accurate when there are two antennas at the tag but becomes less accurate when the number of antennas is increased. Moreover, compared to single-input single-output (SISO) AmBC systems, OSTBC and differential OSTBC can effectively enhance BER performance.

Table X shows the STCs for BackCom.

Discussion: MIMO tags and the reader can use STCs and OSTBCs for diversity and multiplexing gains. Some STCs can provide diversity gains without needing CSI at the transmitter. Moreover, for differential OSTBCs, neither the transmitter nor the receiver requires CSI. Multiple antennas at the reader also improve the coding gain and SNR threshold, ultimately deciding the diversity order. To this end, different STCs have been developed for BackCom systems. Unexpectedly, some may perform worse than the Alamouti code in conventional MIMO wireless channels but achieve almost the same performance as the former in backscatter channels, with lower tag complexity [179]. Thus, one may trawl existing codes to identify the ones that perform well in backscatter channels.

Signal detection when the reader has no CSI is a critical challenge in BackCom systems. This is because the channels have different fading characteristics than the traditional one-way channels (Section IV). As well, pilot-based channel estimation methods may not be feasible for passive tags. In AmBC, the reader does not know the RF source parameters (such as bandwidth, transmit power, and waveforms). Non-coherent detection and decoding methods may overcome those limitations. In the following, we describe them.

D. Non-coherent Detection/Decoding for BackCom

Coherent detection requires good CSI. Pilot sequences (i.e., predetermined known symbols) are sent for this purpose. However, with time-division-duplexing, we can exploit channel reciprocity. Thus, CSI can be obtained from the reverse-direction channel estimates on the same frequency range. For example, the base station can perform channel estimates in cellular networks and feed them back to the users.

However, such techniques may not adapt to BackCom networks. The reason is that the tags have strict energy limitations and may not transmit their own pilots [201], [202]. A solution could be non-coherent detection/decoding methods [42], [62], [125]. In particular, reference [125] investigates a non-coherent decoding scheme for a BiBC setup. The tag adopts an interleaved RM code with FSK modulation. The receiver uses a square-law detector to generate the soft LLR information. For the same system, a non-coherent decoding rule is developed in [62] based on the composite hypothesis

TABLE X: Summary of the STCs in BackCom.

Setup†	Ref.	Quary signal	Coding	Modulation	Performance gain & summary
MoBC	[113]	UFQ/BUTQ	mOSTBC/OSTBC	BPSK/2-ASK	The BER of 2-ASK degrades $3\,\mathrm{dB}$ than that of the BPSK. mOSTBC+BUTQ reduced to the Repetition code of order N, when $L=1$.
	[198]	UFQ/UTQ/BUTQ	Rotated Alamouti	BPSK/QPSK	Same BER as that of the Alamouti under BUTQ and UFQ. Better BER performance than that of the Alamouti under UTQ. Higher outage capacity than that of the Alamouti.
BiBC	[112]	UFQ	OSTBC/STTC	QPSK	Adding additional transmit/receive antennas has no impact on the asymptotic PEP. Receive antennas affects the coding gain and the SNR threshold for the maximum diversity order.
	[176]	UTQ	STC	BPSK	BER improvement as large as $5\,\mathrm{dB}$ to $10\,\mathrm{dB}$ in mid-range SNR regimes, compared with UFQ.
	[114]	UFQ/UTQ/BUTQ	mOSTBC/OSTBC	BPSK/QPSK	The data rate of mOSTBC+BUTQ is $1/M$ of that of UTQ and UFQ under the same modulation. Under the same data rate, mOSTBC+BUTQ achieves $\sim 7\,\mathrm{dB}$ coding gain at BER 10^{-5}, compared to the OSTBC with UTQ and UFQ.
	[198]	UFQ/UTQ/BUTQ	Rotated Alamouti	BPSK/QPSK	Same BER as that of the Alamouti under BUTQ and UFQ. Better BER performance than that of the Alamouti under UTQ. Higher outage capacity than that of the Alamouti.
	[179]	UTQ/BUTQ	Simple STC	BPSK	Same BER as that of the Alamouti under UTQ. Slight BER degradation compared to Alamouti under BUTQ. Reduced tag circuit complexity compared to that of Alamouti.
	[199]	Unmodulated carrier signal	Alamouti+GSM (GSMA)	BPSK/QPSK	Enhanced performance in terms of SER compared to the GSM with the use of combined spatial and time modulation; a coding gain of $\sim 8\,\mathrm{dB}$ at BER 10^{-2}, with a spectral efficiency $3\,\mathrm{bps/Hz}$.
AmBC	[180]	Complex Gaussian signal	OSTBC/Differential OSTBC	BPSK	Enhanced BER performance compared to SISO AmBC under both coherent and non-coherent detection.

† These works consider multiple-antenna source and reader, except [180] which considers single-antenna RF source, and [199] which considers single-antenna RF source and reader.

test. For depth-6 interleaved BCH(31,11,11) code, the coherent ML detector offers a $3\,\mathrm{dB}$ performance gain compared to the non-coherent one. However, the BER gap narrows for higher interleaving depth. The non-coherent receiver has less computational complexity.

Differential coding (Remark 1) and non-coherent detectors are investigated for AmBC systems [50], [138]–[140]. In particular, [50] uses the difference between two consecutive symbols to design the optimal detector and the detection threshold. Reference [139] also designs an ML detector from the joint PDF of the received signals corresponding to two consecutive differentially encoded symbols. An energy detector is also derived to alleviate the computational complexity. With 8-PSK ambient RF source, the BER can be reduced to 10^{-4} at an SNR of $20\,\mathrm{dB}$. However, in [50] and [139], the detection threshold should be estimated first, causing a communication delay. To overcome that, reference [140] adopts differential Manchester coding at the tag and develops a non-coherent Manchester detector. This detector jointly considers the energy difference of two adjacent symbol intervals. Thus, decision threshold estimation is no longer needed and the symbols can be detected immediately. This approach reduces the BER that those in [50], [139]. The BER can also be reduced under unknown deterministic ambient signals than complex Gaussian ambient signals.

A non-coherent detector is also derived when the tag uses NRZ coding (OOK modulation) [203]. A key insight is that its performance cannot be improved by simply increasing the ambient RF source power without interference avoidance/cancellation or increasing the number of primary samples. However, the signal-to-interference can be improved for short tag-to-reader distances. Two detectors are designed in [152], which require neither CSI nor the knowledge of RF source power and noise variance. In the high SNR regime, they can achieve the performance of a chi-squared detector, which tests if the sample variance equals a specified value.

Experiment: To provide insights, we consider a BiBC system and investigate the effects Repetition-5, Hamming$(7,4)$, BCH$(31,11)$, and RS$(3,15)$ with 4-bit per symbol, on the BER performance. Here, bits are interleaved with FSK modulation, and the reader performs coherent and non-coherent detection/decoding [62], [63], [125].

Fig. 26 and Fig. 27 respectively depict the BER of the codes with coherent and non-coherent detection techniques. As observed, using interleaved short codes can enhance the BER performance. In particular, with coherent detection, interleaved Hamming, Repetition, BCH, and RS codes offer gains of respectively $2.1\,\mathrm{dB}$, $7.37\,\mathrm{dB}$, $10.7\,\mathrm{dB}$, and $12.8\,\mathrm{dB}$ at BER 10^{-2}, compared to the uncoded setup. Moreover, with non-coherent detection, the same codes offer $4.5\,\mathrm{dB}$, $8.89\,\mathrm{dB}$, $11.8\,\mathrm{dB}$, and $15.6\,\mathrm{dB}$ gains at BER 0.02, compared to uncoded non-coherent detection. It is also observed that the uncoded non-coherent detection experiences $4.21\,\mathrm{dB}$ loss at BER 0.2.

Discussion: Coherent detection/decoder requires accurate CSI, which is typically acquired via pilot symbols. However, passive tags have limited power and cannot support long pilot sequences. For short channel codes, pilot overhead considerably reduces the rate at low to intermediate SNRs [204]. Better decoding is thus required with short channel codes [33]. Non-coherent detection can be viewed as a joint estimation of the channel and the data. Hence, if properly optimized, it can be efficient, albeit at the expense of higher complexity [205]. Recently, a pilot-free polar-coded scheme was proposed for conventional channels. It jointly estimates CSI and data with

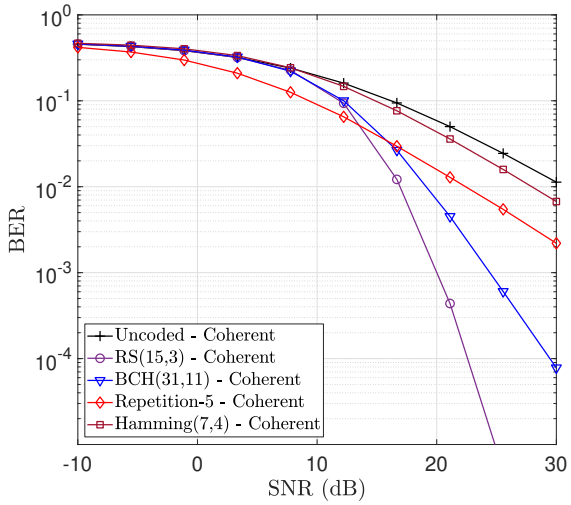

Fig. 26: The BER versus the transmit power at the RF source for an interleaved-coded bistatic setup with $d_{\mathrm{ST}} = 5\,\mathrm{m}$, $d_{\mathrm{TR}} = 2\,\mathrm{m}$, and $\alpha = 0.8$. The channel coherence time and the interleaver depth are $T_c = 32$ and $D_{in} = 8$. The channels are Rayleigh faded, i.e., $\{h_1, h_2\} \sim \mathcal{CN}(0, 1)$, and the tag uses binary FSK.

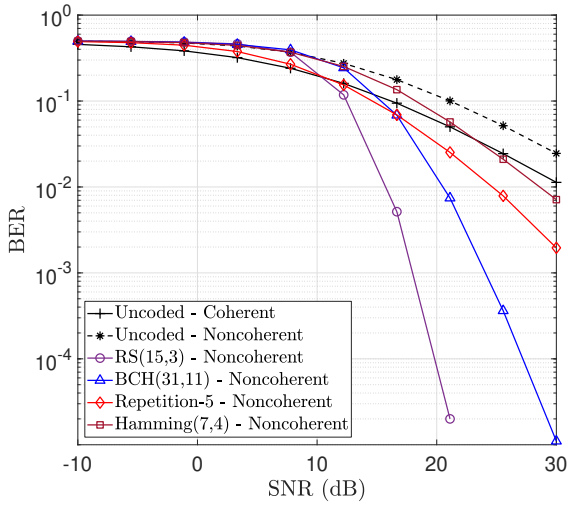

Fig. 27: The BER versus the transmit power at the RF source for an interleaved-coded bistatic setup with $d_{\mathrm{ST}} = 5\,\mathrm{m}$, $d_{\mathrm{TR}} = 2\,\mathrm{m}$, and $\alpha = 0.8$. The channel coherence time and the interleaver depth are respectively $T_c = 32$ and $D_{in} = 8$. The channels are Rayleigh faded, i.e., $\{h_1, h_2\} \sim \mathcal{CN}(0, 1)$, and binary FSK is used at the tag.

a similar complexity of the coherent receiver with perfect CSI [206]. Such novel ideas may also work for BackCom systems.

Fig. 28 provides an outline of existing BackCom codes.

VII. Multiple Access Codes for BackCom

Multiple access algorithms are fundamental to support reliable massive connectivity for low-cost and hardware-limited tags. We review several solutions for that.

Of course, the two classical multiple-access methods are (i) FDMA [63], [190] and (ii) time-division multiple-access (TDMA) [210], [211]. In FDMA, each tag will use a different frequency to communicate with the reader. Thus, it must be able to shift the frequency of the incident RF signal during the reflection process. However, the basic tag design does not readily support frequency shifting operations (Section II-A). Although a tag can be suitably modified to generate multiple frequencies, that will increase its cost. Additionally, the energy expenditure for generating multiple operating frequencies may exceed the energy harvesting capacity. Thus, adopting FDMA could be challenging for large-scale deployments of tags.

On the other hand, TDMA is more often used [211], which requires timing synchronization. A preamble of a sequence of known bits is typically transmitted to help synchronization purposes [42], [212], [213]. Tags thus access the medium with either deterministic (e.g., tree-search) or probabilistic such as FSA-based schemes (EPC protocol in Section V-A) [5]. However, the reader serves as a centralized control node, coordinating frame size. For example, in the EPC protocol, the reader divides time into N_s slots ($N_s = 2^q$, where q controls the number of time slots). Tags randomly selects a slot for their data transmission. To reduce the risk of collisions, N_s should be large enough, which tends to reduce spectral efficiency due to many empty slots. In large-scale deployments, TDMA is thus inefficient and fails to meet the distributed network requirements.

A. Sparse Code Multiple Access

Sparse code multiple access (SCMA), a code domain approaches for non-orthogonal multiple access (NOMA), maps input bits to codewords using multi-dimensional constellations [124], [214]–[219]. SCMA allocates each resource block to only a subset of active users, resulting in a sparse structure. In contrast to low-density signature/spreading (LDS), SCMA users map their input bits to multi-dimensional constellations to spread their information rather than repeating QAM throughout their pre-assigned resource blocks, making it more robust and complex [216]–[218]. For example, if each user is allocated to two resource blocks, LDS repeats one QAM symbol across both resource blocks, while SCMA transmits a separate symbol across each resource block. To this end, LDS can be considered a special case of SCMA, which employs the repetition of QAM in multi-dimensional constellations. SCMA systems can be overloaded depending on the spreading factor, i.e., the number of multiplexed users can exceed the number of resource blocks. Due to the sparsity of codewords, the message passing algorithm (MPA) detection is feasible with a moderate degree of complexity [216]–[218]. In addition, the shaping gain of the multi-dimensional codebook is a primary source of performance improvement for SCMA over LDS.

SCMA has been proposed to facilitate uplink MTC services [216]–[218]. The SCMA codebook is designed using lattice constellation design principles, and the steps are summarized as follows [217]:

1) Design a multi-dimensional constellation based on the required rate. For instance, heuristic optimization is used for low-rate constellation design, whereas the N-fold Cartesian product of $\mathbf{Z}^2$ is used for higher-rate constellation design, where $\mathbf{Z}$ is a set of integers.
2) An optimal rotation matrix is applied to the base constellation to control the dimensional dependence, power variation, modulation diversity or signal space diversity order, and the minimum product distance of the constellation while preserving a constant Euclidean distance.

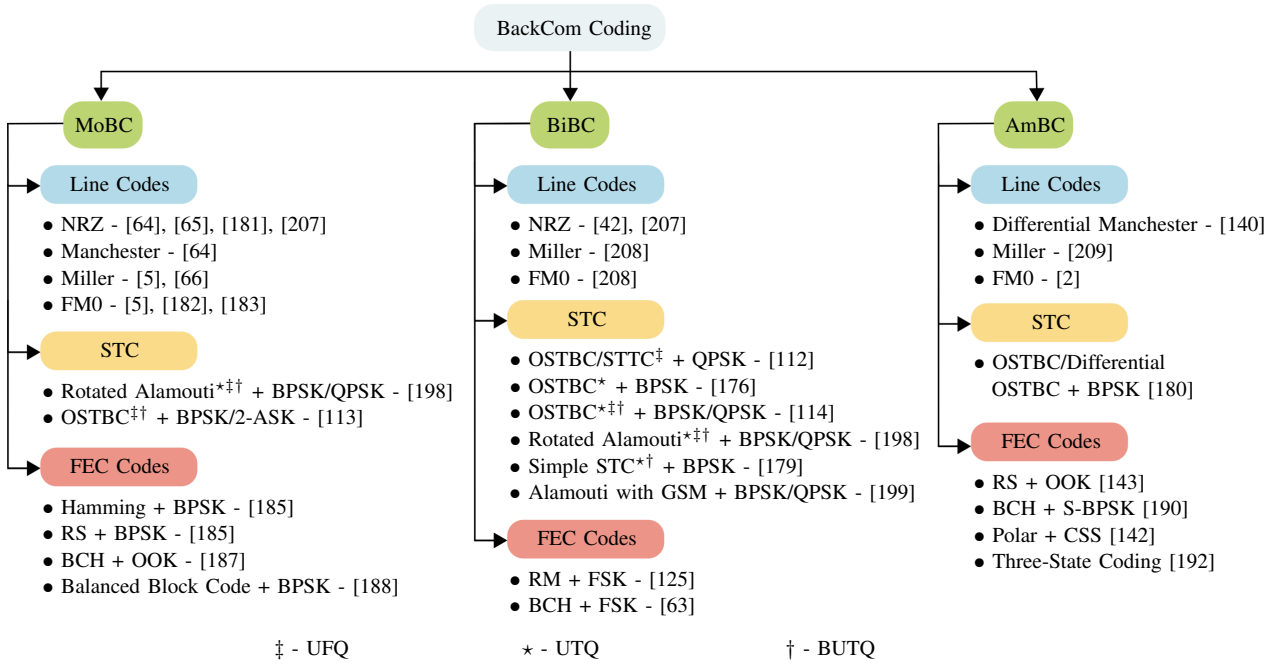

Fig. 28: Summary of the BackCom codes.

3) Shuffling the multi-dimensional constellation along real and imaginary axes to reduce decoding complexity while maintaining dependency among the complex dimensions of the resultant multi-dimensional constellation.

As mentioned before, the tag implements passive modulation by switching among load impedances (Section II-B). These can be chosen to create 2D signal constellations. As a result, tags can implement multi-dimensional modulation and coding schemes. However, advanced modulation and coding schemes, such as an adaptive power ratio in conventional power-domain NOMA or infinite-length channel coding, may not be available with low-complexity tags. Therefore, code-domain NOMA based on sparse coding is preferable over power-domain NOMA in BackCom, particularly in AmBC applications [124]. Specifically, SCMA offers three desirable properties that are suitable for massive connectivity:

1) *Grant-free Uplink Transmission*: Backscatter tags can employ sparse coding to transmit data using a predefined codebook. It can accommodate massive and burst uplink traffic in the absence of a request-grant method. Thus, low latency is achievable without scheduling and resource allocation [124].
2) *NOMA*: Sparse code encodes data in multi-dimensional complex codewords, which provide additional degrees of freedom than conventional two-dimensional BackCom modulation. As a consequence, sparse coding can enable concurrent RF transmissions, and an iterative MPA can efficiently handle multiple-access interference [124].
3) *Projected $\bar{M}$-Ary Modulation*: The conventional tag modulators can achieve $\bar{M}$-ary modulation by load modulation (Section II-B), which, however, increases the form factor of the tag for large $\bar{M}$. On the other hand, sparse coding can represent $\bar{M}$-ary data with a few constellation symbols using the codeword projection/expansion approach. Therefore, tags can implement $\bar{M}$-ary modulation without affecting their form factors.

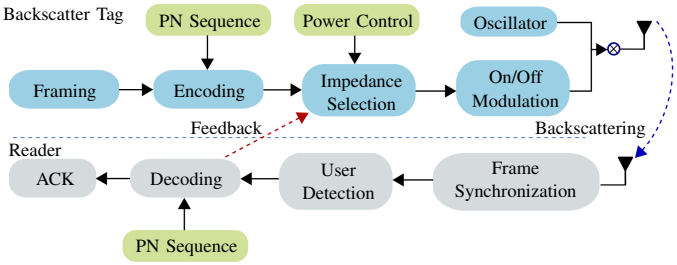

Fig. 29: Structure of the backscatter tag and the receiver for coded backscatter [221].

The duty cycle is defined as the ratio between the times taken to transmit data and harvest RF energy. It can be exploited to support massive connectivity by utilizing sparse coding and NOMA [124], [220] In addition, the data rates of backscatter tags tend to be low. Thus, when tags modulate their data signals via high-rate legacy RF signals, the latter becomes a virtual spreading sequence that provides a diversity gain [124]. Therefore, the combination of SCMA and BackCom may achieve the goals of massive connectivity, high data rates, and cooperative diversity, which can help to achieve IoT networks [124].

B. Coded-Backscatter Multiple Access

To meet the requirements of high capacity and distributed control of large-scale networks, in [221], a coded-backscatter multiple access (CBMA) scheme has been proposed based on a direct sequence spread spectrum, which is resistant to fading and can support simultaneous transmissions. CBMA employs a correlation-based detector because it is challenging to coordinate all tags via sending control signals, resulting

in asynchronous transmission, which significantly impacts the spread sequence's orthogonality [221]. The backscatter signal is weak and strongly affected by the distance between the tag and the reader, degrading performance because of the well-known near-far effect. The tag may not use conventional power control because of its circuit limitations and not having RF circuits to generate RF signals. Thus, CBMA helps in this context by allowing the tags to adjust their antenna impedance to achieve a power control mechanism [221].

CBMA utilizes pseudo-noise (PN) codes to encode tag data like asynchronous code division multiple access (CDMA). Unlike synchronous CDMA, if all tag signals have the same received power, the signals from other tags will appear as noise when the reader decodes one tag's signal. Therefore, the power control scheme adaptively adjusts the tag impedance to optimize the overall system capacity. The backscatter tag performs framing, encoding, power selection (impedance selection), on/off modulation, and frequency shifting. The encoding block at the tag uses a PN code to generate the transmit bit sequence. For instance, if the tag transmits "10" with a PN code "01001", the encoded data is then "0100110110". The tag transmits this sequence via on/off modulation. The reader exploits the mutual orthogonality of PN sequences to decode the data (Fig. 29). This scheme can achieve a multi-tag bit rate up to 8 Mbps with tag-receiver distance up to $5\,\mathrm{m}$.

C. Buzz Multiple Access

Due to limited tag resources, there are two major challenges in deploying BackCom networks.

1) *Device Identification*: a tag depends on the reader to schedule its medium access because they cannot hear other tags [222]. However, the reader does not know which tag wants to transmit. As a result, current backscatter systems use an identification phase before access, which consumes significant time, e.g., the RFID EPC Gen 2 standard requires $30\%-60\%$ of transmission time for device identification [5]. At a high level, the reader splits the total time into slots, and each tag that wants to transmit selects a random temporary ID and transmits it in a random slot. Some tag signals may then collide. Collisions must be eliminated to improve the reliability. However, to avoid collisions, the total number of time slots must be fairly large, which reduces spectral efficiency because of the number of unoccupied slots.
2) *Rate Adaptation*: Due to their ultra-low power, tags employ passive backscatter modulation of on-off keying and BPSK [65]. This limits the capacity of tags to adapt their rate depending on channel conditions, i.e., they cannot transmit more bits per symbol to boost the bandwidth efficiency when the channel is better, and also to drop the bit rate in a poor channel to improve the robustness [223]. Such adaptation requires the reader to send feedback to each tag to adjust its redundancy level. However, since backscatter signals are short and bursty, such feedback is not cost-effective [222].

Therefore, to improve both reliability and efficiency, Buzz multiple access has been developed [220]. It considers tags as if they were a single virtual sender, and then treats collisions as a code across the bits sent by different tags. However, instead of simply allowing tags to collide repeatedly, resulting in multiple copies of the same collision and hence ineffective decoding, Buzz allows each tag to transmit only in a small random subset of collisions. This also reduces the amount of overhead on the tags themselves. Thus, the resultant code is sparse and rateless, which means that nodes can collide indefinitely until the reader acquires enough collisions to decode [220]. Consequently, Buzz makes use of the code's sparsity and ratelessness to enable fast identification and distributed rate adaptation. Moreover, Buzz considers the entire network and adapts the aggregate bit rate of all backscatter tags to channel conditions. In Buzz, since each tag only contributes to a small random subset of collisions, the resulting sparse codes with a low density can be decoded using a linear time decoder based on belief propagation, similar to LDPC codes. Nonetheless, unlike LDPC codes, which are centralized block codes, codes of Buzz are distributed as well as rateless. Because of these properties, Buzz enables automated bit rate adaptation in BackCom [220].

D. μ-Code

Some of the conventional coding principles can be leveraged to increase the BackCom range. For example, CDMA uses a pseudo-random sequence to encode the information; and the receiver synchronizes with the transmit signal and decodes the information by correlating with the pseudo-random codes. However, the tag may find correlation and synchronization are complicated and challenging. Thus, these conventional coding approaches must be modified for BackCom systems. To this end, reference [224] introduces a low-power encoding technique to increase the communication range and ensure concurrent transmissions for AmBC. The μ code employs a periodic signal rather than a pseudo-random sequence to represent data. The intuition is that periodic signals can be detected without the need for phase synchronization when the receiver knows their frequency. Hence, a code is designed to mimic the sine wave. Since the backscatter tag supports only two states, i.e., absorbing and reflecting states, a periodic alternating sequence of bits "0" and "1" is adopted. Specifically, the one bit is encodes by the chip sequence "$101010\cdots10$" and the zero bit is encoded by the chip sequence "$0000\cdots00$". Moreover, a decoding algorithm is designed which can decode the backscatter signal with neither phase information nor analog-to-digital Converters.

The receiver design has four main components: an envelope detector circuit, In-phase (I)/ Quadrature phase (Q) correlation circuits to compute $|I|$ and $|Q|$, an addition circuit to compute $|I|+|Q|$ and a thresholding circuit that outputs "0" and "1" bits. This structure enables backscatter tags to communicate directly with each other at distances of tens of meters and while separated by multiple walls. It can also provide orders of magnitude increase in the communication rate and range of AmBC systems. In particular, with $1\,\mathrm{kHz}$ analog hardware, RFID tags can mutually communicate at a rate of 3.33 bps at ranges greater than 90 feet, given an incident RF power of

TABLE XI: Multiple access coding techniques.

Ref.	Coding technique	Setup	Tag type	Number of tags	Data rate	Distance
[124]	SCMA	AmBC	Passive	8	8.26 Mbps†	5 m
[220]	Buzz	MoBC	Passive/Semi-passive	16	Rateless	<1.8 m
[221]	CBMA	AmBC	Active	10	8 Mbps†	≤5 m
[224]	μ-code	AmBC	Passive	–	1 kbps‡	<24.4 m
[225]	NetScatter	MoBC	Active	256	500 kbps†	2 m

† Throughput, ‡ Per tag.

0 dBm. Moreover, it supports multiple concurrent transmissions in a battery-free tag network.

E. Distributed Chirp Spread Spectrum Coding

Achieving a reliable and high coverage transmission for a tag is a challenging task due to the weak backscatter signal, which may be near to or below the noise level. Therefore, establishing reliable connectivity of many tags is even more difficult. To accomplish this goal, reference [225] proposes NetScatter, a unique network protocol with a multiple access coding scheme. It combines chirp spread spectrum modulation and on-off keying. It can support up to a thousand concurrent tags while requiring just 2 MHz of total bandwidth, and the coding scheme satisfies four essential constraints: (i) it allows hundreds of devices to transmit simultaneously on the same frequency band, (ii) it can operate below the noise level while maintaining reasonable bit rates, (iii) low-power tags perform the coding procedure, and (iv) the reader can decode all tag signals with a single fast Fourier transform operation, reducing receiver complexity. In contrast, the AP of an existing chirp spread spectrum system transmits a continuous wave signal to each tag for backscattering and encoding bits with distinct chirp cyclic shifts. The method [225] allocates a separate chirp cyclic shift to each concurrent device. Each tag then conveys bits by using on-off keying over these cyclically shifted chirps. Additionally, in existing chirp spread spectrum systems with N_D number of tags, each one sends $\log_2(N_D)$ bits using N_D cyclic shifts, whereas the proposed design allows for N_D concurrent tags, each of which transmits a single bit utilizing on-off keying, resulting in a potential gain of $N_D/\log_2(N_D)$. However, practical implementation of this system is difficult due to two reasons.

1) *Near-Far Effect*: The signal from a nearby tag can dominate the signal from a tag far away.
2) *Timing Synchronization*: It is difficult to accurately synchronize hundreds of tags in time due to hardware variations and propagation delays of different tags.

Reference [225] provides several techniques to overcome those issues: (i) a power-aware cyclic shift allocation method in which lower SNR tags employ different cyclic shifts than higher SNR tags, (ii) a zero-overhead power adaptation technique that accounts for channel variations over time by having backscatter devices estimate their SNR at the AP using the signal intensity of the AP's query signal, and (iii) to address the time synchronization issue, introduce gaps between cyclic shifts to guarantee that concurrent tags can be distinguished and decoded.

Table XI summarizes BackCom multiple access codes.

Remark 2. *The concurrent transmissions of multiple tags by exploiting coding schemes might incur overhead on the tag side [226]. One solution is to extend the reader's decoding capacity and shift the workload from the tag to the reader [226]–[230]. Specifically, reference [226] design a parallel decoding scheme where the reader decodes the collided tag signals according to signals' transition probabilities between different combined states, which are shown to be highly stable and traceable*[18]*. A graphical model is thus constructed based on the trajectory of the signals in the I-Q domain, and the collided tags are then decoded by tracking the graph. This approach can work and resolve the collided signals under highly dynamic and unpredictable backscatter systems without relying on the stability of signal features. In particular, in a* 5*-tag collision case, the throughput of* 450 kbps *is achieved.*

Discussion: BackCom systems require innovative codes to achieve massive connectivity. SCMA, CBMA, Buzz multiple access, μ code, and distributed chirp spread spectrum coding support this goal. These schemes are explicitly designed for BackCom while considering its limitations and channel characteristics. Thus, they can provide massive connectivity, high capacity, enhanced reliability and efficiency, and extended communication range. Parallel decoding also supports these goals by extending the reader's decoding capacity.

VIII. Open Issues and Future Research Directions

BackCom research has advanced its capabilities and coexistence with other wireless technologies. However, suitable coding standards are yet to emerge. Thus, this section outlines some challenges, open issues, and future research directions.

A. Encoder and Decoder Complexity

The complexity of a channel encoder and decoder impacts hardware resource requirements and energy consumption. In 5G NR, mMTC applications impose strict complexity restrictions, especially for passive tags (Section II-A). Thus, these IoT devices must work continuously without recharging while requiring minimal hardware resources and energy. These constraints impact the channel encoder and decoder [89].

Existing channel codes (Section V) require numerous computational resources, significant power, and accurate channel

[18]A typical backscatter tag encodes its data by reflecting and absorbing the carrier wave, resulting in two possible states: High and Low; a N_D-tag collision case creates 2^{N_D} combined states, each state is a linear combination of N_D tag's signal state, i.e., $\mathbf{S} = [S_1, \ldots, S_{N_D}]$, where S_i = High or Low.

estimation. Hence, adapting such codes to power-constrained, low-complexity backscatter tags brings many practical challenges [142]. For instance, these codes incur significant encoding overhead (e.g., storing the generating matrix). Rate adaptation codes require the transmitter to adjust the code rate depending on the channel state. However, CSI estimation is difficult because of tag hardware limitations. On the other hand, reducing the decoding complexity will decrease the latency and power consumption, but at the penalty of increasing BER. These trade-offs call for careful design of low-complexity encoders and decoders while taking into account tag limitations [142]. For instance, to reduce the encoding complexity and storage requirements of rate adaptation codes, coding matrices for several code lengths can be generated by matrix iterations, instead of storing them [142]. Besides, optimal code designs can be shifted from the tag to the reader, and the results can be fed back to the tag [143]. GRAND decoders also offer low complexity and delays with good BER performance [195].

B. Reliability

Reliability is the accuracy of delivered information bits from one node to another within a specified latency constraint [231], [232]. Increasing it reduces retransmissions and latency. However, if mMTC and other IoT systems use backscatter, reliability is affected by wireless interference, eavesdropping, routing issues, distance limitations, and others. Although channel coding can mitigate them, significant research advances may be needed.

To find viable codes for BackCom, the following four factors are important: (i) a low error floor, (ii) simple decoding algorithms with simple hardware realizations, (iii) high throughput decoding, and (iv) the burst error correction capability [232]. Thus, increasing the minimum Hamming distance, using concatenated or derived codes, adopting optimized decoding algorithms, and integrating interleaving/de-interleaving, have been tried [232]. Specifically, non-binary codes, e.g., non-binary polar codes [233], increase the minimum Hamming distance. Thus, they achieve higher error-correcting ability, and non-binary symbols map readily to high-order modulations [234]. Concatenated RS and polar codes [235], [236], can improve the BER and reduce the error floor, depending on different combinations of inner and outer code rates. Parallel decoding structures and sophisticated low-complexity decoding algorithms can also reduce latency and power consumption while reducing the BER [237].

However, such coding techniques may have to be carefully adopted for BackCom because of the dyadic path-loss and the limited capability of tags. Hence, further research is needed.

C. Physical Layer Security

Critically, 6G technologies need enhanced security and privacy [238]. However, because tags have limited computing and communication capabilities, BackCom systems cannot support robust protection schemes with highly secure encryption. Thus, they are vulnerable to potential security attacks, reducing their performance and reliability [239]–[241]. The most common such attacks are jamming, eavesdropping, and detection of covert (DoC). Jamming is an active attack that intentionally causes malfunctions (e.g., denial of service). For instance, an attacker can generate artificial noise to cause the target nodes to suffer from the denial of service as long as their operating channels can be identified. By contrast, eavesdropping and DoC are passive forms of attack, which extract private information or detect the presence of a target by monitoring wireless channels. Compared with active attacks, passive attacks are challenging to detect [240].

Physical layer security techniques, which exploit properties of the wireless medium to achieve secure communication, are another solution for BackCom [240]. For instance, strong jamming signals can be leveraged to facilitate BackCom. The tag can then harvest energy from them for its operations [242]–[244]. Deception strategies defend against the jammers that only attack the channels once they detect the activities of target nodes. For instance, the tag sends a fake signal to mislead the jammers and weaken them by wasting their energy [245]. Beamforming design, transmit antenna selection, directional transmission, artificial noise generation, and relay-aided transmission are some other physical-layer techniques [240]. In particular, to combat eavesdropping attacks, the legitimate transmitter may adopt a beamforming design to direct the information signals towards its legitimate destinations and the artificial noise signals towards illegitimate destinations, thereby improving the secrecy rate [246]. In addition, depending on the channel condition, the legitimate transmitter may select one (or more) of its antennas to transmit artificial noise to jam the eavesdropper while causing minimal interference to its legitimate destinations [247].

The adaptation of sophisticated codes can also contribute to security enhancement [238]. However, the inherent characteristics of BackCom networks are (1) the tags have limited energy availability and limited processing capabilities and (2) the cascaded channels cause deeper fading events. Thus, designing secure channel codes that match these inherent characteristics is still an open problem. One possibility may be developing secure polar coding schemes.

D. Machine Learning for Channel Coding

Machine learning techniques are increasingly being leveraged in wireless networks. Their application for coded systems is emerging [248]–[253]. For example, neural decoders trained using gradient-based methods [249] can improve the belief propagation (BP) algorithm. This approach generalizes the basic BP algorithm by assigning weights to the edges of the Tanner graph, which are subsequently trained using deep learning techniques. These decoders can learn both the channel and the linear code simultaneously, improving decoder performance without increasing computational complexity [249]. Moreover, [250] proposes a concatenated polar and LDPC code. It encodes data blocks with a polar code and applies an LDPC code. The receiver first applies the Belief propagation algorithm to recover each LDPC codeword. This decoded sequence is subsequently segmented and fed into multiple parallel deep neural networks for further decoding, which reduces

decoding delays. This scheme has a reduced time complexity and provides BER gains [250], [254]. In particular, AmBC systems, which rely on legacy ambient signals, can use a separate channel coding scheme on top of the primary system's channel coding scheme, and the receiver can recover data from both systems using a machine learning-based decoder. Overall, there is ample room for further development of machine-learning coding techniques in the BackCom space.

Machine learning-based signal detection may overcome the necessity for channel estimate in traditional BackCom signal detection methods [255]. They aim to use only a few (training) pilots without explicitly estimating relevant channel parameters. Specifically, signal detection algorithms for AmBC systems are developed in [256]–[260]. To this end, the signal detection problem can be transformed into a clustering problem [256]. As a result, two constellation learning-based signal detection algorithms are developed for when the tags reflect constellation-modulated ambient RF signals. Moreover, the authors in [257] develop supervised machine learning techniques, including the support vector machine and the random forest method. Moreover, reference [258] uses a deep transfer learning approach to detect the tag's signal. The works [259] and [260] further address the channel estimation. The pilot-based channel estimation problem is modeled as a denoising problem. A deep residual learning approach is developed to learn the residual noise and recover the channel coefficients from the noisy pilot signals. This method achieves the performance of the optimal minimum mean square error (MMSE) estimator given the knowledge of the channel correlation matrix.

E. Synchronization

This refers to the timing alignment between the transmitter and receiver. Timing offsets and carrier frequency offsets cause synchronization errors. Tight synchronization enables the functioning of multiple access schemes and serves many purposes, including location, proximity, energy efficiency, mobility, and others. Synchronization among massive numbers of devices is challenging because of hardware variations and propagation delays. Erroneous synchronization reduces achievable throughput and communication range while increasing inter-symbol interference (ISI).

In the context of BackCom networks, tags must be able to synchronize using incident RF signals. However, synchronization is computationally expensive, and the power consumption increases exponentially at lower incoming signal power levels [213]. Tags may not synchronize well because of their limited hardware and the passive modulation [213]. Thus, much more research is needed on this topic.

Wi-Fi backscattering may use a simple low-power energy detector synchronization scheme, but with low accuracy (of $2\,\mu\mathrm{s}$ at $-20\,\mathrm{dBm}$ input power) [261]. The only work that explicitly investigates the accurate synchronization of BackCom with Wi-Fi is reference [213]. Hence, effective strategies and techniques for BackCom based on various wireless standards must be identified to achieve the minimum required synchronization accuracy and desired high sensitivity with μW level power consumption. Furthermore, synchronization schemes that allow multiple tags to coexist without mutual interference must be investigated further [262].

F. Interference Management/Mitigation

Unlike in conventional channels, interference regeneration occurs in BackCom. The reason is that a backscatter tag reflects all incident signals and interference signals [263]. The reflected signal has the same frequency as the carrier signal (unless the tag shifts the frequency). This causes direct link interference for BackCom systems while generating additional interference for the primary system, particularly in AmBC [264], [265]. Because the same device is used for transmission and reception, the same primary interference causes self-interference in MoBC. Since the tags reflect modulated or unmodulated carrier signals, the amount of interference also depends on the locations of primary transmitters and backscatter tags, as well as the primary transmit power [264]. Multiple access interference and co-channel interference (CCI) are other major limiting factors in large-scale BackCom systems. The former occurs when multiple tags transmit in the same frequency resource, whereas CCI occurs in links that reuse the same frequency channel. To limit interference on primary (legacy) networks, tags may communicate over spectrum holes, which may be identified via energy detection [266]–[268]. Thus, more dynamic and opportunistic spectrum usage by tags should be further investigated.

These interference signals can affect the performances of both the AmBC system and the primary system [263]–[265], [269]. Hence, it is essential to analyze the statistics of these interference distributions and their impact on the primary and BackCom system performances. To do this, research must model and analyze BackCom-generated interference. One analytical tool is the theoretical framework of stochastic geometry. It gives tools for analyzing and modeling the spatial distribution of wireless nodes [265], [270].

Managing interference is possible with spread spectrum techniques in BackCom, taking advantage of its low data rates [263], [271]. Furthermore, interference alignment and interference cancellation techniques also can be used [272]. Large-scale BackCom networks can manage interference through position management, frequency allocation, communication range control, scheduling, and multiple-access schemes.

IX. Conclusion

Coding schemes can improve the reliability and range of BackCom. This paper thus presented a comprehensive overview of such channel codes. First, we reviewed the fundamentals of BackCom and channel codes and their relevant design considerations/parameters. To set the background for potential BackCom codes, we first examined common coding schemes for general communication networks. We addressed the limitations and requirements of BackCom systems and the characteristics of BackCom channels. We identified potential BackCom codes and discussed the multiple access coding schemes. We highlighted potential solutions for dealing with code complexity and reliability. Finally, we discussed some

open issues, challenges, and potential future research directions.

REFERENCES

[1] H. Stockman, "Communication by means of reflected power," *Proc. of the IRE*, vol. 36, no. 10, pp. 1196–1204, 1948.

[2] V. Liu, A. Parks, V. Talla, S. Gollakota, D. Wetherall, and J. R. Smith, "Ambient backscatter: Wireless communication out of thin air," *ACM SIGCOMM Comput. Commun. Rev.*, vol. 43, no. 4, p. 39–50, Aug. 2013. [Online]. Available: https://doi.org/10.1145/2534169.2486015

[3] D. T. Hoang, D. Niyato, D. I. Kim, N. V. Huynh, and S. Gong, *Ambient Backscatter Communication Networks*. Cambridge University Press, 2020.

[4] "3GPP TSG RAN Meeting −94e, Study proposal on Passive IoT, 8A.1 (from RP-213368)," Dec. 2021. Available Online: https://www.3gpp.org/DynaReport/TDocExMtg--RP-94-e--60214.htm.

[5] "EPC radio-frequency identity protocols generation-2, UHF RFID standard, specification for RFID air interface protocol for, communications at 860-960 MHz," July 2018. Available Online: https://www.gs1.org/sites/default/files/docs/epc/gs1-epc-gen2v2-uhf-airinterface_i21_r_2018-09-04.pdf.

[6] D.-L. Yang, F. Liu, and Y.-D. Liang, "A survey of the internet of things," in *Proc. of the 1st Int. Conf. on E-Business Intelli. (ICEBI 2010)*. Atlantis Press, Dec. 2010/12, pp. 524–532. [Online]. Available: https://doi.org/10.2991/icebi.2010.72

[7] A. Al-Fuqaha, M. Guizani, M. Mohammadi, M. Aledhari, and M. Ayyash, "Internet of things: A survey on enabling technologies, protocols, and applications," *IEEE Commun. Surveys Tuts.*, vol. 17, no. 4, pp. 2347–2376, 4th Quart. 2015.

[8] "RFID market by offering (tags, readers, software & services), tag type (passive, active), wafer size, frequency, form factor (card, implant, key fob, label, paper ticket, band), material, application & region - global forecast to 2030," Available Online: https://www.marketsandmarkets.com/Market-Reports/rfid-market-446.html.

[9] "3GPP TR 38.913 - 5G; study on scenarios and requirements for next generation access technologies, V14.3.0 Rel. 14," Aug. 2017. Available Online: https://portal.3gpp.org/desktopmodules/Specifications/SpecificationDetails.aspx?specificationId=2996.

[10] M. Stoyanova, Y. Nikoloudakis, S. Panagiotakis, E. Pallis, and E. K. Markakis, "A survey on the internet of things (IoT) forensics: challenges, approaches, and open issues," *IEEE Commun. Surveys Tuts.*, vol. 22, no. 2, pp. 1191–1221, 2th Quart. 2020.

[11] M. Dohler and T. Nakamura, *5G Mobile and Wireless Communications Technology*, A. Osseiran, J. F. Monserrat, and P. Marsch, Eds. Cambridge University Press, 2016.

[12] "Massive machine type communication market - growth, trends, covid-19 impact, and forecasts (2022 - 2027)," Jan. 2022. Available Online: https://www.researchandmarkets.com/reports/5239364/massive-machine-type-communication-market.

[13] P. Andres-Maldonado, P. Ameigeiras, J. Prados-Garzon, J. Navarro-Ortiz, and J. M. Lopez-Soler, "Narrowband IoT data transmission procedures for massive machine-type communications," *IEEE Netw.*, vol. 31, no. 6, pp. 8–15, Nov. 2017.

[14] N. Xia, H.-H. Chen, and C.-S. Yang, "Emerging technologies for machine-type communication networks," *IEEE Netw.*, vol. 34, no. 1, pp. 214–222, 2020.

[15] S. Andreev *et al.*, "Understanding the IoT connectivity landscape: a contemporary M2M radio technology roadmap," *IEEE Commun. Mag.*, vol. 53, no. 9, pp. 32–40, 2015.

[16] W. Zhou, Y. Jia, A. Peng, Y. Zhang, and P. Liu, "The effect of IoT new features on security and privacy: New threats, existing solutions, and challenges yet to be solved," *IEEE Internet Things J.*, vol. 6, no. 2, pp. 1606–1616, Apr. 2019.

[17] K. Shafique, B. A. Khawaja, F. Sabir, S. Qazi, and M. Mustaqim, "Internet of things (IoT) for next-generation smart systems: A review of current challenges, future trends and prospects for emerging 5G-IoT scenarios," *IEEE Access*, vol. 8, pp. 23 022–23 040, Jan. 2020.

[18] Qualcomm, "Setting off the 5G advanced evolution," Jan. 2022. Available Online: https://www.qualcomm.com/news/onq/2021/12/10/setting-5g-advanced-evolution.

[19] "3GPP TSG Meeting −95e, New SID: Study on ambient power-enabled Internet of Things, SA1 (from SP-220085)," Mar. 2022. Available Online: https://portal.3gpp.org/ngppapp/TdocList.aspx?meetingId=60289.

[20] D. Ma, G. Lan, M. Hassan, W. Hu, and S. K. Das, "Sensing, computing, and communications for energy harvesting IoTs: A survey," *IEEE Commun. Surveys Tuts.*, vol. 22, no. 2, pp. 1222–1250, 2th Quart. 2020.

[21] N. H. Mahmood *et al.*, "White paper on critical and massive machine type communication towards 6G," *arXiv preprint arXiv:2004.14146*, Apr. 2020.

[22] C. Bockelmann *et al.*, "Massive machine-type communications in 5G: Physical and MAC-layer solutions," *IEEE Commun. Mag.*, vol. 54, no. 9, pp. 59–65, Sep. 2016.

[23] R. Duan, X. Wang, H. Yigitler, M. U. Sheikh, R. Jantti, and Z. Han, "Ambient backscatter communications for future ultra-low-power machine type communications: Challenges, solutions, opportunities, and future research trends," *IEEE Commun. Mag.*, vol. 58, no. 2, pp. 42–47, Feb. 2020.

[24] N. Van Huynh, D. T. Hoang, X. Lu, D. Niyato, P. Wang, and D. I. Kim, "Ambient backscatter communications: A contemporary survey," *IEEE Commun. Surveys Tuts.*, vol. 20, no. 4, pp. 2889–2922, 4th Quart. 2018.

[25] F. Rezaei, C. Tellambura, and S. Herath, "Large-scale wireless-powered networks with backscatter communications—A comprehensive survey," *IEEE open j. Commun. Soc.*, vol. 1, pp. 1100–1130, July 2020.

[26] D. Kim, M. Ingram, and W. Smith, "Measurements of small-scale fading and path loss for long range RF tags," *IEEE Trans. Antennas Propag.*, vol. 51, no. 8, pp. 1740–1749, Aug. 2003.

[27] "3GPP TS 25.212 - universal mobile telecommunications system (UMTS); multiplexing and channel coding (FDD), V10.1.0 Rel. 10," May. 2011. Available Online: https://www.etsi.org/deliver/etsi_ts/125200_125299/125212/10.01.00_60/ts_125212v100100p.pdf.

[28] "3GPP TS 36.212 - LTE; evolved universal terrestrial radio access (E-UTRA); multiplexing and channel coding, V13.8.0 Rel. 13," July. 2018. Available Online: https://www.etsi.org/deliver/etsi_ts/136200_136299/136212/13.08.00_60/ts_136212v130800p.pdf.

[29] "3GPP TS 38 212 - 5G; NR; multiplexing and channel coding, V16.2.0 Rel.16," July 2020. Available Online: https://www.etsi.org/deliver/etsi_ts/138200_138299/138212/16.02.00_60/ts_138212v160200p.pdf.

[30] "3GPP TS 38.212 - technical specification group radio access network; NR; multiplexing and channel coding, V17.2.0 Rel. 17," June 2022. Available Online: https://portal.3gpp.org/desktopmodules/Specifications/SpecificationDetails.aspx?specificationId=3214.

[31] M. C. Coşkun *et al.*, "Efficient error-correcting codes in the short blocklength regime," *Physical Commun.*, vol. 34, pp. 66–79, June 2019.

[32] S. L. Howard, C. Schlegel, K. Iniewski, and K. Iniewski, "Error control coding in low-power wireless sensor networks: When is ECC energy-efficient?" *EURASIP J. Wireless Commun. Netw.*, vol. 2006, pp. 1–14, Dec. 2006.

[33] M. Xhemrishi, M. C. Coşkun, G. Liva, J. Östmanl, and G. Durisi, "List decoding of short codes for communication over unknown fading channels," in *53rd Asilomar Conf. Signals, Systems, and Comput.* IEEE, Nov. 2019, pp. 810–814.

[34] D. A. Galappaththige, F. Rezaei, C. Tellambura, and S. Herath, "Link budget analysis for backscatter-based passive IoT," *IEEE Access*, vol. 10, pp. 128 890–128 922, Dec. 2022.

[35] M. L. Memon, N. Saxena, A. Roy, and D. R. Shin, "Backscatter communications: Inception of the battery-free era—a comprehensive survey," *Electronics*, vol. 8, no. 2, p. 129, Jan. 2019.

[36] T. S. Muratkar, A. Bhurane, and A. Kothari, "Battery-less internet of things–a survey," *Computer Networks*, vol. 180, p. 107385, Oct. 2020.

[37] J.-P. Niu and G. Y. Li, "An overview on backscatter communications," *J. Commun. Inf. Netw.*, vol. 4, no. 2, pp. 1–14, June 2019.

[38] C. Yao, Y. Liu, X. Wei, G. Wang, and F. Gao, "Backscatter technologies and the future of internet of things: Challenges and opportunities," *Intelligent and Converged Networks*, vol. 1, no. 2, pp. 170–180, Sep. 2020.

[39] C. Xu, L. Yang, and P. Zhang, "Practical backscatter communication systems for battery-free internet of things: A tutorial and survey of recent research," *IEEE Signal Process. Mag.*, vol. 35, no. 5, pp. 16–27, Sep. 2018.

[40] U. S. Toro, K. Wu, and V. C. M. Leung, "Backscatter wireless communications and sensing in green internet of things," *IEEE Trans. Green Commun. Netw.*, vol. 6, no. 1, pp. 37–55, Mar. 2022.

[41] C. Song *et al.*, "Advances in wirelessly powered backscatter communications: From antenna/RF circuitry design to printed flexible electronics," *Proc. IEEE*, vol. 110, no. 1, pp. 171–192, Jan. 2022.

[42] J. Kimionis, A. Bletsas, and J. N. Sahalos, "Increased range bistatic scatter radio," *IEEE Trans. Commun.*, vol. 62, no. 3, pp. 1091–1104, Mar. 2014.

[43] V. Chawla and D. S. Ha, "An overview of passive RFID," *IEEE Commun. Mag.*, vol. 45, no. 9, pp. 11–17, Sep. 2007.

[44] X. Lu, D. Niyato, H. Jiang, D. I. Kim, Y. Xiao, and Z. Han, "Ambient backscatter assisted wireless powered communications," *IEEE Wireless Commun.*, vol. 25, no. 2, pp. 170–177, Jan. 2018.

[45] G. Yang, Y.-C. Liang, R. Zhang, and Y. Pei, "Modulation in the air: Backscatter communication over ambient OFDM carrier," *IEEE Trans. Commun.*, vol. 66, no. 3, pp. 1219–1233, Mar. 2018.

[46] R. Long, Y.-C. Liang, H. Guo, G. Yang, and R. Zhang, "Symbiotic radio: A new communication paradigm for passive internet of things," *IEEE Internet Things J.*, vol. 7, no. 2, pp. 1350–1363, Feb. 2020.

[47] D. Bharadia, K. R. Joshi, M. Kotaru, and S. Katti, "Backfi: High throughput Wi-Fi backscatter," *ACM SIGCOMM Comput. Commun. Rev.*, vol. 45, no. 4, p. 283–296, Aug. 2015. [Online]. Available: https://doi.org/10.1145/2829988.2787490

[48] "TV query broadcast station search," 2018. Available Online: https://transition.fcc.gov/fcc-bin/tvq?list=0&facid=69571.

[49] "3GPP TS 36.104, LTE; Evolved universal terrestrial radio access (E-UTRA); base station (BS) radio transmission and reception, V15.3.0 Rel. 15," July 2018. Available Online: https://portal.3gpp.org/desktopmodules/Specifications/SpecificationDetails.aspx?specificationId=2412.

[50] G. Wang, F. Gao, R. Fan, and C. Tellambura, "Ambient backscatter communication systems: Detection and performance analysis," *IEEE Trans. Commun.*, vol. 64, no. 11, pp. 4836–4846, Nov. 2016.

[51] C. Boyer and S. Roy, "Backscatter communication and RFID: Coding, energy, and MIMO analysis," *IEEE Trans. Commun.*, vol. 62, no. 3, pp. 770–785, Mar. 2014.

[52] G. Vannucci, A. Bletsas, and D. Leigh, "A software-defined radio system for backscatter sensor networks," *IEEE Trans. Wireless Commun.*, vol. 7, no. 6, pp. 2170–2179, June 2008.

[53] "RFID World." Available Online: https://rfidworldcapr.wpengine.com/.

[54] "GAO RFID Inc." Available Online: https://gaorfid.com/.

[55] J. Qian, A. N. Parks, J. R. Smith, F. Gao, and S. Jin, "IoT communications with M-PSK modulated ambient backscatter: Algorithm, analysis, and implementation," *IEEE Internet Things J.*, vol. 6, no. 1, pp. 844–855, Feb. 2019.

[56] S. J. Thomas, E. Wheeler, J. Teizer, and M. S. Reynolds, "Quadrature amplitude modulated backscatter in passive and semipassive UHF RFID systems," *IEEE Trans. Microw. Theory Techn.*, vol. 60, no. 4, pp. 1175–1182, 2012.

[57] S. J. Thomas and M. S. Reynolds, "A 96 Mbit/sec, 15.5 pJ/bit 16-QAM modulator for UHF backscatter communication," in *IEEE Int. Conf. RFID*, 2012, pp. 185–190.

[58] E. Gong, H. Zhang, X. Chen, L. Ye, and R. Huang, "2.4-GHz 16-QAM passive backscatter transmitter for wireless self-power chips in IoT," in *IEEE Int. Symposium Circuits Syst. (ISCAS)*, 2020, pp. 1–5.

[59] A. Shirane *et al.*, "RF-powered transceiver with an energy- and spectral-efficient IF-based quadrature backscattering transmitter," *IEEE J. Solid-State Circuits*, vol. 50, no. 12, pp. 2975–2987, 2015.

[60] R. Reed, F. L. Pour, and D. S. Ha, "An energy efficient RF backscatter modulator for IoT applications," in *IEEE Int. Symposium on Circuits and Syst. (ISCAS)*, Apr. 2021, pp. 1–5.

[61] A. Bletsas, A. G. Dimitriou, and J. N. Sahalos, "Improving backscatter radio tag efficiency," *IEEE Trans. Microw. Theory Techn.*, vol. 58, no. 6, pp. 1502–1509, May 2010.

[62] P. N. Alevizos, A. Bletsas, and G. N. Karystinos, "Noncoherent short packet detection and decoding for scatter radio sensor networking," *IEEE Trans. Commun.*, vol. 65, no. 5, pp. 2128–2140, May 2017. [Online]. Available: https://doi.org/10.1109/TCOMM.2017.2665494

[63] N. Fasarakis-Hilliard, P. N. Alevizos, and A. Bletsas, "Coherent detection and channel coding for bistatic scatter radio sensor networking," *IEEE Trans. Commun.*, vol. 63, no. 5, pp. 1798–1810, May 2015.

[64] A. Lozano-Nieto, *RFID Design Fundamentals and Applications*, 1st ed. Boca Raton, FL: CRC Press, 2011.

[65] K. Finkenzeller, *RFID Handbook: Fundamentals and Applications in Contactless Smart Cards, Radio Frequency Identification and Near-Field communication*. John wiley and sons, Nov. 2010.

[66] M. Ouroutzoglou, G. Vougioukas, G. N. Karystinos, and A. Bletsas, "Multistatic noncoherent linear complexity Miller sequence detection for Gen2 RFID/IoT," *IEEE Trans. Wireless Commun.*, vol. 20, no. 12, pp. 8067–8080, Dec. 2021.

[67] A. Quddious, M. A. Antoniades, P. Vryonides, and S. Nikolaou, "Voltage-doubler RF-to-DC rectifiers for ambient RF energy harvesting and wireless power transfer systems," in *Recent Wireless Power Transfer Techn.*, P. Pinho, Ed. Rijeka: IntechOpen, Nov. 2019, ch. 10. [Online]. Available: https://doi.org/10.5772/intechopen.89271

[68] L. Ramalingam *et al.*, "The advancement of radio frequency energy harvesters (RFEHs) as a revolutionary approach for solving energy crisis in wireless communication devices: A review," *IEEE Access*, vol. 9, pp. 106 107–106 139, July 2021.

[69] X. Lu, P. Wang, D. Niyato, D. I. Kim, and Z. Han, "Wireless networks with RF energy harvesting: A contemporary survey," *IEEE Commun. Surveys Tuts.*, vol. 17, no. 2, pp. 757–789, 2th Quart. 2015.

[70] A. C. C. Chun, H. Ramiah, and S. Mekhilef, "Wide power dynamic range CMOS RF-DC rectifier for RF energy harvesting system: A review," *IEEE Access*, vol. 10, pp. 23 948–23 963, Feb. 2022.

[71] R. Zhang and C. K. Ho, "MIMO broadcasting for simultaneous wireless information and power transfer," *IEEE Trans. Wireless Commun.*, vol. 12, no. 5, pp. 1989–2001, May 2013.

[72] P. Lu, K. Huang, C. Song, Y. Ding, and G. Goussetis, "Optimal power splitting of wireless information and power transmission using a novel dual-channel rectenna," *IEEE Trans. Antennas Propag.*, vol. 70, no. 3, pp. 1846–1856, Mar. 2022.

[73] Y. Dong, M. J. Hossain, and J. Cheng, "Performance of wireless powered amplify and forward relaying over Nakagami-m fading channels with nonlinear energy harvester," *IEEE Commun. Lett.*, vol. 20, no. 4, pp. 672–675, Feb. 2016.

[74] Y. Chen, K. T. Sabnis, and R. A. Abd-Alhameed, "New formula for conversion efficiency of RF EH and its wireless applications," *IEEE Trans. Veh. Technol.*, vol. 65, no. 11, pp. 9410–9414, Jan. 2016.

[75] B. Clerckx and E. Bayguzina, "Waveform design for wireless power transfer," *IEEE Trans. Signal Process.*, vol. 64, no. 23, pp. 6313–6328, Dec. 2016.

[76] E. Boshkovska, D. W. K. Ng, N. Zlatanov, and R. Schober, "Practical non-linear energy harvesting model and resource allocation for SWIPT systems," *IEEE Wireless Commun. Lett.*, vol. 19, no. 12, pp. 2082–2085, Dec. 2015.

[77] S. Wang, M. Xia, K. Huang, and Y.-C. Wu, "Wirelessly powered two-way communication with nonlinear energy harvesting model: Rate regions under fixed and mobile relay," *IEEE Trans. Wireless Commun.*, vol. 16, no. 12, pp. 8190–8204, Apr. 2017.

[78] D. Wang, F. Rezaei, and C. Tellambura, "Performance analysis and resource allocations for a WPCN with a new nonlinear energy harvester model," *IEEE open j. Commun. Soc.*, vol. 1, pp. 1403–1424, Sep. 2020.

[79] X. Tang, G. Xie, and Y. Cui, "Self-sustainable long-range backscattering communication using RF energy harvesting," *IEEE Internet Things J.*, vol. 8, no. 17, pp. 13 737–13 749, Sep. 2021.

[80] C. Song, Y. Huang, J. Zhou, J. Zhang, S. Yuan, and P. Carter, "A high-efficiency broadband rectenna for ambient wireless energy harvesting," *IEEE Trans. Antennas Propag.*, vol. 63, no. 8, pp. 3486–3495, Aug. 2015.

[81] T. K. Moon, *Error correction coding: mathematical methods and algorithms*. John Wiley & Sons, Dec. 2020.

[82] U. Madhow, *Fundamentals of Digital Communication*. Cambridge University Press, 2008.

[83] R. G. Maunder and L. Hanzo, "Near-capacity irregular variable length coding and irregular unity rate coding," *IEEE Trans. Wireless Commun.*, vol. 8, no. 11, pp. 5500–5507, Nov. 2009.

[84] L. Hanzo, R. G. Maunder, J. Wang, and L.-L. Yang, *Near-Capacity Variable-Length Coding: Regular and EXIT-Chart-Aided Irregular Designs*. Chichester, U.K.: Wiley, 2011.

[85] L. Hanzo, T. H. Liew, B. L. Yeap, R. Y. S. Tee, and S. X. Ng, *Turbo Coding, Turbo Equalisation and Space-Time Coding: EXIT-Chart-Aided Near-Capacity Designs for Wireless Channels*, 2nd ed. New York, NY, USA: Wiley, 2011.

[86] E. Biglieri, *Coding for wireless channels*. Springer Science & Business Media, May 2005.

[87] G. Forney, "The viterbi algorithm," *Proc. IEEE*, vol. 61, no. 3, pp. 268–278, Mar. 1973.

[88] Y. Sun and J. R. Cavallaro, "Efficient hardware implementation of a highly-parallel 3GPP LTE/LTE-advance turbo decoder," *Integration*, vol. 44, no. 4, pp. 305–315, Sep. 2011.

[89] S. Shao *et al.*, "Survey of Turbo, LDPC, and Polar decoder ASIC implementations," *IEEE Commun. Surveys Tuts.*, vol. 21, no. 3, pp. 2309–2333, 3th Quart. 2019.

[90] Z. Tu and S. Zhang, "Overview of LDPC codes," in *7th IEEE Int. Conf. Comput. Inf. Technol. (CIT 2007)*, Oct. 2007, pp. 469–474.

[91] M. Fossorier, M. Mihaljevic, and H. Imai, "Reduced complexity iterative decoding of low-density parity check codes based on belief propagation," *IEEE Trans. Commun.*, vol. 47, no. 5, pp. 673–680, May 1999.

[92] W. Ryan and S. Lin, *Channel Codes: Classical and Modern*. Cambridge University Press, 2009.

[93] K. D. Rao, *Channel coding techniques for wireless communications*. Springer, Mar. 2015.

[94] P. Koopman and T. Chakravarty, "Cyclic redundancy code (CRC) polynomial selection for embedded networks," in *IEEE Int. Conf. Dependable Syst. Netw., 2004*, July 2004, pp. 145–154.

[95] P. Koopman, "Best CRC polynomials," 2018. Available Online: https://users.ece.cmu.edu/~koopman/crc/.

[96] M. P. Clark and M. Clarke, *Wireless Access Networks: Fixed Wireless Access and WLL Networks – Design and Operation*. John Wiley & Sons, Ltd, 2000.

[97] P. Robertson, E. Villebrun, and P. Hoeher, "A comparison of optimal and sub-optimal MAP decoding algorithms operating in the log domain," in *Proc. IEEE Int. Conf. on Commun. ICC '95*, vol. 2, June 1995, pp. 1009–1013 vol.2.

[98] M. Kanj, V. Savaux, and M. Le Guen, "A tutorial on NB-IoT physical layer design," *IEEE Commun. Surveys Tuts.*, vol. 22, no. 4, pp. 2408–2446, 4th Quart. 2020.

[99] A. Ahmed, A. Al-Dweik, Y. Iraqi, H. Mukhtar, M. Naeem, and E. Hossain, "Hybrid automatic repeat request (HARQ) in wireless communications systems and standards: A contemporary survey," *IEEE Commun. Surveys Tuts.*, vol. 23, no. 4, pp. 2711–2752, 4th Quart. 2021.

[100] G. W. Stephen, "Digital modulation and coding," 1996.

[101] A. Huseyin, *Wireless Communication Signals: A Laboratory-based Approach*. John Wiley & Sons, Inc., 2021.

[102] "Modulation and Coding," Available Online: http://vig.pearsoned.com/samplechapter/0672321572.pdf.

[103] G. Ungerboeck, "Channel coding with multilevel/phase signals," *IEEE Trans. Inf. Theory*, vol. 28, no. 1, pp. 55–67, Jan. 1982.

[104] E. Biglieri, D. Divsalar, M. K. Simon, and P. J. McLane, *Introduction to trellis-coded modulation with applications*. Prentice-Hall, Inc., 1991.

[105] A. Goldsmith, *Wireless communications*. Cambridge university press, 2005.

[106] "5G/NR - MCS/TBS/Code Rate," Available Online: https://www.sharetechnote.com/html/5G/5G_MCS_TBS_CodeRate.html.

[107] "4G/LTE - Measurement Report," Available Online: https://www.sharetechnote.com/html/Handbook_LTE_CQI.html.

[108] "5G/NR - CSI Report," Available Online: https://www.sharetechnote.com/html/5G/5G_CSI_Report.html.

[109] E. Biglieri, *Coding for Wireless Channels*, 1st ed. Springer Publishing Company, Incorporated, 2010.

[110] R. Y. Mesleh, H. Haas, S. Sinanovic, C. W. Ahn, and S. Yun, "Spatial modulation," *IEEE Trans. Veh. Technol.*, vol. 57, no. 4, pp. 2228–2241, July 2008.

[111] E. Başar, U. Aygölü, E. Panayirci, and H. V. Poor, "Space-time block coded spatial modulation," *IEEE Trans. Commun.*, vol. 59, no. 3, pp. 823–832, Mar. 2011.

[112] C. Boyer and S. Roy, "Space time coding for backscatter RFID," *IEEE Trans. Wireless Commun.*, vol. 12, no. 5, pp. 2272–2280, May 2013.

[113] C. He, S. Chen, H. Luan, X. Chen, and Z. J. Wang, "Monostatic MIMO backscatter communications," *IEEE J. Sel. Areas Commun.*, vol. 38, no. 8, pp. 1896–1909, Aug. 2020.

[114] C. He, Z. J. Wang, C. Miao, and V. C. M. Leung, "Block-level unitary query: Enabling orthogonal-like space-time code with query diversity for MIMO backscatter RFID," *IEEE Trans. Wireless Commun.*, vol. 15, no. 3, pp. 1937–1949, Mar. 2016.

[115] J. D. Griffin and G. D. Durgin, "Link envelope correlation in the backscatter channel," *IEEE Commun. Lett.*, vol. 11, no. 9, pp. 735–737, Sep. 2007.

[116] ——, "Gains for RF tags using multiple antennas," *IEEE Trans. Antennas Propag.*, vol. 56, no. 2, pp. 563–570, Feb. 2008.

[117] D. Arnitz, U. Muehlmann, and K. Witrisal, "Wideband characterization of backscatter channels: Derivations and theoretical background," *IEEE Trans. Antennas Propag.*, vol. 60, no. 1, pp. 257–266, Sep 2012.

[118] M. Nakagami, "The m-distribution—A general formula of intensity distribution of rapid fading," in *Statistical Methods in Radio Wave Propagation*. Pergamon, 1960, pp. 3–36.

[119] C. Tellambura, "Evaluation of the exact union bound for trellis-coded modulations over fading channels," *IEEE Trans. Commun.*, vol. 44, no. 12, pp. 1693–1699, 1996.

[120] Y. Chen and C. Tellambura, "Infinite series representations of the trivariate and quadrivariate Rayleigh distribution and their applications," *IEEE Trans. Commun.*, vol. 53, no. 12, pp. 2092–2101, 2005.

[121] D. Chizhik, G. Foschini, and R. Valenzuela, "Capacities of multi-element transmit and receive antennas: Correlations and keyholes," *Electron. Lett.*, vol. 36, pp. 1099–1100(1), June 2000.

[122] R. S. Hassan, T. B. A. Rahman, and A. Y. Abdulrahman, "LTE coverage network planning and comparison with different propagation models," *TELKOMNIKA Telecommun. Comput. Electron. Control*, vol. 12, pp. 153–162, Mar. 2014.

[123] S. M. Kay, *Fundamentals of Statistical Signal Processing: Estimation Theory*. Englewood Cliffs, NJ, USA: Prentice-Hall, 1993.

[124] T. Y. Kim and D. I. Kim, "Novel sparse-coded ambient backscatter communication for massive IoT connectivity," *Energies*, vol. 11, no. 7, p. 1780, July 2018.

[125] P. N. Alevizos, N. Fasarakis-Hilliard, K. Tountas, N. Agadakos, N. Kargas, and A. Bletsas, "Channel coding for increased range bistatic backscatter radio: Experimental results," in *IEEE RFID Technol. Appl. Conf. (RFID-TA)*, Sep. 2014, pp. 38–43.

[126] J. H. Bae, A. Abotabl, H.-P. Lin, K.-B. Song, and J. Lee, "An overview of channel coding for 5G NR cellular communications," *APSIPA Trans. on Signal and Inf. Process.*, vol. 8, p. e17, June 2019.

[127] A. G. I Fabregas and A. J. Grant, "Capacity approaching codes for non-coherent orthogonal modulation," *IEEE Trans. Wireless Commun.*, vol. 6, no. 11, pp. 4004–4013, Nov. 2007.

[128] J. G. Proakis, *Digital Communications 5th Edition*. McGraw Hill, 2007.

[129] L. Tong, B. Sadler, and M. Dong, "Pilot-assisted wireless transmissions: general model, design criteria, and signal processing," *IEEE Signal Process. Mag.*, vol. 21, no. 6, pp. 12–25, Nov. 2004.

[130] T. Cui and C. Tellambura, "Semiblind channel estimation and data detection for OFDM systems with optimal pilot design," *IEEE Trans. Commun.*, vol. 55, no. 5, pp. 1053–1062, May 2007.

[131] S. Ma, G. Wang, R. Fan, and C. Tellambura, "Blind channel estimation for ambient backscatter communication systems," *IEEE Commun. Lett.*, vol. 22, no. 6, pp. 1296–1299, June 2018.

[132] N. Sagias and G. Karagiannidis, "Effects of carrier phase error on EGC receivers in correlated Nakagami-m fading," *IEEE Commun. Lett.*, vol. 9, no. 7, pp. 580–582, July 2005.

[133] K. H. Ngo, "Non-coherent wireless communications : fundamental limits and system design," Ph.D. dissertation, Université Paris-Saclay, Jun. 2020.

[134] F. Yuan, *CMOS circuits for passive wireless microsystems*. Springer Science & Business Media, 2010.

[135] Y. Li, H. Wu, and Y. Zeng, "Signal coding in physical layer separation for RFID tag collision," in *Proc. of the Int. Conf. on Wireless Commun., Network and Multimed. Eng. (WCNME), Guilin, China*, vol. 10, Apr. 2019.

[136] D. Dobkin, *The RF in RFID: UHF RFID in practice*. Newnes, Nov. 2012.

[137] J. D. Gibson, *The communications handbook*. CRC press, 2018.

[138] J. K. Devineni and H. S. Dhillon, "Ambient backscatter systems: Exact average bit error rate under fading channels," *IEEE Trans. Green Commun. Netw.*, vol. 3, no. 1, pp. 11–25, Mar. 2019.

[139] J. Qian, F. Gao, G. Wang, S. Jin, and H. Zhu, "Noncoherent detections for ambient backscatter system," *IEEE Trans. Wireless Commun.*, vol. 16, no. 3, pp. 1412–1422, Mar. 2017.

[140] Q. Tao, C. Zhong, H. Lin, and Z. Zhang, "Symbol detection of ambient backscatter systems with Manchester coding," *IEEE Trans. Wireless Commun.*, vol. 17, no. 6, pp. 4028–4038, June 2018.

[141] G. A. Vitetta, D. P. Taylor, G. Colavolpe, F. Pancaldi, and P. A. Martin, *Wireless communications: Algorithmic techniques*. John Wiley & Sons, 2013.

[142] G. Song, W. Wang, H. Yang, D. Zhang, P. Gao, and T. Jiang, "Exploiting channel polarization for reliable wide-area backscatter networks," *IEEE Trans. Mobile Comput.*, pp. 1–1, Apr. 2021.

[143] X. He, W. Jiang, M. Cheng, X. Zhou, P. Yang, and B. Kurkoski, "Guardrider: Reliable WiFi backscatter using Reed-Solomon codes with QoS guarantee," in *IEEE/ACM 28th Int. Symposium on Quality of Service (IWQoS)*, June 2020, pp. 1–10.

[144] L. W. F. Chaves, M. Schwuchow, A. Schmidt, and A. Taherivand, "Radio frequency identification reading by using error correcting codes on sets of tags," Sep. 2013, uS Patent 8,542,103.

[145] M. Shirvanimoghaddam *et al.*, "Short block-length codes for ultra-reliable low latency communications," *IEEE Commun. Mag.*, vol. 57, no. 2, pp. 130–137, 2019.

[146] J. Van Wonterghem, A. Alloum, J. J. Boutros, and M. Moeneclaey, "On performance and complexity of OSD for short error correcting codes in 5G-NR," *Proc. 1st Int. Balkan Conf. on Commun. and Netw. (BalkanCom 2017)*, vol. 6, June 2017.

[147] J. G. Proakis and M. Salehi, *Digital communications*. McGraw-hill New York, 2001, vol. 4.

[148] G. Ricciutelli, M. Baldi, and F. Chiaraluce, "Interleaver design for short concatenated codes," *IEEE Commun. Lett.*, vol. 22, no. 9, pp. 1762–1765, July 2018.

[149] R. J. McEliece, *The theory of information and coding*. Cambridge University Press, July 2004, no. 86.

[150] W. Zhao, G. Wang, S. Atapattu, R. He, and Y.-C. Liang, "Channel estimation for ambient backscatter communication systems with massive-antenna reader," *IEEE Trans. Veh. Technol.*, vol. 68, no. 8, pp. 8254–8258, Aug. 2019.

[151] D. Darsena, "Noncoherent detection for ambient backscatter communications over OFDM signals," *IEEE Access*, vol. 7, pp. 159 415–159 425, Oct. 2019.

[152] C. Chen, G. Wang, H. Guan, Y.-C. Liang, and C. Tellambura, "Transceiver design and signal detection in backscatter communication systems with multiple-antenna tags," *IEEE Trans. Wireless Commun.*, vol. 19, no. 5, pp. 3273–3288, May 2020.

[153] S. Choi, H. K. Ahn, B. K. Song, J. P. Kim, S. H. Kang, and S.-O. Jung, "A decoder for short BCH codes with high decoding efficiency and low power for emerging memories," *IEEE Trans. VLSI Syst.*, vol. 27, no. 2, pp. 387–397, Feb. 2019.

[154] G. Forney Jr, "Introduction to binary block codes," *Principles of Digital Communication II, MIT*, 2005.

[155] S. Lin and D. J. Costello, *Error control coding*, 2nd ed. Prentice hall New York, June 2004, no. 4.

[156] E. Arikan, "Channel polarization: A method for constructing capacity-achieving codes for symmetric binary-input memoryless channels," *IEEE Trans. Inf. Theory*, vol. 55, no. 7, pp. 3051–3073, 2009.

[157] V. Bioglio, C. Condo, and I. Land, "Design of Polar codes in 5G new radio," *IEEE Commun. Surveys Tuts.*, vol. 23, no. 1, pp. 29–40, 1th Quart. 2020.

[158] M. Indoonundon and T. Pawan Fowdur, "Overview of the challenges and solutions for 5G channel coding schemes," *J. Inf. Telecommun.*, vol. 5, no. 4, pp. 460–483, Oct. 2021.

[159] I. Tal and A. Vardy, "List decoding of Polar codes," *IEEE Trans. Inf. Theory*, vol. 61, no. 5, pp. 2213–2226, May 2015.

[160] S. A. Hashemi, C. Condo, and W. J. Gross, "Fast simplified successive-cancellation list decoding of Polar codes," in *IEEE Wireless Commun. Netw. Conf. Workshops (WCNCW)*, May 2017, pp. 1–6.

[161] G. Sarkis, P. Giard, A. Vardy, C. Thibeault, and W. J. Gross, "Fast list decoders for Polar codes," *IEEE J. Sel. Areas Commun.*, vol. 34, no. 2, pp. 318–328, Nov. 2016.

[162] Y. Fan *et al.*, "A low-latency list successive-cancellation decoding implementation for Polar codes," *IEEE J. Sel. Areas Commun.*, vol. 34, no. 2, pp. 303–317, Nov. 2016.

[163] D. MacKay and R. Neal, "Near Shannon limit performance of low density parity check codes," *Electronics Lett.*, vol. 32, pp. 1645–1646(1), Aug. 1996.

[164] D. V. Nguyen and B. Vasic, "Two-bit bit flipping algorithms for LDPC codes and collective error correction," *IEEE Trans. Commun.*, vol. 62, no. 4, pp. 1153–1163, 2014.

[165] B. Vasic and S. K. Chilappagari, "An information theoretical framework for analysis and design of nanoscale fault-tolerant memories based on low-density parity-check codes," *IEEE Trans. Circuits Syst.*, vol. 54, no. 11, pp. 2438–2446, 2007.

[166] S.-Y. Chung, G. Forney, T. Richardson, and R. Urbanke, "On the design of low-density parity-check codes within 0.0045 dB of the Shannon limit," *IEEE Commun. Lett.*, vol. 5, no. 2, pp. 58–60, 2001.

[167] X.-Y. Hu, E. Eleftheriou, D.-M. Arnold, and A. Dholakia, "Efficient implementations of the sum-product algorithm for decoding LDPC codes," in *IEEE Global Telecommun. Conf.*, vol. 2, 2001, pp. 1036–1036E vol.2.

[168] L. Ping and W. Leung, "Decoding low density parity check codes with finite quantization bits," *IEEE Commun. Lett.*, vol. 4, no. 2, pp. 62–64, 2000.

[169] S. Viraktamath and G. Attimarad, "Performance analysis of Min-Sum LDPC decoding algorithm,," *Int. J. Adv. Eng. Research Sci.*, vol. 1, pp. 1–5, 08 2014.

[170] C. He and Z. J. Wang, "Gains by a space-time-code based signaling scheme for multiple-antenna RFID tags," in *CCECE 2010*, May 2010, pp. 1–4.

[171] G. Yang, C. K. Ho, and Y. L. Guan, "Multi-antenna wireless energy transfer for backscatter communication systems," *IEEE J. Sel. Areas Commun.*, vol. 33, no. 12, pp. 2974–2987, Sep. 2015.

[172] J. D. Griffin and G. D. Durgin, "Multipath fading measurements at 5.8 GHZ for backscatter tags with multiple antennas," *IEEE Trans. Antennas Propag.*, vol. 58, no. 11, pp. 3693–3700, Nov. 2010.

[173] H. Jafarkhani, *Space-time coding: theory and practice*. Cambridge university press, 2005.

[174] L. Poo, "Space-time coding for wireless communication : A survey," in *Report from Standford University*, 2002.

[175] V. Tarokh, N. Seshadri, and A. Calderbank, "Space-time codes for high data rate wireless communication: performance criterion and code construction," *IEEE Trans. Inf. Theory*, vol. 44, no. 2, pp. 744–765, Mar. 1998.

[176] C. He, Z. J. Wang, and V. C. M. Leung, "Unitary Query for the $M \times L \times N$ MIMO backscatter RFID channel," *IEEE Trans. Wireless Commun.*, vol. 14, no. 5, pp. 2613–2625, May 2015.

[177] I. S. Gradshteyn and I. M. Ryzhik, *Table of Integrals, Series, and Products, 7th edition*. Academic Press, 2007.

[178] S. M. Alamouti, "A simple transmit diversity technique for wireless communications," *IEEE J. Sel. Areas Commun.*, vol. 16, no. 8, pp. 1451–1458, Oct. 1998.

[179] C. He, H. Luan, X. Li, C. Ma, L. Han, and Z. Jane Wang, "A simple, high-performance space–time code for MIMO backscatter communications," *IEEE Internet Things J.*, vol. 7, no. 4, pp. 3586–3591, Apr. 2020.

[180] W. Liu, S. Shen, D. H. K. Tsang, and R. Murch, "Enhancing ambient backscatter communication utilizing coherent and non-coherent space-time codes," *IEEE Trans. Wireless Commun.*, vol. 20, no. 10, pp. 6884–6897, Oct. 2021.

[181] A. I. Barbero, E. Rosnes, G. Yang, and O. Ytrehus, "Near-field passive RFID communication: Channel model and code design," *IEEE Trans. Commun.*, vol. 62, no. 5, pp. 1716–1727, May 2014.

[182] Y. Zhu, E. Li, and K. Chi, "Encoding scheme to reduce energy consumption of delivering data in radio frequency powered battery-free wireless sensor networks," *IEEE Trans. Veh. Technol.*, vol. 67, no. 4, pp. 3085–3097, Nov. 2018.

[183] Y. Zhang, E. Li, Y. Zhu, K. Chi, and X. Tian, "Energy-efficient prefix code based backscatter communication for wirelessly powered networks," *IEEE Wireless Commun. Lett.*, vol. 8, no. 2, pp. 348–351, Sep. 2019.

[184] M. Simon and D. Divsalar, "Some interesting observations for certain line codes with application to RFID," *IEEE Trans. Commun.*, vol. 54, no. 4, pp. 583–586, Apr. 2006.

[185] C. A. Albright, S. A. Kaiser, L. W. Oglesbee, and D. W. Engels, "Forward error correction in passive UHF Gen2 communications," in *IEEE Int. Conf. RFID*, Apr. 2015, pp. 17–24.

[186] M. Khan *et al.*, "On the use of Reed-Solomon codes to extend link margin and communication range in low-power wireless networks," in *Proc. 22nd Irish Signals Syst. Conf.(ISSC)*, June 2011, pp. 124–130.

[187] G. Smietanka, J. Geldmacher, and J. Götze, "Error detection based on correlation analysis for BCH encoded UHF RFID communication," in *IEEE Int. Conf. Ind. Technol. (ICIT)*. IEEE, Feb. 2013, pp. 1666–1670.

[188] G. D. Durgin and B. P. Degnan, "Improved channel coding for next-generation RFID," *IEEE J. Radio Freq. Identif.*, vol. 1, no. 1, pp. 68–74, Mar. 2017.

[189] K. A. S. Immink, *Codes for mass data storage systems*. Shannon Foundation Publisher, 2004.

[190] G. Vougioukas and A. Bletsas, "Switching frequency techniques for universal ambient backscatter networking," *IEEE J. Sel. Areas Commun.*, vol. 37, no. 2, pp. 464–477, Feb. 2019.

[191] Y. Peng *et al.*, "PLoRa: A passive long-range data network from ambient LoRa transmissions," in *Proc. of the 2018 Conf. of the ACM Special Interest Group on Data Commun.*, ser. SIGCOMM '18, Aug. 2018, p. 147–160.

[192] Y. Liu, G. Wang, Z. Dou, and Z. Zhong, "Coding and detection schemes for ambient backscatter communication systems," *IEEE Access*, vol. 5, pp. 4947–4953, Mar. 2017.

[193] V. Talla, B. Kellogg, B. Ransford, S. Naderiparizi, J. R. Smith, and S. Gollakota, "Powering the next billion devices with Wi-Fi," *Commun. ACM*, vol. 60, no. 3, p. 83–91, Dec. 2015.

[194] K. R. Duffy, J. Li, and M. Médard, "Capacity-achieving guessing random additive noise decoding," *IEEE Trans. Inf. Theory*, vol. 65, no. 7, pp. 4023–4040, 2019.

[195] W. An, M. Médard, and K. R. Duffy, "CRC codes as error correction codes," in *IEEE Int. Conf. Commun. (ICC)*, June 2021, pp. 1–6.

[196] ——, "Keep the bursts and ditch the interleavers," *IEEE Trans. Commun.*, May 2022.

[197] D. Mishra and E. G. Larsson, "Optimal channel estimation for reciprocity-based backscattering with a full-duplex MIMO reader," *IEEE Trans. Signal Process.*, vol. 67, no. 6, pp. 1662–1677, Mar. 2019.

[198] H. Luan, X. Xie, L. Han, C. He, and Z. J. Wang, "A better than Alamouti OSTBC for MIMO backscatter communications," *IEEE Trans. Wireless Commun.*, vol. 21, no. 2, pp. 1117–1131, Feb. 2022.

[199] E. Goudeli, C. Psomas, and I. Krikidis, "Spatial-modulation-based techniques for backscatter communication systems," *IEEE Internet Things J.*, vol. 7, no. 10, pp. 10 623–10 634, Oct. 2020.

[200] A. Younis, N. Serafimovski, R. Mesleh, and H. Haas, "Generalised spatial modulation," in *Conf. Record of the 44th Asilomar Conf. on Signals, Syst. and Comput.*, Nov. 2010, pp. 1498–1502.

[201] C. Chen, G. Wang, P. D. Diamantoulakis, R. He, G. K. Karagiannidis, and C. Tellambura, "Signal detection and optimal antenna selection for ambient backscatter communications with multi-antenna tags," *IEEE Trans. Commun.*, vol. 68, no. 1, pp. 466–479, Jan. 2020.

[202] J. Qian, F. Gao, G. Wang, S. Jin, and H. Zhu, "Semi-coherent detection and performance analysis for ambient backscatter system," *IEEE Trans. Commun.*, vol. 65, no. 12, pp. 5266–5279, Dec. 2017.

[203] S. Guruacharya, X. Lu, and E. Hossain, "Optimal non-coherent detector for ambient backscatter communication system," *IEEE Trans. Veh. Technol.*, vol. 69, no. 12, pp. 16 197–16 201, Dec. 2020.

[204] J. Östman, G. Durisi, E. G. Ström, M. C. Coşkun, and G. Liva, "Short packets over block-memoryless fading channels: Pilot-assisted or noncoherent transmission?" *IEEE Trans. Commun.*, vol. 67, no. 2, pp. 1521–1536, Feb. 2019.

[205] D. Warrier and U. Madhow, "Spectrally efficient noncoherent communication," *IEEE Trans. Inf. Theory*, vol. 48, no. 3, pp. 651–668, Mar. 2002.

[206] P. Yuan, M. C. Coşkun, and G. Kramer, "Polar-coded non-coherent communication," *IEEE Commun. Lett.*, vol. 25, no. 6, pp. 1786–1790, June 2021.

[207] A. Varshney, O. Harms, C. Pérez-Penichet, C. Rohner, F. Hermans, and T. Voigt, "LoRea: A backscatter reader for everyone!" *ArXiv, abs/1611.00096*, 2016.

[208] Y.-H. Kim, H.-S. Ahn, C. Yoon, Y. Lim, S. Lim, and M.-H. Yoon, "Implementation of bistatic backscatter wireless communication system using ambient wi-fi signals," *KSII Trans. Internet Inf. Syst. (TIIS)*, vol. 11, no. 2, pp. 1250–1264, Feb. 2017.

[209] Y.-H. Kim, H.-S. Ahn, C. Yoon, Y. Lim, and S. Lim, "Self-powered and backscatter-communicated IoT device system for zero-energy wireless communication in a Wi-Fi environment," in *Proceedings of the 6th Int. Conf. Internet of Things*, Nov. 2016, pp. 163–164.

[210] A. V. Padaki and M. Zawodniok, "TDMA for wireless passive backscatter networks: An information theoretic approach," in *Proc. of IEEE 37th Conf. on Local Comput. Netw.*, Oct. 2012, p. 264–267.

[211] W. Liu, Y.-C. Liang, Y. Li, and B. Vucetic, "Backscatter multiplicative multiple-access systems: Fundamental limits and practical design," *IEEE Trans. Wireless Commun.*, vol. 17, no. 9, pp. 5713–5728, Sep. 2018.

[212] A. Alma'aitah, H. S. Hassanein, and M. Ibnkahla, "Tag modulation silencing: Design and application in RFID anti-collision protocols," *IEEE Trans. Commun.*, vol. 62, no. 11, pp. 4068–4079, Nov. 2014.

[213] M. Dunna, M. Meng, P.-H. Wang, C. Zhang, P. Mercier, and D. Bharadia, "SyncScatter: Enabling WiFi like synchronization and range for WiFi backscatter communication," in *18th USENIX Symposium on Netw. Syst. Design and Implement. (NSDI 21)*. USENIX Association, Apr. 2021, pp. 923–937. [Online]. Available: https://www.usenix.org/conference/nsdi21/presentation/dunna

[214] H. Nikopour and M. Baligh, "Systems and methods for sparse code multiple access," *US patent, US20140140360 A*, vol. 1, Jan 2016.

[215] T. Y. Kim and D. I. Kim, "Sparse-coded ambient backscatter communication method and system," May 4 2021, uS Patent 10,999,848.

[216] M. Vameghestahbanati, "Designing multidimensional constellations and efficient detection schemes for sparse code multiple access (scma) systems," Ph.D. dissertation, Carleton University, Jan. 2020.

[217] M. Vameghestahbanati, I. D. Marsland, R. H. Gohary, and H. Yanikomeroglu, "Multidimensional constellations for uplink SCMA systems—A comparative study," *IEEE Commun. Surveys Tuts.*, vol. 21, no. 3, pp. 2169–2194, 3th Quart. 2019.

[218] D. Cai, P. Fan, X. Lei, Y. Liu, and D. Chen, "Multi-dimensional SCMA codebook design based on constellation rotation and interleaving," in *IEEE 83rd Veh. Technol. Conf. (VTC Spring)*. IEEE, May 2016, pp. 1–5.

[219] M. Taherzadeh, H. Nikopour, A. Bayesteh, and H. Baligh, "SCMA codebook design," in *IEEE 80th Veh. Technol. Conf. (VTC2014-Fall)*. IEEE, Sep. 2014, pp. 1–5.

[220] J. Wang, H. Hassanieh, D. Katabi, and P. Indyk, "Efficient and reliable low-power backscatter networks," *ACM SIGCOMM Comput. Commun. Rev.*, vol. 42, no. 4, pp. 61–72, Aug. 2012.

[221] N. Mi *et al.*, "CBMA: Coded-backscatter multiple access," in *IEEE 39th Int. Conf. Distrib. Comput. Syst. (ICDCS)*, July 2019, pp. 799–809.

[222] M. Buettner and D. Wetherall, "A software radio-based UHF RFID reader for PHY/MAC experimentation," in *IEEE Int. Conf. RFID*, Apr. 2011, pp. 134–141.

[223] ——, "A "Gen 2" RFID monitor based on the USRP," *ACM SIGCOMM Comput. Commun. Rev.*, vol. 40, no. 3, p. 41–47, July 2010.

[224] A. N. Parks, A. Liu, S. Gollakota, and J. R. Smith, "Turbocharging ambient backscatter communication," *ACM SIGCOMM Comput. Commun. Rev.*, vol. 44, no. 4, p. 619–630, Aug. 2014. [Online]. Available: https://doi.org/10.1145/2740070.2626312

[225] M. Hessar, A. Najafi, and S. Gollakota, "Netscatter: Enabling large-scale backscatter networks," in *Proc. of the 16th USENIX Conf. on Networked Syst. Design and Implementation*, ser. NSDI'19. USA: USENIX Association, 2019, p. 271–283.

[226] M. Jin, Y. He, X. Meng, Y. Zheng, D. Fang, and X. Chen, "FlipTracer: Practical parallel decoding for backscatter communication," *IEEE/ACM Trans. Netw.*, vol. 27, no. 1, pp. 330–343, Feb. 2019.

[227] P. Hu, P. Zhang, and D. Ganesan, "Leveraging interleaved signal edges for concurrent backscatter," *SIGMOBILE Mob. Comput. Commun. Rev.*, vol. 18, no. 3, p. 26–31, Jan. 2015. [Online]. Available: https://doi.org/10.1145/2721896.2721902

[228] J. Ou, M. Li, and Y. Zheng, "Come and be served: Parallel decoding for COTS RFID tags," *IEEE/ACM Trans. Netw.*, vol. 25, no. 3, pp. 1569–1581, June 2017.

[229] P. Hu, P. Zhang, and D. Ganesan, "Laissez-Faire: Fully asymmetric backscatter communication," *ACM SIGCOMM Comput. Commun. Rev.*, vol. 45, no. 4, p. 255–267, Aug. 2015. [Online]. Available: https://doi.org/10.1145/2829988.2787477

[230] A. Bletsas, J. Kimionis, A. G. Dimitriou, and G. N. Karystinos, "Single-antenna coherent detection of collided FM0 RFID signals," *IEEE Trans. Commun.*, vol. 60, no. 3, pp. 756–766, Feb. 2012.

[231] K. Arora, J. Singh, and Y. S. Randhawa, "A survey on channel coding techniques for 5G wireless networks," *Telecommun. Syst.: Modelling, Analysis, Design and Management, Springer*, vol. 73, no. 4, pp. 637–663, Apr. 2020.

[232] M. Zhan, Z. Pang, D. Dzung, and M. Xiao, "Channel coding for high performance wireless control in critical applications: Survey and analysis," *IEEE Access*, vol. 6, pp. 29 648–29 664, May 2018.

[233] R. Mori and T. Tanaka, "Non-binary Polar codes using Reed-Solomon codes and algebraic geometry codes," in *IEEE Inf. Theory Workshop*, Aug. 2010, pp. 1–5.

[234] K. Saied, A. C. A. Ghouwayel, and E. Boutillon, "Short frame transmission at very low SNR by associating CCSK modulation with NB-code," *IEEE Trans. Wireless Commun.*, vol. 21, no. 9, pp. 7194–7206, Sep. 2022.

[235] J. Zhao, W. Zhang, Y. Liu, J. Gao, and R. Zhang, "A rate-matching concatenation scheme of Polar codes with outer Reed-Solomon codes," *IEEE Wireless Commun. Lett.*, vol. 10, no. 3, pp. 459–463, Mar. 2021.

[236] Y. Wang, W. Zhang, Y. Liu, L. Wang, and Y. Liang, "An improved concatenation scheme of Polar codes with Reed–Solomon codes," *IEEE Commun. Lett.*, vol. 21, no. 3, pp. 468–471, Mar. 2017.

[237] O. Dizdar and E. Arıkan, "A high-throughput energy-efficient implementation of successive cancellation decoder for Polar codes using combinational logic," *IEEE Trans. Circuits Syst.*, vol. 63, no. 3, pp. 436–447, Mar. 2016.

[238] Y. Liu, H.-H. Chen, and L. Wang, "Physical layer security for next generation wireless networks: Theories, technologies, and challenges," *IEEE Commun. Surveys Tuts.*, vol. 19, no. 1, pp. 347–376, 1th Quart. 2017.

[239] Y. Wang, S. Yan, W. Yang, Y. Huang, and C. Liu, "Energy-efficient covert communications for bistatic backscatter systems," *IEEE Trans. Veh. Technol.*, vol. 70, no. 3, pp. 2906–2911, Mar. 2021.

[240] X. Lu, N. Cong Luong, D. T. Hoang, D. Niyato, Y. Xiao, and P. Wang, "Secure wirelessly powered networks at the physical layer: Challenges, countermeasures, and road ahead," *Proc. IEEE*, vol. 110, no. 1, pp. 193–209, Jan. 2022.

[241] J. Liu, J. Yu, X. Chen, R. Zhang, S. Wang, and J. An, "Covert communication in ambient backscatter systems with uncontrollable RF source," *IEEE Trans. Commun.*, vol. 70, no. 3, pp. 1971–1983, Mar. 2022.

[242] N. Van Huynh, D. N. Nguyen, D. Thai Hoang, E. Dutkiewicz, and M. Mueck, "Ambient backscatter: A novel method to defend jamming attacks for wireless networks," *IEEE Wireless Commun. Lett.*, vol. 9, no. 2, pp. 175–178, Feb. 2020.

[243] N. Van Huynh, D. N. Nguyen, D. T. Hoang, and E. Dutkiewicz, ""Jam Me If You Can": Defeating jammer with deep dueling neural network architecture and ambient backscattering augmented communications," *IEEE J. Sel. Areas Commun.*, vol. 37, no. 11, pp. 2603–2620, Nov. 2019.

[244] Z. Fang, T. Song, and T. Li, "Energy harvesting for two-way OFDM communications under hostile jamming," *IEEE Signal Process. Lett.*, vol. 22, no. 4, pp. 413–416, Apr. 2015.

[245] D. T. Hoang, D. Niyato, P. Wang, and D. I. Kim, "Performance analysis of wireless energy harvesting cognitive radio networks under smart jamming attacks," *IEEE Trans. on Cogn. Commun. Netw.*, vol. 1, no. 2, pp. 200–216, June 2015.

[246] M. Alageli, A. Ikhlef, and J. Chambers, "Optimization for maximizing sum secrecy rate in MU-MISO SWIPT systems," *IEEE Trans. Veh. Commun.*, vol. 67, no. 1, pp. 537–553, Jan. 2018.

[247] X. Jiang, C. Zhong, Z. Zhang, and G. K. Karagiannidis, "Power beacon assisted wiretap channels with jamming," *IEEE Trans. Wireless Commun.*, vol. 15, no. 12, pp. 8353–8367, Dec. 2016.

[248] Y.-M. Chang, A. I. V. Casado, M.-C. F. Chang, and R. D. Wesel, "Lower-complexity layered belief-propagation decoding of LDPC codes," in *IEEE Int. Conf. Commun.*, 2008, pp. 1155–1160.

[249] E. Nachmani, Y. Be'ery, and D. Burshtein, "Learning to decode linear codes using deep learning," in *54th Annual Allerton Conf. on Commun., Control, and Computing (Allerton)*, Sep. 2016, pp. 341–346.

[250] X. Wang, J. Li, H. Chang, and J. He, "Optimization design of Polar-LDPC concatenated scheme based on deep learning," *Comput. and Electr. Eng.*, vol. 84, p. 106636, June 2020. [Online]. Available: https://www.sciencedirect.com/science/article/pii/S0045790620304912

[251] L. Lugosch and W. J. Gross, "Neural offset Min-Sum decoding," in *IEEE Int. Symposium Inf. Theory (ISIT)*, June 2017, pp. 1361–1365.

[252] N. Shah and Y. Vasavada, "Neural layered decoding of 5G LDPC codes," *IEEE Commun. Lett.*, vol. 25, no. 11, pp. 3590–3593, Sep. 2021.

[253] Y. Jiang, H. Kim, H. Asnani, S. Kannan, S. Oh, and P. Viswanath, *Turbo Autoencoder: Deep Learning Based Channel Codes for Point-to-Point Communication Channels*. Red Hook, NY, USA: Curran Associates Inc., 2019.

[254] L. Mostari and A. Taleb-Ahmed, "High performance short-block binary regular LDPC codes," *Alexandria Eng. J.*, vol. 57, no. 4, pp. 2633–2639, Dec. 2018. [Online]. Available: https://www.sciencedirect.com/science/article/pii/S1110016818300619

[255] U. S. Toro, B. M. ElHalawany, A. B. Wong, L. Wang, and K. Wu, "Machine-learning-assisted signal detection in ambient backscatter communication networks," *IEEE Netw.*, vol. 35, no. 6, pp. 120–125, Dec. 2021.

[256] Q. Zhang, H. Guo, Y.-C. Liang, and X. Yuan, "Constellation learning-based signal detection for ambient backscatter communication systems," *IEEE J. Sel. Areas Commun.*, vol. 37, no. 2, pp. 452–463, 2019.

[257] Y. Hu, P. Wang, Z. Lin, M. Ding, and Y.-C. Liang, "Machine learning based signal detection for ambient backscatter communications," in *IEEE Int. Conf. Commun. (ICC)*, 2019, pp. 1–6.

[258] C. Liu, Z. Wei, D. W. K. Ng, J. Yuan, and Y.-C. Liang, "Deep transfer learning for signal detection in ambient backscatter communications," *IEEE Trans. Wireless Commun.*, vol. 20, no. 3, pp. 1624–1638, Mar. 2021.

[259] X. Liu, C. Liu, Y. Li, B. Vucetic, and D. W. K. Ng, "Deep residual learning-assisted channel estimation in ambient backscatter communications," *IEEE Wireless Commun. Lett.*, vol. 10, no. 2, pp. 339–343, Feb. 2021.

[260] C. Liu, X. Liu, D. W. Kwan Ng, and J. Yuan, "Deep residual network empowered channel estimation for IRS-assisted multi-user communication systems," in *IEEE Int. Conf. Commun.*, June 2021, pp. 1–7.

[261] P. Zhang, D. Bharadia, K. Joshi, and S. Katti, "HitchHike: Practical backscatter using commodity Wi-Fi," in *Proc. of the 14th ACM Conf. Embedded Netw. Sensor Syst. CD-ROM*, ser. SenSys '16. New York, NY, USA: Association for Computing Machinery, Nov. 2016, p. 259–271. [Online]. Available: https://doi.org/10.1145/2994551.2994565

[262] P. Jia, X. Wang, and X. Shen, "Passive network synchronization based on concurrent observations in industrial IoT systems," *IEEE Internet Things J.*, vol. 8, no. 18, pp. 14 028–14 038, Sep. 2021.

[263] W. Liu, K. Huang, X. Zhou, and S. Durrani, "Next generation backscatter communication: systems, techniques, and applications," *EURASIP J. Wireless Commun. Netw.*, vol. 2019, pp. 1–11, Mar. 2019.

[264] Q. Wang, Y. Zhou, H.-N. Dai, G. Zhang, and W. Zhang, "Performance on cluster backscatter communication networks with coupled interferences," *IEEE Internet Things J.*, vol. 9, no. 20, pp. 20 282–20 294, 2022.

[265] L. Shi, R. Q. Hu, Y. Ye, and H. Zhang, "Modeling and performance analysis for ambient backscattering underlaying cellular networks," *IEEE Trans. Veh. Technol.*, vol. 69, no. 6, pp. 6563–6577, 2020.

[266] S. Atapattu, C. Tellambura, and H. Jiang, "Energy detection of primary signals over $\eta - \mu$ fading channels," in *2009 International Conference on Industrial and Information Systems (ICIIS)*, 2009, pp. 118–122.

[267] ——, *Energy detection for spectrum sensing in cognitive radio*. Springer, vol. 6.

[268] S. P. Herath, N. Rajatheva, and C. Tellambura, "Unified approach for energy detection of unknown deterministic signal in cognitive radio over fading channels," in *2009 IEEE International Conference on Communications Workshops*, 2009, pp. 1–5.

[269] C. Chen, G. Wang, Y. Wang, and Q. Miao, "Interference analysis of ambient backscatter on existing wireless communication systems," in *IEEE 85th Veh. Technol. Conf. (VTC Spring)*, 2017, pp. 1–5.

[270] X. Lu, H. Jiang, D. Niyato, D. I. Kim, and Z. Han, "Wireless-powered device-to-device communications with ambient backscattering: Performance modeling and analysis," *IEEE Trans. Wireless Commun.*, vol. 17, no. 3, pp. 1528–1544, 2018.

[271] W. Liu, K. Huang, X. Zhou, and S. Durrani, "Full-duplex backscatter interference networks based on time-hopping spread spectrum," *IEEE Trans. Wireless Commun.*, vol. 16, no. 7, pp. 4361–4377, 2017.

[272] M. Noura and R. Nordin, "A survey on interference management for device-to-device (D2D) communication and its challenges in 5G networks," *J. Netw. Comput. Appl.*, vol. 71, no. C, p. 130–150, Aug. 2016.